The Effect of Configurational Asymmetries on Projectile Aerodynamics, Stability, and Performance

by

Sean George

Applied Physics (B.S.),
Harvey Mudd College, Claremont, CA (1996)

Submitted to the Department of Aeronautics and Astronautics
in partial fulfillment of the requirements for the degree of

Master of Science

at the

MASSACHUSETTS INSTITUTE OF TECHNOLOGY

May 1998

Author .....
Department of Aeronautics and Astronautics
April 1, 1998

Certified by .....
Eric Feron
Assistant Professor of Aeronautics and Astronautics
Thesis Supervisor

Accepted by .....
Professor Jaime Peraire
Chairman, Department Committee on Graduate Students

The Effect of Configurational Asymmetries on Projectile Aerodynamics, Stability, and Performance

by

Sean George

Submitted to the Department of Aeronautics and Astronautics
on April 1, 1998, in partial fulfillment of the
requirements for the degree of
Master of Science

Abstract

Designs for a guided, spin-stabilized projectile using configurational asymmetries to produce fixed-trim control authority were tested using modern computational fluid dynamic simulations. These tests provided a aerodynamic basis for an evaluation of both the dynamic performance and stability of the projectiles over the Mach regime of a typical ordnance flight envelope. A complete set of analysis tools, suitable for vehicle design and evaluation, were developed for this investigation from previously established components.

The aerodynamic behavior of two classes of non-axisymmetric geometries have been parametrically investigated. The two geometry classes consist of two operations performed on the axisymmetric NATO standard fuze: slicing and bending. Slicing produces a non-circular cross-section with a centroid displaced from the original axis of revolution, while bending produces a near-circular cross-section with a displaced centroid. Aerodynamic characteristics and flow fields have been computed with both a three-dimensional structured Navier-Stokes solver and an unstructured Euler solver. Axisymmetric predictions have been validated with spark-range and windtunnel measurements obtained from the literature.

Initial studies have resulted in several conclusions concerning the strengths and weaknesses of using configurational asymmetries for the trajectory command of modern munitions. In addition the usuage of two distinctly different CFD formulations has provided valuable insight into the proper modelling of the relevant flow features and aerodynamic effects for transonic vehicles. A more indepth look at the dynamics of asymmetric projectiles under fixed-trim flight has been attempted, leading to several conclusions concerning possible stability and performance problems.

Thesis Supervisor: Eric Feron
Title: Assistant Professor of Aeronautics and Astronautics

Thesis Supervisor: Eugene Covert
Title: Emeritus Professor of Aeronautics and Astronautics

Acknowledgments

Over the past two years I have met many people who have made my time here at MIT worthwhile. I'd like to extend my gratitude to my advisors Professor Eric Feron and Professor Eugene Covert for their encouragement and help. Without their experience and knowledge, this thesis could never have been completed. I would also like to thank Professor Jaime Peraire who adopted me into his lab and gave me a place to hang my hat every morning. Another big thanks goes out to Bob Haimes, who provided me with the computer resources necessary to complete this project.

My biggest thanks goes out to Alex Budge, my research partner on this project. How many hours of simulations did we run? It was truly a pleasure working with you on this project Alex, thanks for helping me out when I needed it, and maintaining my sanity during the bumpy moments over the last two years.

The research for this thesis was sponsored by the Charles Stark Draper Laboratory. I would like to acknowledge our main project monitors Brent Appleby and Tim Henderson, who were extremely patient and helpful throughout many meetings and discussions.

To everyone in the ICE and FDRL labs, it was great to have worked with all of you. I feel privileged to have been part of two great offices in my tenure here at MIT.

Thanks to Suzanne Wallace for proofreading this monstrosity. Basically, I'm really happy you high-lighted such a myriad of errors. I guess I'm a bit verbose sometimes, you'll have to pardon me.

Cambridge, Spring 1998

Sean George

Contents

List of Figures

Chapter 1

Introduction

1.1 Background

The concept of guided, unpowered munitions has become more attractive due to a number of inherent advantages and technical improvements. The enhanced accuracy of the guided projectiles translates into a higher rate of successful hits on a target, as well as a reduction in the exposure time of armed forces near a hostile environment. Studies have shown a definite potential improvement with actively controlled trajectory command of field artillery [20, 8]. Projectile guidance has been made more practical due to the advent of miniaturized inertial and global positioning units, which allow a completely integrated control system to be implemented under severe volume constraints.

At the same time, numerous investigations have also demonstrated the fidelity of applying Navier-Stokes and Euler computations to generic shell configurations, even within transonic flow regimes [25, 9, 32, 38]. These studies have illustrated the usefulness of computational simulations for predicting aerodynamic characteristics in problems involving a large space of possible design parameters. Wind tunnel studies require significantly higher development costs for each design modification or iteration, making aerodynamic predictions prohibitively expensive for even small design studies. As computational speed increases, the effort in producing a complete aerodynamic design profile using only simulation data is becoming more practical.

This thesis will attempt to bridge the gap between these two technologies by making use of computational fluid dynamics to accurately predict the aerodynamic qualities of a class of guided projectile designs. Prior related studies have focused on investigating the aerody-

namics of projectiles guided by movable canard lifting surfaces of various geometries [30]. This design has the potential for allowing controlled variable-trim maneuvering, but suffers due to its complexity and lack of durability. By far the simplest and cheapest possible design is a fixed-trim configuration, whereby the control force and maneuvering power of the projectile is entirely set by the specific body geometry. The basic idea behind this type of design is to develop a vehicle with a fixed surface asymmetry which generates nominal forces and moments at zero angle of attack. The unbalanced moment would cause the vehicle to trim at an angle capable of generating sufficient control authority for guidance. Roll control of the vehicle, through some means of a surface aero-torque feature, would then allow reasonable command of the vehicle's trajectory.

Fixed-trim guidance is a fairly common method used for re-entry vehicles and free rolling ballistic missiles. Terminal guidance laws have been proposed by Gracey [11] and various modifications have been performed specifically for ordnance projectiles [36, 37]. Spin-stabilized projectiles offer several difficult problems for fixed trim guidance, which are not seen in the slowly rotating re-entry vehicles.

1. The static instability of the projectiles necessitates a high spin rate, making a roll-controlled actuation scheme impossible without mechanically decoupling the control surface from the shell body.

2. The destabilizing static moment of the projectiles under angle of attack perturbations, demonstrated by the positive value of the pitch moment coefficient, results in a trim angle opposite in direction to the control force which generated it.

3. *Magnus-type* side forces caused by the spin rate of the projectiles at the trim angle of attack could be potentially destabilizing without sufficient augmented damping of the shell dynamics.

In order to address these problems, a potential initial flight plan and projectile design have been devised. The scheme currently envisioned is to replace the standard projectile fuze with a separate section which could be independently despun after launch. The projectile would be launched in an axisymmetric state, then after inertial and global positioning estimations have been acquired, the shell fuze would be augmented in flight. Launching symmetrically alleviates the potential for instability prior to the onset of control. The aero-torque surface feature, used to initially despin the projectile fuze, would then be available to

provide roll directional control of the resultant force and moment on the shell fuze section. The controlled portion of the flight, in which the projectile flew at a trim angle of attack, would then allow limited trajectory command for improved target accuracy.

1.2 Requirements and Evaluation

The requirements for fixed-trim guidance, from an aerodynamic standpoint, deal with the magnitude of control force which can be produced by the specific vehicle geometry. This force translates directly into the amount of control authority and trajectory command available during the flight. The control force available is a rather complicated function of several aerodynamic qualities of the projectiles, each interacting to produce a specific trim angle and resultant force. The aim of this study is to develop the basic computational tools necessary for modeling projectile aerodynamics and to implement these tools to evaluate a class of actuation schemes for guided munitions. These schemes rely on utilizing configurational asymmetries to generate sufficient control authority. Accurate predictions, over a range of Mach numbers, must be made on integrated forces and moments and include simulations at different angles of attack.

Evaluation of the different projectile designs must incorporate as much of the physics of the problem as possible, without becoming unnecessarily cumbersome and difficult to implement. For this study, a design metric was derived based solely on the static aerodynamic coefficients predicted using the computational tools at specific Mach number flight points. Justification of this static approximation must include some reasonable account of both the relation between the design metric and the actual projectile trajectory offset, as well as some assurance that the chosen design points are representative of the flight envelope. In addition, characteristics such as available internal volume within the fuze have caused hard constraints to be initiated limiting the space of possible projectile designs.

The physical constraints mentioned above, as well as the practicality of schemes for in-flight augmentation, have lead to three basic design strategies: remove volume from the projectile fuze, add volume, or distort the initial volume in a mechanically viable way. Each of these strategies has the potential to produce asymmetric shell geometries, but the number of possible designs is extremely large. In order to reduce the design space to a reasonable level, the aerodynamic behavior of only two classes of non-axisymmetric fuze

designs have been parametrically investigated. The two geometry classes consist of two operations performed on an axisymmetric, standard projectile fuze: slicing and bending. Slicing produces a noncircular cross section with a centroid displaced from the original axis of revolution, while bending produces a near-circular cross section with a displaced centroid.

The *sliced fuze* design, shown in Figure 1-1, represents a simple method of asymmetric volume extraction which could be accomplished during the flight. The two design parameters initially investigated were the angle of the slice cut and the position of the slice along the length of the fuze. Slicing the fuze creates an actuation surface on the front of the projectile which has the potential to generate a force and moment at zero angle of attack. The two parameters, slice angle and position, effect the degree of asymmetry by altering the relative amount and distribution of internal volume in the fuze section. The hard constraint of minimum internal volume plays an extremely important role in the range of available parameters for this design.

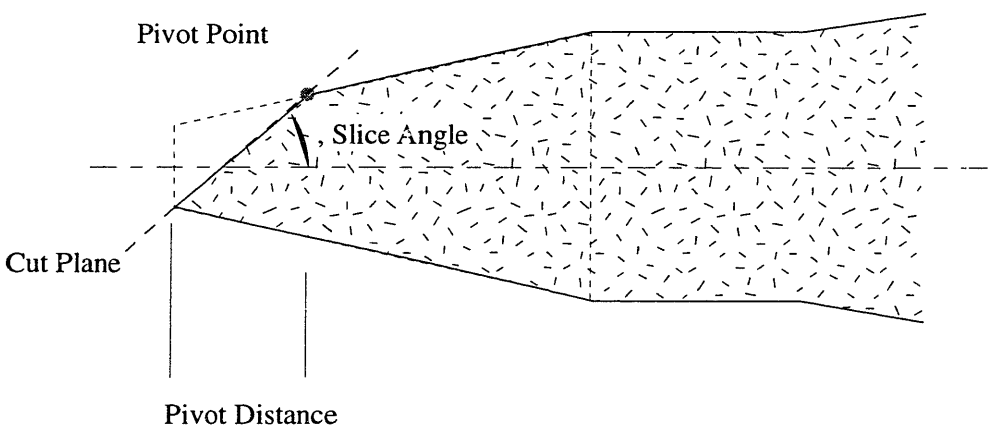

Figure 1-1: Geometry of the Sliced Fuze Design

Figure 1-2 is a diagram of the second design concept, the *bent fuze*. This scheme calls for a simple rotation of the fuze section at a prescribed bend angle and hinge location. Bending the front section of the projectile creates a relative angle of attack in this region with respect to the free-stream flow, resulting in the generation of forces and moments on the shell. This geometry distortion does not alter the amount of volume in the fuze, as in the sliced fuze case, but rather it is the displacement of the projectile centroid which affects the degree of asymmetry. The internal volume constraint on the fuze places no restriction on the magnitude of the parameters for the bent fuze design.

The other requirement of this design, in addition to the production of a sufficient trim

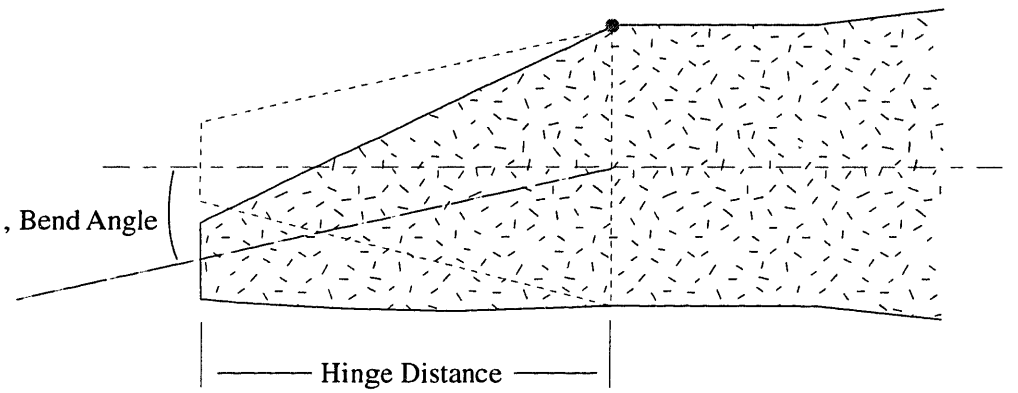

Figure 1-2: Geometry of the Bent Fuze Design

force, is the ability to generate some form of roll-torque on the fuze section. Although the use of internal motors has been suggested, a far better scheme would be to make use of aerodynamic torque generation by external surface features on the fuze. Internal motors would then only be required to hold the fuze at a specific roll orientation, rather than producing all the torque necessary for sufficient angular acceleration. Figure 1-3 shows two views of a possible design for these features, which most closely resemble cork-screw strakes.

There are two separate roll control goals for this design, which effectively act as bounds on the magnitude of aero-torque required. The first design goal is to generate a large amount of torque at the beginning of the projectile's flight in order to quickly despin the fuze from the main body. The second requirement is that, after the initial despinning process, sufficient roll control of the fuze must be produced by the aero-torque features in order to adequately control the azimuthal direction of the trim force. The difficulty lies in maintaining a relatively constant amount of roll control throughout the flight, despite the large changes in dynamic pressure, while still producing a huge amount of torque for the despinning process. Several geometric designs have been tested, which are parameterized by width, height, and cant angle. Evaluations have been made based on the magnitude of roll-torque produced at several different Mach numbers within the flight envelope.

The two fixed-trim concepts mentioned above represent by no means an exhaustive investigation of all possible design geometries, but they do provide an initial study into the effects of configuration asymmetries on projectile aerodynamics. Although the two schemes represent the initial simplified geometric distortions examined in this study, further

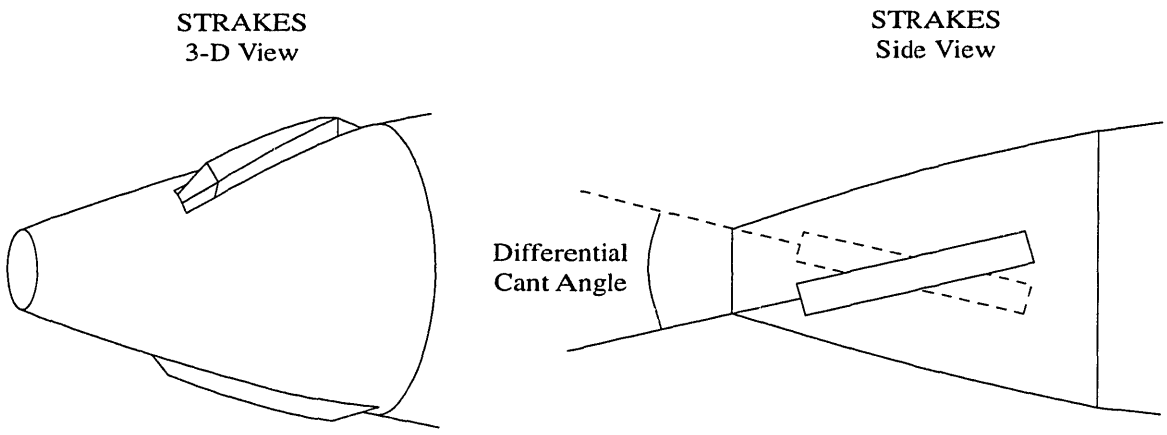

Figure 1-3: Pictures of the Aero-Torque Strake Design

modifications on these basic designs have been completed to more fully address the potential design space. Lessons learned from the basic designs have motivated these subsequent iterations and produced a better perspective on the overall aerodynamic behavior of this class of projectiles.

1.3 Thesis Outline

Chapter 2 of this thesis presents the computational background behind this study. The main theme of this chapter addresses the requirements and limitations of using numerical simulation tools for analysis and design. Inherent in this idea is an assessment of the basic theoretical framework behind Navier-Stokes solvers, and the simplifying assumptions which lead to the Euler equations. The relationship between viscous numerical formulations, which incorporate the effects of boundary layers, and inviscid modeling plays a pivotal role in this investigation. The chapter also discusses the specific computational tools utilized for this study, and our development of them into a useful set of components suitable for accurate aerodynamic modeling and prediction.

Chapter 3 presents the validation attempts made using the computational simulation tools discussed in Chapter 2. The validation cases come from several experimental investigations taken from the literature, completed on projectile geometries which closely match the shell profiles examined in this study. The chapter ends with an evaluation of the two main codes used in this study; FELISA, an unstructured, inviscid, Euler solver; and OVERFLOW, a structured, fully viscous, Navier-Stokes solver. This chapter is used to motivate

confidence in the results found for this design study, and to outline the difficulties in properly modeling the flow physics of a typical projectile flight regime.

Chapter 4 presents the results from all of the preliminary aerodynamic studies performed for this investigation. The methodology for the chosen parameterizations is the initial topic, followed by presentation and discussion of actual results. Baseline characteristics of the control vehicle, used as the platform for the various fuze distortions, is presented first. The main focus of the chapter is based on a design study completed on parameterizations of the two design concepts. Predictions of normal force and pitch moment coefficients, for each of the fuze designs, are presented, as well as pressure distribution results for more indepth explanation. This is followed by results from a study on various geometries for the aero-torque surface features. Roll moments generated by the different strake geometries are presented as the main aerodynamic characteristic. The chapter is concluded by two studies detailing the Mach sensitivity of the forces and moments produced by the shell augmentations, as well as a section detailing the effects of the deformations on the baseline aerodynamic derivatives. These studies attempt to present a broader look at the ramifications of using asymmetric projectile distortion over a complete ballistic flight.

Chapter 5 details the evaluation of the projectile designs shown in Chapter 4 based on the criteria mentioned in Section 1.2. The chapter begins with a numerical simulation on the angular dynamics of a spinning projectile under trim moments. This simulation is made to support the derivation of a trim condition metric, which is used to distinguish the behavior and worthiness of the different projectile fuze designs. A complete design evaluation, based on this design metric, is then displayed for all the initial fuze configurations. The assessment of the different designs is followed by a section detailing the physical relationship between the simplified design metric and the actual trajectory offset using a 3-DOF simulation tool which treats the projectile as a point mass with a roll-angle commanded control force. This simulation tool is used to perform maximum terminal cross range offset and footprint studies on augmented projectile trajectories. The chapter concludes with some discussion on other secondary metrics used in this study to evaluate performance, which are not directly related to the trim performance of the asymmetric shells. This chapter is meant to act as a justification for our conclusions about the overall aerodynamic performance of each design.

Chapter 6 addresses the next step in the design process; assessment of design weaknesses and iterative modifications based on these conclusions. Two additional fuze configurations,

based on simple alterations to the initial design concepts, have been numerically tested. These second phase concepts show substantially improved trim performance, without significant influence on the baseline aerodynamic properties of the projectile. They are meant to provide an example of possible improvements on the initial design schemes and strategy. The chapter ends with some final conclusions based on all the numerical results from the augmented projectiles, as well as suggestions on future work needed to support the fixed-trim guidance concepts investigated in this design study.

Appendix A examines the aerodynamic investigation completed on the CMATD projectile, an experimental shell designed by Draper laboratory. The projectile was the initial focus of this design study, and a substantial series of predictions over a range of Mach numbers has been collected in order to compare with experimental data. The numerical results completed on the CMATD illustrate some very interesting aerodynamic behavior and support the usefulness of applying computational simulations for vehicle analysis.

1.4 Thesis Contributions

This thesis presents the culmination of work completed for the Charles Stark Draper Laboratory on the aerodynamic characteristics of a class of fixed-trim projectiles with asymmetric fuzes. The following contributions have been made toward this endeavour:

1. Implementation of two computational simulation codes, an inviscid Euler solver and a viscous Navier-Stokes formulation, which have been developed using additional components into useful aerodynamic design tools.

2. Validation and analysis of the computational tools, which has lead to several conclusions on the limitations of their aerodynamic prediction capabilities.

3. Development of a series of programs which generate surface grids for an axisymmetric projectile, as well as the various augmented shells used in this design study.

4. Investigation of the baseline aerodynamic characteristics for a standard projectile configuration over the Mach range of a typical ballistic trajectory.

5. Analysis of two asymmetric projectile configurations based on predicted static coefficients and flow field results.

6. Derivation of a suitable design metric used for comparison of the various augmented projectile concepts, which is based on the angular motion of spinning shells under trim forces and moments.

7. Evaluation of a series of possible aero-torque generating features (strakes), which could be suitable for trim force roll control.

8. Assessment of the sensitivity of Magnus forces and moments to the various projectile augmentations.

9. Generation and analysis of several additional asymmetric projectile designs, which demonstrate substantially improved aerodynamic performance.

Chapter 2

Computational Approach

The purpose of this chapter is to indicate the precise computational framework and tools which have been used for this study. Two completely separate formulations have been implemented, each with different assumptions and limitations. The most rigorous description of continuum mechanics comes in the form of the Navier-Stokes equations, a completely non-linear, coupled set of equations incorporating conservation of mass, momentum, and energy. All computational fluid dynamic subsets of these equations use various assumptions or approximations in order to create a tractable set of equations which can be discretized and solved using a stable integration scheme. Section 2.1 of this chapter outlines the various subsets of the Navier-Stokes equations relevant to this study. An attempt is also made in Section 2.2 to establish the computational requirements necessary to complete the investigation of the aerodynamics of projectiles in a typical flight profile.

Most of the time spent on this project has been focused on the development of a complete set of computational tools for aerodynamic design analysis. Section 2.3 of this chapter discusses the specific components used in this investigation. Along with the formulation of the continuum equations mentioned above, the other distinguishing factor that separates the different simulation tools is the method of flow field discretization. There are many established schemes for grid generation which follow from these specific discretizations and the two codes initially used for this study fall at opposite ends of the gridding spectrum. Section 2.3 outlines these differences in addition to discussing the other tools developed to analyze the raw data produced by the flow solver codes.

2.1 Basic Framework

The computation of the flow fields around the projectile configurations was accomplished by performing simulations using the structured, thin-layer, Navier-Stokes solver OVERFLOW [5] as well as the unstructured, Euler (inviscid) solver FELISA [28]. The severe modeling differences between these two codes seem to demand some explanation of the link that exists in the formulation of their basic equations. This section aims to provide an overview of computational fluid dynamics modeling with the Navier-Stokes equations and subsets, including Reynolds averaged, thin-layer (TLNS), parabolized (PNS), and Euler formulations. The limitations of the assumptions made at each level are noted, in order to provide the proper framework for the results obtained with each code. The discussion has primarily been distilled from Hirsch [13].

2.1.1 Navier-Stokes Equations

The fundamental laws of fluid dynamics are that the properties of mass, momentum and energy are conserved during the evolution of a fluid. The most general description of these conservative laws comes from the full system of Navier-Stokes equations. This system can be written in a relatively compact form for the basic quantities ρ, $\rho\vec{v}$, and ρE as

$$\frac{\partial}{\partial t}\begin{vmatrix} \rho \\ \rho\vec{v} \\ \rho E \end{vmatrix} + \vec{\nabla}\cdot\begin{vmatrix} \rho\vec{v} \\ \rho\vec{v}\otimes\vec{v} + p\overline{\overline{I}} - \overline{\overline{\tau}} \\ \rho\vec{v}H - \overline{\overline{\tau}}\cdot vecv - k\vec{\nabla}T \end{vmatrix} = \begin{vmatrix} 0 \\ \rho\vec{f_e} \\ W_f + q_H \end{vmatrix} \tag{2.1}$$

where $\overline{\overline{I}}$ is the unit tensor, $\overline{\overline{\tau}}$ is the viscous shear stress tensor, H is the total enthalpy, k is the coefficient of thermal conductivity, T is the temperature, $\vec{f_e}$ are the external volume forces, W_f is the work performed by the external forces and q_H are the heat sources. The constitutive equation of state relates pressure to the other flow variables

$$p = (\gamma - 1)\left(e - \frac{1}{2}\rho\left(u^2 + v^2\right)\right) \tag{2.2}$$

where e is the specific energy and for newtonian fluids, the viscous shear stresses and the thermal conductivity are written in terms of the Reynolds number Re, dynamic viscosity μ, the Prandtl number Pr and the ratio of specific heats γ.

This system of equations, supplemented by empirical laws for the dependence of viscosity and thermal conductivity on other flow variables, completely describe all flow phenomena. Fortunately for computational fluid dynamicists, whose research rely on the intractability of these equations, an insidious form of instability called *turbulence* exists in most natural flow situations which is characterized by statistical fluctuations in all flow quantities. The complete numerical description of these fluctuations is outside the present level of computational power for most relevant flow problems, making successive approximations of the Navier-Stokes equations the only viable option for fluid flow prediction. These levels of approximations come at a huge range of complexity and computational cost. Proper choice of a flow simulation scheme, for a particular flow problem and required level of accuracy, is perhaps the most demanding aspect of using computational fluid dynamics. The differences, weaknesses, and strengths of each of these schemes is outlined in the following sections, in hopes of supplying the basis from which the computational tools in this study were chosen.

2.1.2 Reynolds-Averaged Approximation

One of the highest levels of approximation is the Reynolds-Averaged Navier Stokes equations. The influence of the *mean* turbulent quantities in Equation 2.1 is obtained by a time averaging process which attempts to preserve the time-dependent flow phenomena which occur at time scales different from the turbulence. In this formulation the turbulent mean momentum is composed of an *average* viscous shear stress as well as a component dependent on the interaction between the turbulent velocity fluctuations and the main flow, called the Reynolds stress.

$$\bar{\bar{\tau}} = -\overline{\rho \vec{v}'' \otimes \vec{v}''} \tag{2.3}$$

In this equation $\vec{v}''$ represents the turbulent fluctuating velocity vector. The relationship between the mean flow quantities and the Reynolds stress is unknown, making the system of equations intractable without further modeling based on theoretical assumptions and empirical data. The difficulty, at this level, is choosing the most accurate turbulence model for the specific flow situation. Typical models are Baldwin-Lomax [2], Baldwin-Barth [1], and the two equation k-ϵ model; each with varying degrees of complexity and computational difficulty. Validation of these turbulence models, for the particular flow problem of interest, is essential to accurate modeling and closure of the equations.

2.1.3 Thin-Layer Approximations

The next level of approximation deals with high Reynolds number viscous flows, which tend to have the influence of viscosity dominated by gradients normal to the main flow direction. The thin-layer approximation (TLNS) of the Navier-Stokes equations follows from neglecting all derivatives in the turbulent and viscous shear stress terms of Equation 2.1 transverse to the local surface orientation. The approximation amounts to neglecting the viscous diffusion which occurs in a direction parallel to the local boundary surface, while maintaining contributions in the normal direction. This approximation does not affect the general form of the conservation equations and is made in the interest of computational efficiency. In TLNS simulations grid points can be concentrated normal to the surface allowing the more substantial viscous terms to be resolved. The TLNS approximation is valid for high Reynolds number attached and mildly separated flows.

2.1.4 Parabolized Approximations

The parabolized Navier-Stokes (PNS) approximation is based on the same kind of flow arguments as the TLNS approximation but applies only to the steady state formulation of the Navier-Stokes equations. It is developed to handle flow situations that have a predominant main flow direction, with cross-flow velocity components of a substantially lower order of magnitude. Viscous regions along body surfaces are assumed to be dominated by normal gradients, allowing the streamwise diffusion of momentum and energy to be neglected. The PNS approximation represents a significant departure from the general form of the Navier-Stokes equations. The approximations change the character of the mainstream flow equations from elliptic to parabolic. Due to this change, the numerical methods for solving the PNS approximation over a discretized flow field vary significantly from those used for TLNS approximations. Solutions to the equations can be obtained by advancing in the direction of the main flow and solving an elliptic problem in each discretized cross section. The directional nature of the space-marching PNS approximation makes it suitable for supersonic flows, where disturbances propagate only downstream. The approximation breaks down completely in regions of reverse flow of the streamwise velocity, which can occur over areas of sharp geometry changes or large flow gradients.

2.1.5 Euler Equations

A wide array of inviscid formulations marks the final plateau in the succession of approximations to Equation 2.1. These models neglect all shear stresses and heat conduction terms in the Navier-Stokes equations. While this approximation may seem too drastic to model real flows, inviscid models are valid for high Reynolds numbers where the influence of viscous phenomena is extremely small. High Mach number flows can be accurately modeled with full consideration for compressible effects. The Euler equations are the most general and popular form of the five equation system for inviscid flow. They represent a considerable simplification to Equation 2.1, normally requiring far less computational power and effort. The large decrease in complexity and cost is what makes the Euler equations so attractive for modeling flow problems where estimations are needed in relatively viscous-free situations.

The Euler approximation changes the mathematical form of the basic flow equations, with respect to the previous viscous models. The system of partial differential equations reduces from second order to first order, thus fundamentally changing the numerical computation of these flows. The number of allowable boundary conditions is reduced and the equations become hyperbolic in time. Despite the absence of viscosity, entropy variations in directions normal to the local velocity, such as shock wave phenomena, will generate vorticity; and inversely, vorticity will create entropy variations. Large flow field gradients, resulting from shocks or surface discontinuities, are allowed by the Euler equations but the stability of the numerical discretization, without the dampening effects of viscosity, must be closely considered. Most Euler schemes introduce a form of artificial viscosity into the calculation which stabilizes the flow solution in the presence of severe gradients, but still allow shock surfaces to be accurately resolved. The method of stabilizing the equations is what separates the proper treatment of the Euler equations from schemes which are poor modeling tools.

2.2 Simulation Requirements

Proper identification of simulation requirements for a particular flow problem is absolutely crucial for effective computational modeling. Given the large number of computational schemes and levels of approximation, an important job of the researcher is to properly match

his requirements with the strengths of each simulation tool. Characteristics contained in these requirements include not only the relevant flow regimes and particular flight points, but also the level of desired computational cost, the basic quantities needed to be calculated, and the required level of precision. Questions must also be addressed about the complexity of the particular surface geometry, and the availability of grid generating tools for proper discretization of the flow field. It is often difficult to make *a priori* decisions regarding these questions, since detailed simulation is often required to ascertain what the important flow features and phenomena will be. This computational Catch-22 can only be resolved by attempting to validate the simulation tools for flow problems closely related to the unknown situation. The first step in this validation process is to carefully access the relevant questions needed to be answered by the simulation, and then produce a basic list of requirements to answer these questions.

The most difficult aspect to this particular fluid flow problem is the range of Mach numbers which occur within the flight envelope of a standard ordnance projectile. The projectile is initially launched at a Mach number of approximately 2.5, well within the supersonic regime, but then subsequently loses a significant portion of its speed, cruising at around 0.90 for a large period of the flight. This Mach range stretches the limits of present day computational simulations, since it requires predictions within the transonic flight regime. Transonic flight is characterized by an extreme sensitivity, of all flow quantities present in the conservative equations, to particular surface features and flight speed. Radical changes occur in the structure and position of shock waves even for simple geometries, making complex bodies very difficult to model. Projectile and airplane dynamicists are well acquainted with the large changes in most force and moment coefficients which occur in passing through the Mach 1 barrier. For simulations within the flight profile of ordnance projectiles, it was absolutely necessary to make use of a computational scheme that properly modeled transonic compressibility effects. This conclusion negated the use of panel methods or other potential equation schemes, requiring at a minimum one of the flow field discretization schemes mentioned in Section 2.1.

The next basic requirement for this projectile study dealt with the aerodynamic quantities necessary for accurate evaluation of the different asymmetric shell designs. At a minimum the simulation tool needed to accurately calculate the drag, normal forces, and pitching moment generated by the experimental shells. The initial validation of the com-

putational tools focused on their ability to make accurate predictions of these basic static coefficients. In addition, due to the abnormal geometries of the experimental shells, shock positions on the surface needed to be reasonably modeled, so that subtle changes in the fuze designs could be examined. Confirmation was also required that the computational schemes predicted, with relatively high precision, the variations of aerodynamic coefficients due to changes in the angle of attack. These requirements facilitated not only the choice of simulation tools necessary for the study, but in addition the analysis tools and post-simulation data that should be available in order to make a reasonable evaluation of the designs.

The final requirement of the simulation tools was concerned with the relative importance of viscous effects and secondary flow features in the design evaluation process. Initially, it was uncertain how prominently changes in the boundary layer and turbulent quantities would affect the prediction of the asymmetric shell's control capabilities. Two different simulation codes were developed in parallel in order to assess the level of simulation complexity required for the study. The ability to make use of an inviscid formulation has the potential to greatly diminish the computational power and time required for each simulation. Since this study dealt mostly with a parametric investigation, in which the relative effectiveness of many designs would be tested, it was initially decided that an inviscid Euler code could provide reasonable prediction capabilities. The Navier-Stokes code could then be used only for a more complete and accurate investigation of a few candidate designs.

The lack of viscous modeling in the simulations meant neglecting the relative boundary layer growth due to the fuze distortions. Several possible consequences for this secondary flow effect were considered.

1. Separation of the flow due to *adverse* pressure gradients along the surface of the projectile.

2. Shock wave-boundary layer interaction in regions of high surface gradients.

3. Control blanking, in which the growth of the boundary layer greatly impairs the efficiency of the control surfaces.

4. A change in the *Magnus-type* force, which has been strongly linked to boundary layer thickness [19, 17].

Of these four concerns, the first two were the initial focus of attention since they directly

affected predictions of the static aerodynamic coefficients. The surface finishes of most ordnance projectiles are designed to enhance the transition to turbulence, therefore a turbulent boundary layer was assumed to fall over the entire shell profile. Turbulent boundary layers are more resistant to separation from adverse pressure gradients. This fact cast some uncertainty on how significant surface discontinuities would have to be for separation to be induced, either due to shock wave interaction or the basic acceleration of the flow around severe surface slope changes. An additional problem was that the absence of viscous effects, specifically reflected in the lack of a *no-slip condition* at the surface, could have significant influences on the position of shocks along the projectile. It was decided to develop the two codes in parallel to account for these possible discrepancies, in the event that results showed a significant dependence on viscous effects.

The initial reason for developing the Navier-Stokes code OVERFLOW, was to attempt to make predictions about Magnus forces and moments. Magnus effects result from a spin induced distortion of the viscous boundary layer, which exists on a spinning shell at angle of attack. This prediction requires a significant amount of work, since Magnus forces are commonly one-tenth to one-hundredth of the magnitude of static forces, and require implementation of a spinning surface boundary condition. The predictions may be important though, since studies have shown significant variations in Magnus effects on projectiles with different nose-cap or fuze shapes [14]. This result can be explained by the fact that the fuze surface influences the pressure distribution on the front of the shell, which affects the growth and propagation of the boundary layer downstream. Studies have shown that Magnus effects are sensitive to boundary layer thickness, therefore they should also be sensitive to fuze shapes and other surface features upstream. The degree of sensitivity to a particular surface geometry distortion is the question of interest in this case.

Fortunately, experimental results have shown that the static coefficients, normal force and pitch moment, are only very weakly dependent on the spinning shell boundary condition [24], therefore the specific requirements for evaluation of the fixed-trim designs can be met in a more simplified manner. Capturing spinning boundary effects require a full three-dimensional projectile geometry, due to boundary layer asymmetries, but static coefficients can be predicted using a mirror symmetry boundary condition. This simplification halves the number of grid points necessary for each simulation, reducing the computational time in the same manner. This simplification has been used in nearly all predictions of the

static coefficients, and has additionally been justified by comparisons between full-grid and half-grid simulations.

All the questions mentioned above about the requirements for computational simulation capabilities have resulted in the development of two separate codes for this investigation. This project has proven to be an excellent case study on the decision techniques employed in CFD validation for a specific flow problem. There are a vast array of codes available for conducting aerodynamic analysis, each with various approximate schemes and levels of computational cost. The simulation complexity necessary for accurate engineering analysis is a very difficult question to answer without prior information on the essential flow features. While there is an abundance of work completed on CFD simulations of projectile aerodynamics, the differences resulting from the asymmetric fuze designs created enough uncertainty to require a lot of conservatism with respect to code choice. The next section is dedicated to discussing the specific computational tools and components for this investigation, including a brief look at the full solution process.

2.3 Computational Tools

Computational fluid dynamics provides a great measure of versatility and usefulness because it allows complicated flow problems to be investigated without costly wind tunnel studies. The development of an integrated design package is a difficult task which requires a great deal of initial investment of time to realize any reward. The basic solution process can be broken down into several important categories.

1. Geometry Specification and Decomposition
2. Surface and Volume Grid Generation (Discretization)
3. Fluid Flow Computation
4. Solution Post-Processing and Analysis

The full implementation of this sequence of steps involves considerable adaptation, so a series of feedback loops can occur throughout the process as errors are recognized and fixed. Work done on the actual flow solution is actually only a small aspect of the development. This can be the source of much consternation on the part of individuals wishing to implement

CFD simulations, since there is a significant lag time from initialization of the problem to the recovery of any seemingly useful information.

The particular choice of a flow solver for computation practically dictates all other aspects of the solution process. In this study, two different codes, FELISA and OVERFLOW, have been developed for use in the projectile aerodynamics investigation. Each code, due to its different structure and requirements, has a distinct solution methodology. The following subsections provide the essential features of each code, in light of the discussion given in Section 2.1, and with regard to the importance each code has on the steps in the solution process.

2.3.1 The Inviscid Code: FELISA

The FELISA code is a research Euler flow solver which uses unstructured, adaptable mesh generation. It has been developed by Professor Peraire of the Aero/Astro department of M.I.T. for the simulation of 3-D inviscid flows around complex geometrical bodies. FELISA has been developed as a complete flow solution package; incorporating mesh generation, flow solution, adaption, and post-processing into several main modules. The modules are run independently, with interaction taking place through input and output files, and consist of the following:

- SURFACE: a surface triangulator
- VOLUME: a three-dimensional volume generator
- PREPRO: a flow solver pre-processor
- SOLVE: an unstructured mesh Euler flow solver
- REMESH: an adaptive remeshing procedure
- XPLT: for mesh geometry and flow visualization

The geometry specification and decomposition process for FELISA comes in the form of two input files; the geometry definition and the background source file. The geometric description consists of a large series of points defining composite curves and surfaces, similar in style to CAD systems, which completely describe the model's outer boundary. The geometry of the various projectiles is broken up into easily described surface pieces. The

connectivity and orientation of each individual surface region is also defined in the geometry definition, resulting in a structure which allows extreme ease in the inclusion of additional geometric features or objects. The background file is a user defined spatial distribution of sources which dictate node spacing within the final volume mesh. This localized scheme allows intricate surface features, such as the projectile strakes, to be well resolved; without severely altering the node density throughout the domain.

The main feature, which sets FELISA apart from other Euler solvers, lies in its unstructured surface and volume grid generation. The technique is based on a variant of the 2-D advancing front method [18], extended to three dimensions [27], which allows considerable flexibility in the level of complexity of the discretized surfaces. Information for the surface grid is taken from the geometry and background description; and then a complete surface mesh is generated by an algorithm which attempts to optimize the placement, relative orientation, and number of nodal points. The resultant triangulated surface is used to produce a 3-D volume grid, which consists of a mesh of tetrahedral elements that completely describe the physical domain. Examples of several unstructured surface grids generated by the FELISA system are shown in Figure 2-1. There is a severe overhead using an unstructured gridding system, since more information about the connectivity, position, and orientation of each node relative to its local neighboring nodes must be stored. Despite this overhead, unstructured generators allow for the gridding of extremely complex surfaces with local resolution of important geometric features.

The basic structure of the Euler flow algorithm is a variational formulation using a Galerkin finite element method, with central difference approximations to derivative operators. The steady state solution is found by advancing the system using an explicit Runge-Kutta time marching scheme. Artificial viscosity is included in the scheme with the purpose of stabilizing the solution without deteriorating the overall accuracy. Since the code was not developed to model transient flow, several techniques have been implemented to improve convergence including mass lumping, local time-stepping, and residual smoothing. In addition to these techniques, a novel and extremely efficient data structure has been used, resulting in a solver which is optimized in terms of computational performance and resources.

The post-processing module (XPLT) for FELISA allows for geometry, flow, and mesh visualization. XPLT is able to organize the output system files and display the interpolated

geometry of the body; iso-contours on the surface such as density, pressure, and Mach number; as well as velocity vectors of the flow. Aerodynamic quantities such as lift, drag, and pitching moment can be computed over the entire body or on individual sections. XPLT is a relatively simple flow visualization program, which can be easily modified to suit the specific needs of the analysis. Filter programs have also been written for use with the more general and robust visualization program VISUAL3 [12]. These two codes allow for a considerable level of post-processing information detailing flow field, surface, and edge distributions of all relevant flow quantities.

In general, FELISA is a highly flexible code which can be run on several different computer systems. Its benefits lie in its speed, gridding capabilities, and ease of use. FELISA's modular nature makes it particularly useful for adapting flow solutions using a more highly resolved nodal mesh. Although the remeshing capabilities were not used for this investigation, FELISA includes a module (REMESH) designed specifically to adapt the volume grid using initial flow solutions. Since the focus of this study was on many different surface designs, the adaption process proved to be too time consuming given the design requirements. The limitations for using FELISA lie in its inviscid approximations, but in situations where boundary layer effects are not prominent it is a very effective simulation tool.

2.3.2 The Viscous Code: OVERFLOW

The OVERFLOW code is a production-level structured Navier-Stokes flow solver that has been developed by researchers in the Aeronautical Technologies Division, NASA Ames Research Center. OVERFLOW has been in use for many years with a long heritage of successful flow solutions from an evolution of past schemes. The solver algorithm incorporates a finite-difference formulation of the basic flow equations. In the hierarchy of Navier-Stokes subsets, OVERFLOW incorporates Reynolds averaging and thin-layer approximations to viscous derivatives. It has a wide variety of turbulence models which can be implemented depending on the flow problem including the one equation Baldwin-Barth, one equation Spalart-Allmaras, Baldwin-Lomax algebraic, and two equation k-ϵ models. The specific turbulence model as well as boundary conditions, flow parameters, and numerical settings are all inputted in a namelist file format. The set of parameters and different conditions available for a flow simulation is considerable and requires significant pre-planning.

Unlike the Euler code FELISA, OVERFLOW was designed to facilitate only the flow

simulation step in the solution process. It relies on additional software packages to perform the other necessary tasks, which requires a high degree of standardization with respect to grid and flow field file formats. All solution and grid definitions are specified in the PLOT3D file format [6]. Structured surface grids, in this format, can be generated by many commercially available programs such as GRIDGEN or ICEM-CFD. For this study, specific codes were written to perform the necessary gridding routines. An array of programs now exists to generate the specific fuze augmentations on a standard axisymmetric projectile such as bending, slicing, and the inclusion of additional surface features.

OVERFLOW is part of a collection of overset (Chimera), structured grid CFD software programs developed at NASA Ames. This capability allows complex geometries, ordinarily impossible to grid in a structured format, to be split up and defined in specific, much simpler sections. The other programs which facilitate the Chimera gridding scheme are Collar Grid Tools [26], a grid manipulation and surface grid generation package; and PEGSUS [34], a boundary interpolation code which calculates the connectivity between the different grids. Unstructured codes were developed largely to address the difficulty of generating structured grids for complex bodies, but the Chimera gridding scheme solves these difficult gridding problems while still maintaining the same relative speed and computational power requirements. The final volume grid generation was accomplished using the hyperbolic grid generator HYPGEN [4], which takes the PLOT3D surface definition and *grows* a 3-D domain to a user-defined free stream outer boundary. Several structured grids, produced using these gridding software programs, are shown in Figure 2-2.

Post-processing for OVERFLOW simulation results was accomplished using several software packages. The NASA Ames software package FOMOCO [3] was used for calculating forces and moments on the overset grids. Programs were also developed to output pressure, Mach number, and force distributions; both within the flow field and over specific regions of the projectile. Since OVERFLOW is equipped to be run in a time accurate mode, outputs of residual and flow state histories are available. In addition to the actual calculation of various quantities, visualization of the flow field was performed by the VISUAL3 program.

The OVERFLOW simulation package is an amalgam of software codes and components for performing specific analysis functions. It has been developed in this style so that no one component is dependent on another, and various sets of tools can be placed together according to the specific simulation problem. The standardized PLOT3D format of the

grid and flow field files is widely used in many grid generation packages and visualization software, facilitating OVERFLOW's ease of usage. The code does suffer somewhat due to the complexity and overall number of the individual programs which comprise the complete system. Despite the difficulties, OVERFLOW is a mature, production level code, with a vast library of validation studies in flow regimes closely resembling the relevant features in this investigation.

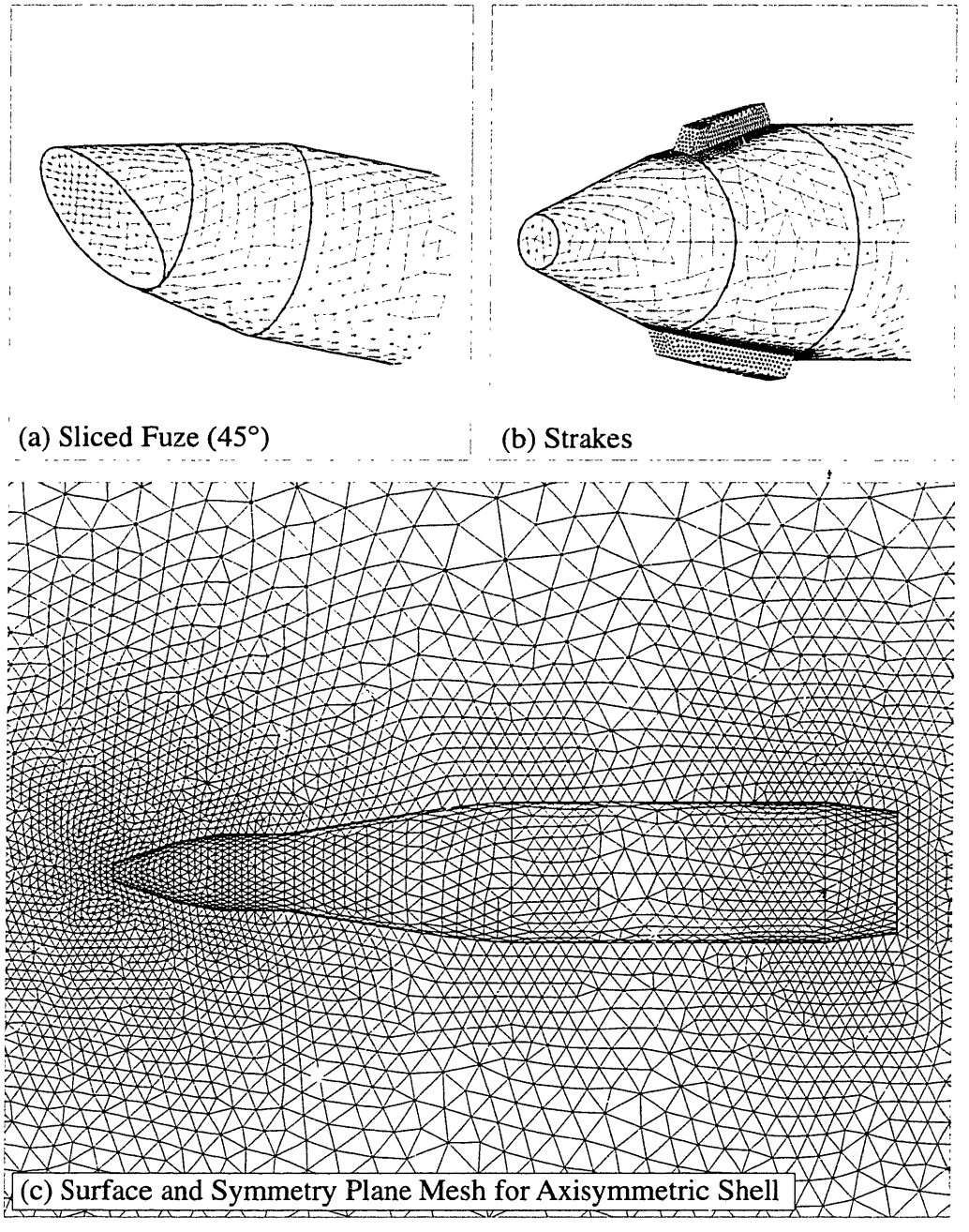

Figure 2-1: Examples of Unstructured Grids for FELISA

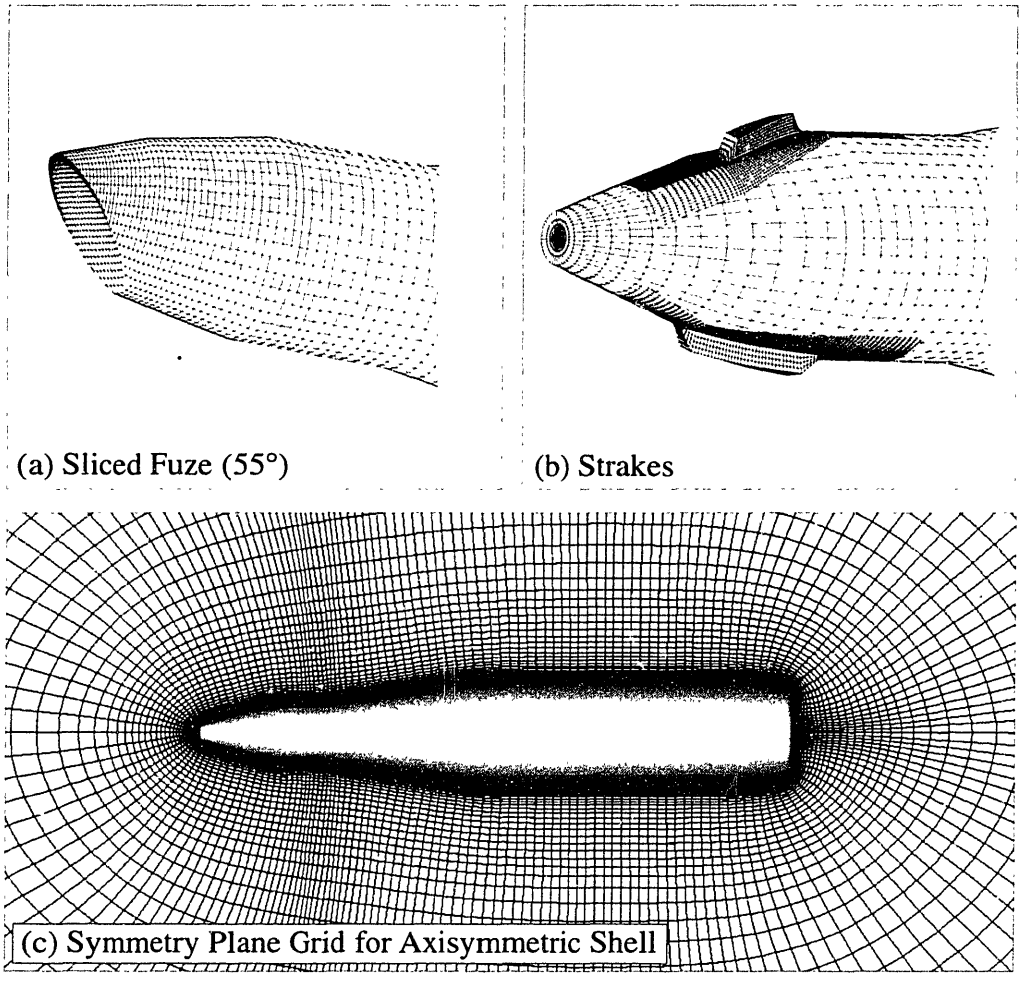

Figure 2-2: Examples of Structured Grids for OVERFLOW

Chapter 3

Computational Tool Analysis

The framework and unique features have now been discussed for the two codes used in this projectile investigation. Section 3.1 begins with the initial validation studies completed using the two codes, using experimental data taken from the literature. Comparisons have been made at various Mach numbers and angles of attack, using both longitudinal pressure distributions and integrated quantities. Justification for the choice of codes, based on their ability to predict nominal aerodynamic characteristics, was addressed prior to the evaluation of the various design augmentations. Section 3.1 ends with a brief validation study completed using the viscous code OVERFLOW for investigating Magnus effects. This capability, while not required for the initial phase of this design study, could provide useful information on the strengths and weaknesses of the two asymmetric projectile configurations.

Section 3.2 is devoted to a discussion of the relative merits of the two codes, with respect to providing useful information for this specific investigation. Although validation studies provide a *first cut* comparison of a code's abilities to accurately predict flow features of interest, it was essential in this study to compare actual predictions concerning the various projectile modifications. Results from the two main shell augmentations, the bent and sliced fuze designs, are used to properly assess the prediction characteristics of the two software packages. This discussion makes direct use of points outlined in Section 2.1 concerning the differences between Euler and Navier-Stokes formulations. Section 3.2 also presents some reasonable benchmarks for the two codes; based on speed of computation, memory requirements, and overall ease of usage. This evaluation is important, in addition to the

direct prediction accuracy, since computational resource requirements are a large factor in the decision process of researchers seeking to use CFD simulations.

3.1 Validation

Validation is an essential part of using computational tools for aerodynamic design. Comparisons with reliable experimental results can greatly enhance the effectiveness of using CFD simulations, since the ability of the code to model specific flow regimes can be addressed. This particular investigation provided a difficult flow problem because it required predictions in transonic Mach regions, where small perturbations can greatly affect the overall flow. Small geometry discrepancies and other modeling problems can produce severe errors in simulating the relevant pressures, velocities, and forces. Validation of the codes with projectiles similar in geometry to the baseline shell for this study, within the pertinent Mach envelope, was necessary to insure that proper flow modeling was being accomplished.

Numerous problems have been completed by both FELISA and OVERFLOW prior to this study, leaving some measure of confidence in the two codes' ability to accurately model some basic flow situations. This project's investigation into inherently uncommon grid configurations, though, required additional validation to be undertaken on geometries closely related to the deformed projectiles. The major sources of experimental results came from studies performed by both the Ballistics Research Lab (BRL) [32, 25], and the U.S. Naval Weapons Lab [7]. High quality wind tunnel or spark-range data is difficult to produce in the transonic Mach region, so validation data had to be procured from several different studies. Initial validation attempts with OVERFLOW and FELISA focused on simple comparisons of longitudinal pressure distributions at various Mach numbers. The final comparisons were set on the much more difficult task of computing integrated force and moment coefficient derivatives.

3.1.1 Pressure Distribution Comparisons

Studies by the Ballistic Research Lab were completed on the SOCBT (Secant-Ogive Cylinder with Boat Tail), which is shown in Figure 3-1. This projectile configuration has had numerous experimental and numerical studies performed on it. Pressure distributions along

the shell were calculated using both codes and comparisons were made at three flight points: (1) Mach 3.0 at 10.4° attack angle (2) Mach 1.1 at 4° and (3) Mach 0.91 at 2°. These three validation points are intended to push the prediction limits of the codes, since they represent both supersonic and transonic behavior, as well as angles of attack well in excess of normal flight conditions.

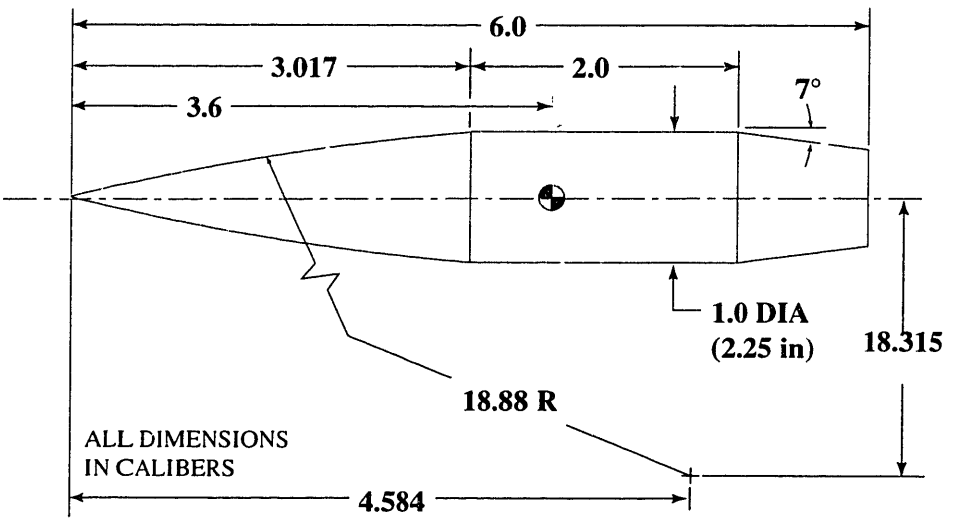

Figure 3-1: Geometry of the SOCBT Test Projectile

Comparisons for the Mach 3.0, $\alpha = 10.4°$, case are displayed in Figure 3-2. The OVERFLOW results are extremely accurate, predicting the severe jumps in the pressure distribution due to the shocks generated across the various shell surface regions with large slope changes. The boat tail region on the projectile is also well modeled by OVERFLOW, despite the extremely large angle of attack used in the comparison. The FELISA predictions are not as accurate, but despite the inviscid assumptions and high attack angle, the deviation is only severe in two regions. The strength of the shock at the surface transition from ogive to cylinder on the SOCBT is poorly predicted. This result could be improved greatly by FELISA's mesh adaption scheme, which models shocks more precisely by increasing the node density in that region, but since the adaption technique was too costly to be used in the design study it was decided to maintain that condition for the validation. The other region poorly modeled by FELISA is the projectile base, which is not surprising considering the flow conditions which exist in that region as well as the severe angle of attack of the shell. The base region is characterized by severe gradients in the flow velocity and pressure,

often leading to re-entry flow and other viscous phenomena. It was understood from the onset that this region would be poorly predicted given the inviscid assumptions used in FELISA.

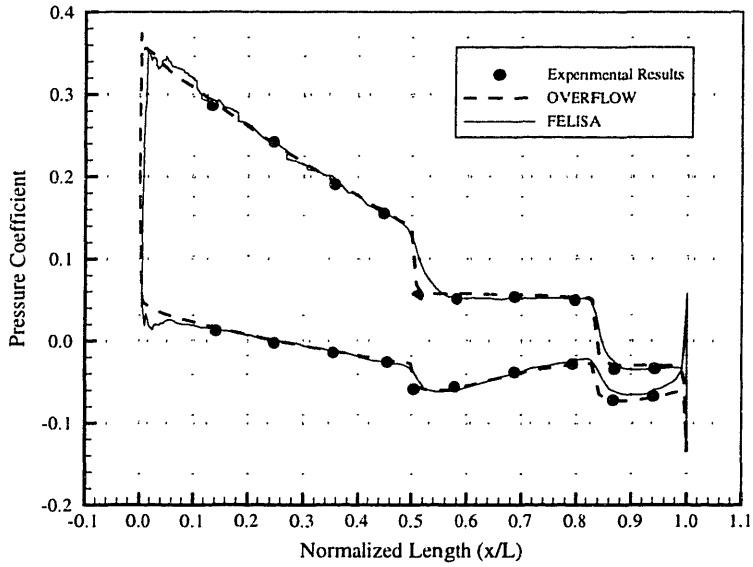

Figure 3-2: SOCBT Comparison at Mach 3.0, AOA = 10.4°

The next two validation cases are for flight conditions within the transonic flow regime. Figure 3-3 shows a pressure distribution comparison taken on the SOCBT at a Mach number of 1.1, $\alpha = 4°$. In this case the predictions of both OVERFLOW and FELISA closely match the wind tunnel data. The less severe angle of attack reduces the level of compressible-viscous interaction present in the flow, making the position and strength of the shock regions less dependent on the boundary layer. This leads to much better flow modeling using inviscid assumptions. The accurate comparisons using both codes at this angle of attack is important since the angle represents a reasonable upper-bound on a stable trajectory of an ordnance projectile.

The second transonic case, shown in Figure 3-4, was taken at Mach 0.91, $\alpha = 2°$. This Mach regime is quite challenging to make accurate comparisons within, since even slight surface geometry differences between the experimental and numerical model can lead to large changes in the pressure distribution. It is also extremely difficult to produce accurate experimental data in this region since wind tunnel walls and other artificial effects can have a drastic influence on the flow quantities. Despite these difficulties the validation

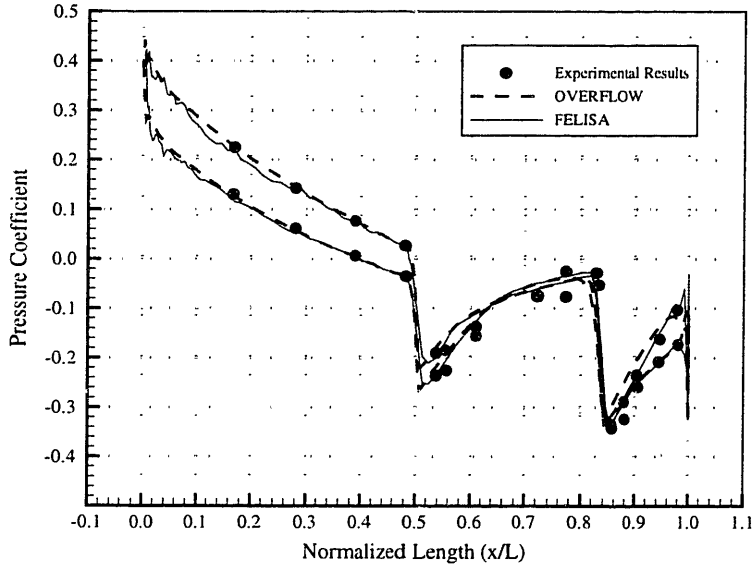

Figure 3-3: SOCBT Comparison at Mach 1.1, AOA = 4°

results produced using the two codes compare favorably with the wind tunnel data. Some irregularities exist between the experimental data and the numerical pressure coefficient predictions, but the character of the distributions is reasonably accurate. It is interesting to note that the inviscid predictions are consistent with the viscous results over the majority of the projectile surface.

The reasonable accuracy of the three pressure coefficient comparisons just outlined represent an initial confidence check confirming the usefulness and accuracy of both codes in modeling the flow around a standard projectile even in transonic conditions. The next validation sequence was completed in order to test the codes prediction capabilities with regard to actual force and moment coefficient derivatives. Computed results of coefficients represent a much more difficult step in validation because they require good pressure predictions at several angles of attack, and over the entire surface of the model. Since this design study is driven by predictions of normal force and pitch moment, as well as the drag coefficient, it is absolutely essential to make accurate predictions of these quantities.

3.1.2 Force and Moment Coefficient Comparisons

Investigations done by the Naval Weapons Lab on the 5-Inch/54 RAP (Rocket Assisted Projectile) provided measurements of drag, pitch moment derivative, and normal force

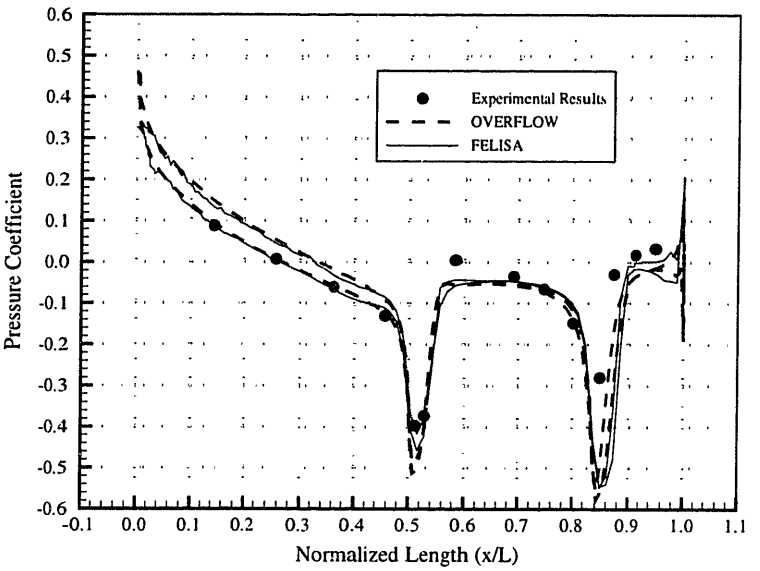

Figure 3-4: SOCBT Comparison at Mach 0.91, AOA = 2°

derivative; using both wind tunnel and spark range data at a wide range of Mach numbers. A computational investigation, to predict these basic aerodynamic derivatives, was completed on the 5-inch-54 shell using both codes. The drag coefficient comparison, shown in Figure 3-5, indicates good agreement with experiment over a substantial Mach range. FELISA slightly under-predicts the magnitude of the drag coefficient. This is reasonable since the inviscid assumptions used in the calculation exclude the presence of viscous, *skin friction* on the surface of the projectile. Estimates of the relative magnitude of the viscous component of the drag, calculated using OVERFLOW, ranged from 5-10% in the subsonic region, to 3-5% in the supersonic regime. These estimates account for the slightly lower values of drag predicted by FELISA in the specific Mach regions mentioned.

The quality of experimental data for the normal force and pitch moment coefficient derivatives of the 5-inch-54 projectile is poor, demonstrated by an extremely large spread in the measured results. This is not unexpected considering the difficulty obtaining experimental transonic measurements. Much of the data for this particular comparison was taken using spark-range data, where conditions at a specific Mach number are difficult to isolate and measure. The computed predictions and the experimental data for the normal force derivative are shown in Figure 3-6. Considering the rather imprecise nature of the experimental results, the numerical results compare very favorably in all of the flight conditions.

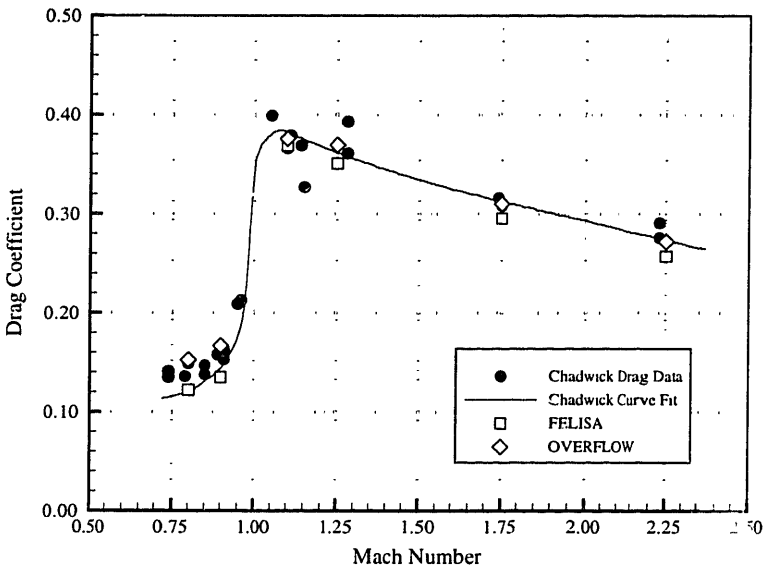

Figure 3-5: Drag Coefficient Comparisons for 5in54 RAP

The results from the two codes are consistent and closely follow the given experimental Chadwick curve fit.

The pitch moment derivative comparison, shown in Figure 3-7, also demonstrates that the simulations made by the two codes are capable of accurately predicting important static derivatives. The pitch moment derivative has a rather noteworthy and important feature in the transonic flight regime, shown by the large bump in the magnitude of the pitch slope. This pitch moment characteristic is seen in most ordnance projectiles which have a substantial boat tail. It is an important validation result that both codes captured the relative position of the peak of this derivative, which occurs for the 5in54 RAP at approximately Mach 0.92. This result is an excellent measure that flow solutions generated by both of the codes for nominal projectile geometries, in the transonic regime, have reasonable accuracy and validity.

Small discrepancies exist between the results from the two codes; but these differences were expected given the nature of the two flow solvers as stated previously in Section 2.3. Certain regions of the projectile, particularly the base of the shell, are definitely poorly modeled by FELISA. Base region flow is an extremely difficult area to model, even for a Navier-Stokes solver, making the necessity for highly resolved flow features in this region impractical in a design study of this nature. The predictions made using OVERFLOW are

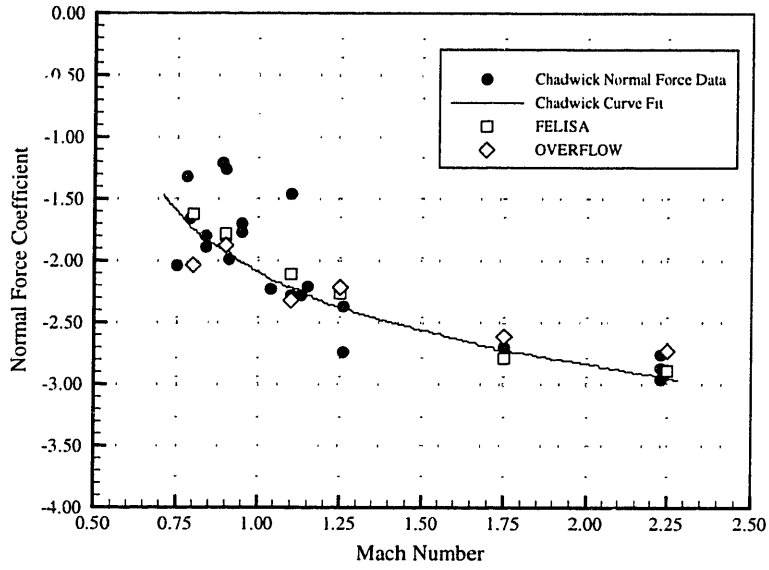

Figure 3-6: Normal Force Derivative Comparisons for 5in54 RAP

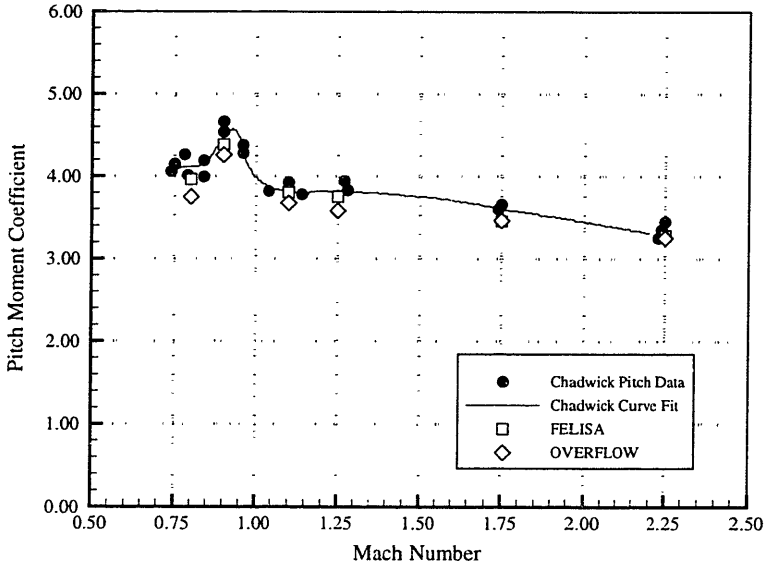

Figure 3-7: Pitch Moment Derivative Comparisons for 5in54 RAP

certainly more accurate within extreme flight conditions, however this design study is being conducted at reasonable angles of attack where the influence of viscous separation is not as great. Despite the limitations of the Euler code FELISA, knowledge of the poorly predicted features renders it a viable design tool.

In general, the basic validation studies confirmed that both codes provide good predictions of the coefficients of importance to the shell fuze design study. The comparisons were used to probe the weaknesses of the two codes due to their modeling assumptions, and in addition they served as a information source for subsequent grid and numerical parameter refinement. The validation studies were essential to insure the fidelity and accuracy of the two codes in the prediction of nominal flow characteristics for ordnance projectiles.

The next section outlines the validation study completed using the viscous code OVERFLOW on Magnus effects. This validation represents a brief departure from the comparisons between the two codes, but Magnus forces are a purely viscous phenomena requiring the use of a Navier-Stokes code for correct prediction. The investigation into the influence of the shell distortions on Magnus effects represents only a secondary issue in this design study, but it is an effect which should be accounted for when a candidate design has been reached using prior comparisons.

3.1.3 Magnus Validation

Validation of Magnus effects requires a very computationally costly series of simulations. Since Magnus forces and moments were considered only a secondary effect for this design study, evaluation of the Magnus effects for all the designs was not considered reasonable. Instead, it was decided to narrow the list of possible designs to a few candidate shapes, which would be investigated more fully using the viscous code OVERFLOW. Predictions of the Magnus forces and moments demanded several computational requirements; establishing a spinning boundary condition on the surface, increasing the grid resolution in the boundary layer, and implementing a full, 360° grid without the use of a time-saving, mirror symmetry grid. All three of these requirements caused increased complexity and overall cost for the simulations.

Numerical prediction of Magnus effects has been accomplished in recent years [31, 33, 24, 32]. These studies showed fairly good comparison with wind tunnel and spark range tests, but were mostly focused on supersonic flight conditions. It was understood at the outset

that good predictions in the transonic regime were difficult to perform, and even a relative comparison which showed the correct Magnus trends would be a significant accomplishment. Data from the Chadwick report was again utilized, since it contained information on the variation of Magnus moment with yaw angle. The Magnus moment is a very non-linear function of the angle of attack, demonstrating sign changes over a small range of yaw angles. Predictions at Mach 1.1 were attempted since it represented a flow regime on the border of transonic flight, and was also pertinent to the asymmetric projectile design study.

Figure 3-8 shows a comparison of the predictions made with OVERFLOW and two sources of experimental data from range testing and wind tunnel. The ballistic range data is considered accurate for very small angles of attack less than 1°, while the wind tunnel data was taken over larger angles. The important points to notice in this comparison are that OVERFLOW predicts the correct sign for all angles tested, and the correct magnitude for all but the most extreme angle conditions. Angles of attack greater than 10° are extremely difficult to make predictions about even for static derivatives, because of the presence of severe viscous effects and vorticity development on the leeward side of the shell. The predictions made using OVERFLOW compare quite favorably over a reasonable range of angles. The ability to accurately predict trends in Magnus moment adds an important extra dimension to the prediction capabilities available for this study.

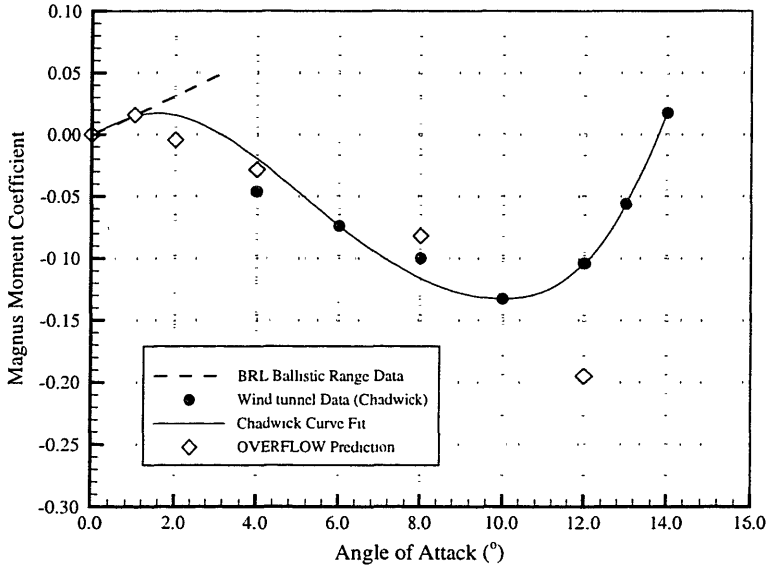

Figure 3-8: Magnus Moment Coefficient Comparisons for 5in54 RAP

The validation study on Magnus effects is the final step in the evaluation of the nominal prediction capabilities for the computational tools used in this aerodynamics investigation. The next section discusses a more indepth evaluation of the two codes used in this study, based on simulation data taken from the two design concepts. This evaluation is of paramount importance to the remainder of the augmented fuze investigation since it establishes a clear limitation on the usage of the inviscid Euler code for the specific analysis goals of this study.

3.2 Inviscid vs. Viscous Code Discussion

The results shown in Section 3.1 for the different validation attempts on standard projectile configurations demonstrated that both OVERFLOW and FELISA had adequate prediction capabilities. The experimental results were taken from Mach regions indicative of a typical projectile flight path, and the angle of attack ranges actually far exceeded normal conditions. The initial assessment of the two codes was that each could perform the design study in question; providing reasonable predictions of the aerodynamic qualities of non-axisymmetric fuze designs. This litmus test, concerning the code's prediction capabilities, is the first, essential requirement for an effective computational analysis tool. It was also necessary to compare other distinguishing qualities of the two codes in order to make a proper decision on which software to implement for this design study.

In Section 2.3, the basic steps in the solution process for implementing computational analysis tools were outlined. An evaluation of the two codes, with respect to the four steps mentioned, was completed resulting in these basic characteristics:

- Inviscid Code: FELISA
  - Complete Integrated Solution Package
  - Flexible Mesh Generation
  - Memory Intensive due to Unstructured Format
  - Simple, Unpolished Post-Processing
- Viscous Code: OVERFLOW
  - Supported by Additional Software

- Complicated Mesh Generation
- Cumbersome Input Parameter List
- Standardized File Format
- Extensive Validation Library

Naturally, this list of the characteristics should be considered along with the basic weaknesses and limitations concerning the two flow formulations. Section 2.1 has already detailed the approximations to the Navier-Stokes equations leading to the Euler equations. These approximations, while possibly neglecting significant flow features, greatly simplify not only the flow equations, but also the computational schemes necessary to effectively solve the equations. There are certainly weaknesses associated with using an inviscid formulation, which have been seen in the validation results in Section 3.1; but often the simplicity of inviscid tools outweighs the benefits of viscous predictions.

The effective modeling of the boundary layer, using a viscous code, requires a significant number of node points to be placed extremely close to the object's surface. This greatly increases the overall size of the discretized, computational domain, leading to higher computer resource and time requirements. For this study, nearly 500,000 grid points were required for a projectile simulation using the viscous code OVERFLOW, while the same shell decomposed using the inviscid grids from FELISA was only 100,000 nodes. The more informative metric for a proper assessment is the relative time required by each of the two codes to produce a single prediction point on the same speed computer. OVERFLOW required nearly twice the time for each flow computation as the inviscid code FELISA. This is not unexpected considering the significant complexity difference between the two codes and the equations they are solving.

3.2.1 Sliced Projectile Comparisons

The nominal prediction capabilities of the two codes, as presented in Section 3.1, were reasonably similar; therefore the initial decision was to implement the inviscid code FELISA for the asymmetric projectile investigation. FELISA was used to compare the various shell designs, in order to assess the relative merits of each concept, since a large parameterization study would require significantly more time to complete using the viscous code. The capability to produce viscous, structured grids for the two guidance concepts was also

undertaken. The plan was to complete the design parameterization using FELISA, and then perform more elaborate simulations on several candidate shapes using OVERFLOW. Magnus validation attempts, presented in Section 3.1.3, suggested that predictions could be made using OVERFLOW on the relative effects of the fuze distortions on Magnus forces and moments. This was deemed a secondary prediction capability, though, since evaluation of various fuze configurations was being completed based solely on static coefficients.

Initial simulations of the sliced fuze concept were completed with FELISA on the CMATD projectile, an experimental shell configuration similar in geometry to Mk64 NATO standard shell, which was designed by the Draper laboratory. This baseline projectile was the initial focus for the design study and a complete analysis of the shell is given in Appendix A. Following a fairly extensive study using FELISA on the CMATD with a sliced configuration, initial results completed using OVERFLOW showed radically different aerodynamic behavior from the inviscid predictions. While this result was a bit disappointing, given the time assessed to the parameterized study, it highlighted several interesting flow characteristics of the asymmetric projectiles.

In Section 2.2 a list of possible consequences for neglecting viscous effects in the design study was outlined. It was assumed early in the investigation that the presence of a fully turbulent boundary layer over the shell surface would perhaps reduce the probability of flow separation due to the fuze distortions. An additional assumption was that any shock wave-boundary layer interaction would be a localized phenomena, making relative comparisons between the different designs still a reasonable pursuit. The strength or weakness of the compressible-viscous interaction is largely determined by the amount of feedback between the boundary layer and the impinging shock wave. The large pressure rise in the presence of a compression shock creates a large adverse pressure gradient in the boundary layer, which is felt upstream through the subsonic flow in the viscous layer. Flow separation can occur depending on the intensity of the shock wave, and the thickness of the boundary layer. In regions of large boundary layer growth, due to sharp surface gradients, a bubble of re-entry flow might occur under very severe conditions. Once the flow has separated from the surface, the tendency is for the flow to reattach itself, but the resulting *dead zone* on the surface can cause abrupt changes in the pressure distribution and in the integrated forces.

The inviscid solutions proposed for the design study take none of these interactions into account, since they completely neglect all viscous terms in the flow equations of motion.

Despite these problems, the computational cost for performing Navier-Stokes computations with OVERFLOW seemed prohibitive, given the number of possible designs and flight points planned for in the study. It was hoped that the viscous effects would be sufficiently small to allow inviscid simulations to provide useful information. While it was realized that the exact flow physics would probably not be accounted for by FELISA, relative strengths of the different designs could perhaps be taken from the predictions. This of course assumed that the change in the different design parameters would not significantly alter the influence of viscous effects in the static coefficients.

The assumption made above concerning the relative unimportance of viscous effects as well as the usefulness of completing inviscid calculations using FELISA for the design study were proven to be absolutely unfounded. This conclusion was reached after a design sequence was completed on the sliced CMATD projectile, and then later verified for the bent shell design as well. While no directly useful information for the design study was produced by the FELISA/OVERFLOW comparisons for the two design concepts, the reasons for the failure of the inviscid predictions are an interesting case study on the various discrepancies that exist between the two flow solver formulations. In addition, the simulations taken at Mach 1.1 provide almost classic examples of shock wave-viscous interaction, influencing not only the local pressure distribution, but also dominating the integrated aerodynamic quantities as well.

The longitudinal pressure distribution predictions from both codes for the sliced CMATD projectile at Mach 1.1 are displayed in Figure 3-9. In this case the fuze is sliced at 50 degrees and the pivot point is 3.737 inches from the original nose. OVERFLOW predicts a severe flow separation region just aft of the slice surface, which is a dominant effect in the transonic regime for this particular design. Although FELISA predicts the strong loss of pressure due to the acceleration of the flow around the slice corner, the lack of boundary layer and viscous forces in the equations of motion inevitably fail to account for the fact that real flows will stall under such severe adverse pressure gradients. It was clear from these results that FELISA was incapable of completing the design study. Viscous effects were far too dominant in the transonic Mach regime for accurate evaluation with an inviscid code. It was decided that OVERFLOW would be used for the rest of the design study, since at least some of the projectile distortions, in some of the flow regimes, required accurate modeling of boundary layer effects.

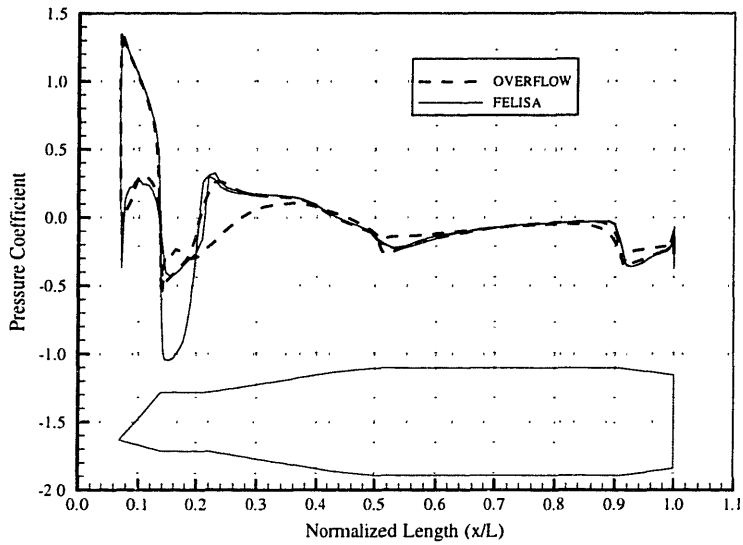

Figure 3-9: Transonic Slice Pressure Distribution Comparison

In an effort to explore when the influence of viscous effects could be neglected for accurate, aerodynamic predictions, further tests were completed using FELISA to investigate flow regions where viscous forces would not dominant. Figure 3-10 shows the longitudinal pressure distribution taken along the same sliced projectile at a Mach number of 2.5. For this case FELISA and OVERFLOW predict very similar pressure distributions on the projectile surface. In this flight regime, compressible effects dominate the propagation of the flow over the shell body. Flow separation, which was seen in the transonic case, is not seen at this high Mach number since the inertia of the main flow is so much greater. The position of the shock coming off the slice is also well predicted by FELISA, which can be seen from the similar pressure drop aft of the slice corner in the recovery region of the flow.

These conclusions can also be illustrated with Figure 3-11 which shows the Mach contour maps on the symmetry plane of the sliced shell for the two Mach cases in question. A large re-entry flow region, which extends nearly half way down the entire projectile body, is visible in the transonic flow case. The pressure distribution plot also attests to the fact that the flow separation at the slice, contrary to the initial assumptions, affects the flow far downstream. In the Mach 2.5 case, although there are severe gradients in the flow velocity field generated by the slice, re-entry flow is not exhibited on the projectile surface due to the high inertia of the main flow. The adverse pressure necessary to turn the flow back into itself is just too great at this supersonic condition.

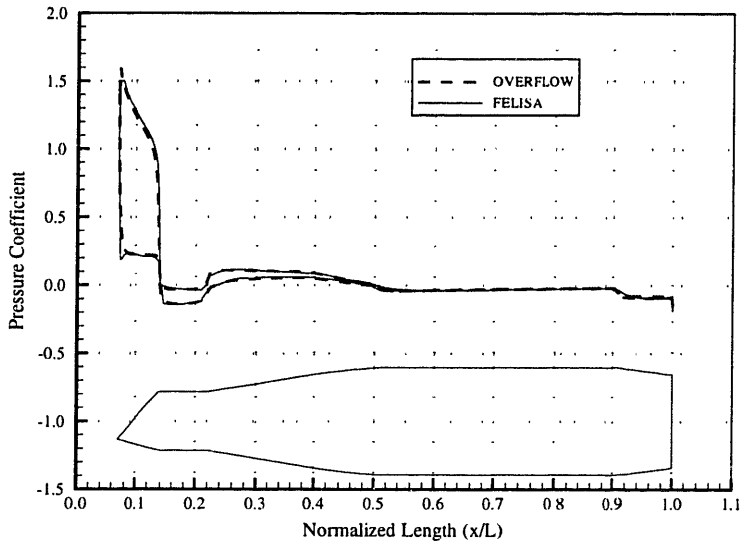

Figure 3-10: Supersonic Slice Pressure Distribution Comparison

Significant differences were found in the normal force and pitch coefficients computed using both FELISA and OVERFLOW for the transonic sliced shell simulations. Static coefficients for the CMATD slice design (shown in Table 3.1), predicted at Mach 1.1, differed by as much as 200% percent between results obtained from the two codes. The supersonic predictions of the coefficients compared much more favorably. Drag, normal force, and pitch moment were all predicted by FELISA within 1-5% of the values given by OVERFLOW at Mach 2.5. The pressure distribution and flow field results outlined above, in addition to the flow solver discussion in Chapter 2, showed that inviscid predictions are completely invalid in the presence of flow separation. Unfortunately, while this viscous phenomena should perhaps have been expected given the large surface gradients in the sliced design, the conclusion was only realized upon comparisons with results from OVERFLOW. Developing the two codes in parallel turned out to be a beneficial and rewarding task, since it really highlighted some essential information concerning the flow surrounding the deformed shells.

3.2.2 Bent Projectile Comparisons

A brief investigation was also initiated on the second design concept, the bent fuze design, using both FELISA and OVERFLOW. Simulations of a projectile with the fuze bent 16° at a 2.7 inch hinge length were completed at Mach numbers of 1.1 and 2.5. The flight points were chosen for comparison with the results from the sliced example outlined above. Comparisons

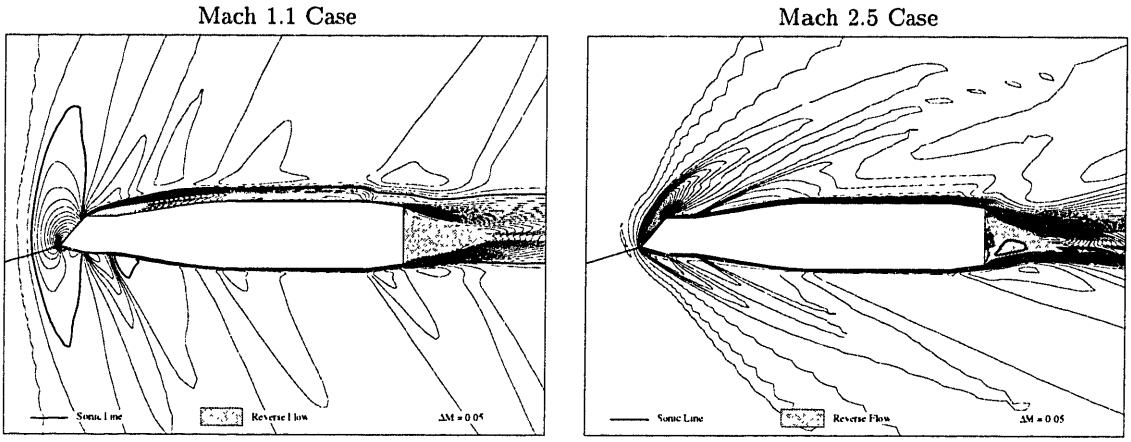

Figure 3-11: Mach Contour Maps for the Sliced Projectile

of predictions made with the two codes differed at the two flow regimes. Figure 3-12 shows the pressure distribution plots at Mach 1.1 for the deformed shell, obtained from FELISA and OVERFLOW. The extremely large bend angle of 16° creates a severe local angle of attack along the fuze which culminates in a sharp surface change at the junction of the bend with the main shell. The pressure distribution over the fuze region is not captured accurately by FELISA, probably due to the viscous effects occurring at this large angle of attack. In addition, the position and strength of the upper and lower shocks generated by the bend hinge are not well predicted by FELISA in the transonic regime. The viscous effects tend to dampen the acceleration of the flow over the hinge region, thereby reducing the shock strength. This can be seen in Figure 3-12 by the difference in the two predictions of the pressure drop occurring aft of the bend hinge on the upper surface of the shell.

The two pressure distributions predicted for the same bend geometry run at Mach 2.5 are shown in Figure 3-13. As in the slice case discussed above, the inviscid predictions compare very favorably with the results obtained using OVERFLOW in the supersonic regime. With the increase in Reynolds number, compressible effects dominate the flow propagation at this high Mach number. The strength and position of the shocks emanating from the bend hinge are properly captured by FELISA for this case. This can be seen from the sharp pressure drop in the region of the junction between the bend and the main body.

The results for the 16° bent shell comparison can be further illustrated by two pictures of the Mach contours of the flow field, shown in Figure 3-14. The location of the sonic line in the transonic figure is an indication of the effect the bend has on the local flow velocity.

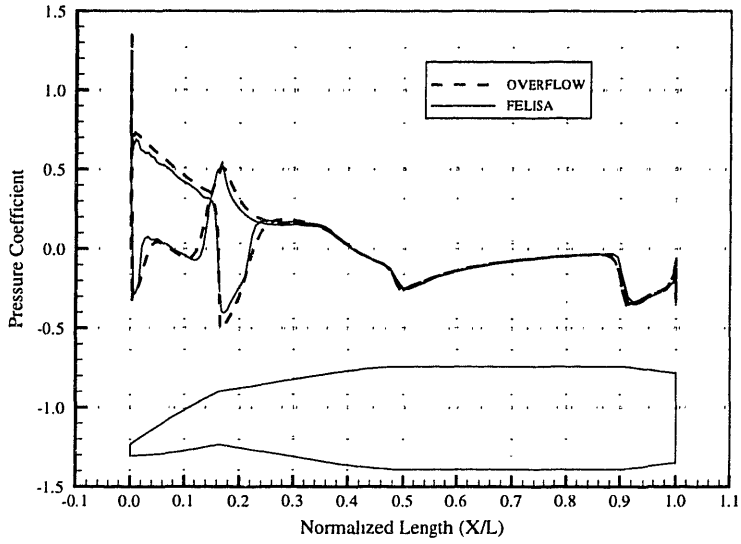

Figure 3-12: Transonic Bend Pressure Distribution Comparison

The subsonic region on the upper surface of the shell is terminated with an expansion shock at the bend hinge. Although separation does not occur in this region, the shock wave-viscous interaction in the recovery region aft of bend is not well modeled by inviscid assumptions. The concave region on the lower section of the fuze has a large subsonic pocket of fluid generated by the large surface gradient. The flow conditions are strongly dependent on viscous effects and subsequently FELISA has a fairly poor prediction of the pressure distribution in this region as well.

The errors seen in the transonic flow case in capturing the shock wave properties produce a significant effect on the aerodynamic coefficients for the bent shell design. Table 3.1 shows that the pitch moment prediction between the two codes is almost 40% different, and the normal force predictions are actually of different signs. The force and moment coefficients in the supersonic case calculated using both codes were all within 5% of each other, attesting to the increased accuracy of modeling large Mach number flows with FELISA. Unfortunately, transonic predictions were needed for this study, and the discrepancies in the results computed for both fuze designs is clearly unacceptable. It was therefore necessary, as mentioned above, to conduct the entire design study using predictions obtained with OVERFLOW.

Validation studies had shown that the two codes produced reasonable predictions of the nominal characteristics of ordnance projectiles. Further studies, motivated by radical

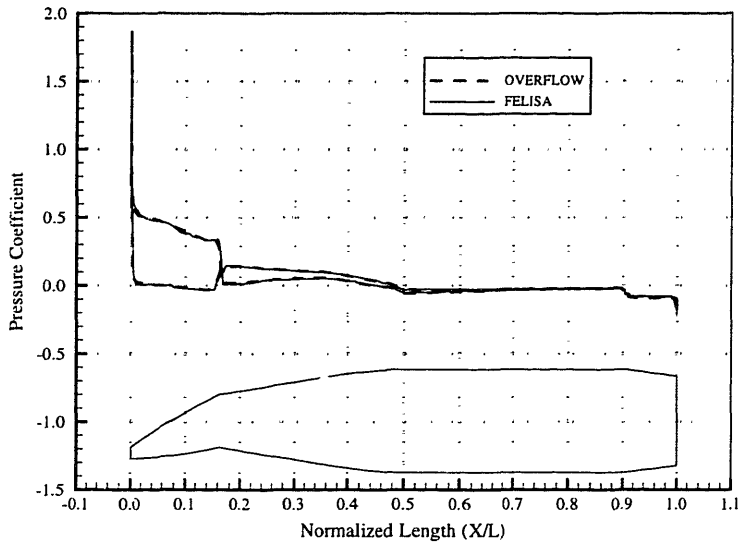

Figure 3-13: Supersonic Bend Pressure Distribution Comparison

	FELISA		OVERFLOW	
	Normal Force	Pitch Moment	Normal Force	Pitch Moment
50° Slice (M 1.1)	-0.0019	-0.0759	-0.0041	-0.0504
50° Slice (M 2.5)	-0.0616	-0.2530	-0.0621	-0.2476
10° Bend (M 1.1)	0.0008	-0.0581	-0.0032	-0.0710
10° Bend (M 2.5)	-0.0306	-0.2337	-0.0310	-0.2348

Table 3.1: FELISA vs. OVERFLOW Design Coefficient Results

discrepancies in initial predictions with FELISA on the forces and moments generated by the slice geometry, have shown that viscous effects need to be accounted for in this study. The pressure distributions and flow field visualization, taken from simulations of the sliced shell configuration, have illustrated that separation of the flow aft of the slice feature is a dominant effect in the transonic flow regime. The size and strength of the separated, re-entry flow region is almost certainly influenced by the slice angle, since the perturbation to the boundary layer is dependent on the surface gradient at the slice pivot point. Predictions of the overall aerodynamic characteristics and performance of the sliced configuration are completely dependent on viscous phenomena.

In the case of the bent shell design, the position of the shock waves generated behind the bend hinge in the transonic flight regime is influenced by the presence of a boundary layer. Comparisons made using FELISA at two Mach numbers, 1.1 and 2.5, differed significantly in their accuracy with respect to viscous predictions from OVERFLOW. In the simulations

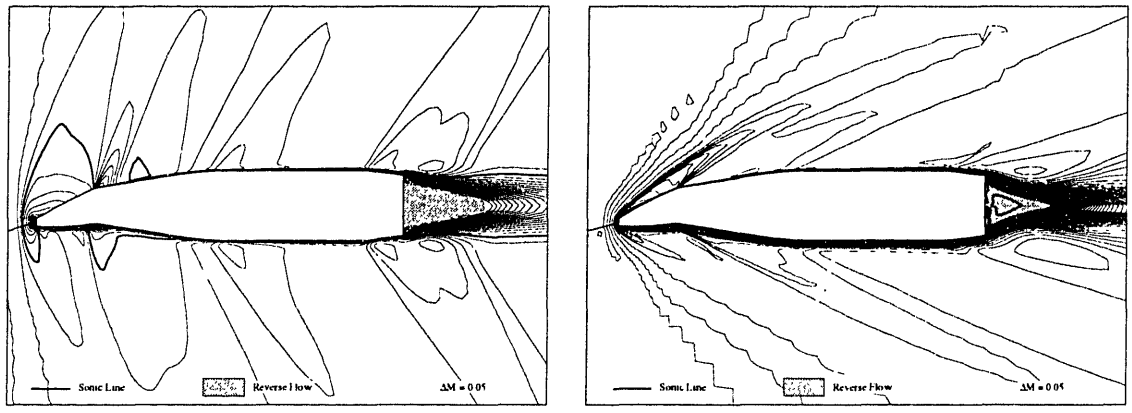

Mach 1.1 Case Mach 2.5 Case

Figure 3-14: Mach Contour Maps for the Bent Projectile

with geometries which have severe bend angles, pockets of subsonic flow were generated by the pressure gradients near the junction between the bent fuze section and the main body. This flow recovery region, characterized by large surface pressure fluctuations, is seen in the viscous computations but is not accurately predicted by simulations made with FELISA. The surface pressure changes are not a localized phenomena and substantially affect the integrated force and moment quantities over the projectile body.

Analysis of the two codes was continued for the sliced and bent shell concepts to investigate the level of viscous effects present in the flows, and the regimes for which accurate predictions could be achieved with FELISA. The fuze distortions investigated in this study cause large divergences in the nominal flow characteristics, introducing viscous and compressible effects which were formally unseen. This is an important consideration for the shell configurations since it suggests that the boundary layer, and forces dependent on its propagation and size, will certainly be altered by the various fuze distortions. Although the initial design study was set up to focus solely on predictions of static coefficients, secondary forces involving the boundary layer need to be taken into account. The Magnus validation study completed using OVERFLOW sets the stage for this kind of viscous analysis. The comparisons between the results with the two fuze distortions have shown that a priori assumptions regarding the essential flow characteristics need to be properly investigated and quantified before useful aerodynamic data can be produced for effective design evaluation.

Chapter 4

Preliminary Design Study

An extensive evaluation of the numerical prediction capabilities available for the asymmetric design concepts have been completed in Chapter 3. The final analysis of the computational tools clearly determined that the Navier-Stokes code OVERFLOW should be the backbone for this study. This chapter sets out from that conclusion to display the background and basic results for the preliminary phase of this investigation. Section 4.1 delves into the methodology behind the choice of simulated flight points and flow parameters used in this study. These decisions are important since limited computational time influences the amount and range of numerical data which can be produced. It was essential to this study to choose reasonable flight points which could provide useful information for the aerodynamics of ordnance projectiles.

Section 4.2 gets to the heart of this investigation by presenting the results obtained from various aerodynamic studies. The initial study is a presentation of the nominal aerodynamic characteristics for the baseline projectile used for this investigation. The majority of the results deal with the pitch moment and normal force predictions for the different parameterizations of the sliced and bent projectile concepts at zero angle of attack. In addition, comparisons were also made on the effect of the fuze distortions on the basic aerodynamic derivatives. This issue is quite important, since changes to these derivatives greatly influence the motion and stability of the shells in flight. Simulations were also completed on several strake geometries, in order to ascertain the amount of aero-torque generated from each design. The section concludes with results obtained from Mach sweeps completed with a candidate design from each of the asymmetric fuze concepts. The Mach range cov-

ered includes speeds in both the transonic and supersonic regime, giving a fairly complete investigation of the projectiles in all reasonable flight points.

4.1 Design Study Background

This investigation was completed to study the effects that configurational asymmetries have on the basic forces and moments generated by a spin-stabilized ordnance projectile in flight. The initial goal of this study was to make use of the nominal characteristics of a standard projectile and generate various distorted designs off of this basic frame. It was therefore necessary to choose a particular projectile geometry to be used as the *control vehicle*, since a reference source was needed for comparisons with the experimental shells. The projectile used as the base for most of this investigation was the NATO standard, 5in54/Mk64 shell, shown in Figure 4-1. The aerodynamic results for this particular projectile, while qualitatively generalizable to other shells, are naturally dependent on the surface geometry and specifically the longitudinal profile of the shell.

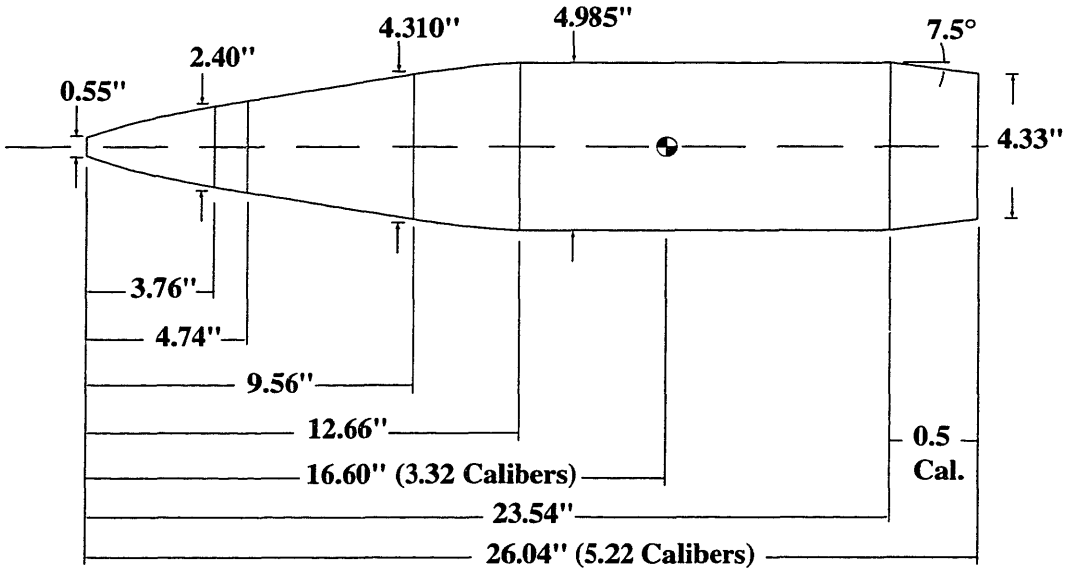

Figure 4-1: Geometry of the Baseline Projectile

The next step in the initiation of any aerodynamic vehicle design study begins with a careful examination of the basic flight envelope within which the vehicle will function. For this computational investigation the flight envelope is a serious consideration since the ordnance projectiles examined in this study are ballistic, and therefore their trajectory is

highly dependent on their aerodynamic characteristics. It was also necessary to choose a characteristic trajectory for this shell, in order to assess a typical flight regime for the investigation. The nominal trajectory of a ballistic shell can be reasonably described by three reference quantities; the initial speed (V_0), roll rate (P_0), and flight path angle (Q_e) of the projectile at launch. The set of initial values assumed for this investigation is shown in Table 4.1.

Quantity	Value	Units
V_0	2650.0	ft/sec
P_0	255.4	Hz (rad/sec)
Q_e	25.0	degrees

Table 4.1: Basic Initial Launch Conditions

These basic initial states can be used to produce a typical flight envelope for a ballistic projectile, using the physical characteristics of the shell in addition to it's baseline aerodynamic properties. A flight envelope, using the initial conditions above, has been generated with a 3-DOF, *point mass* simulation program, which uses an aero-database of values for the standard shell and produces a complete trajectory description during the flight. This 3-DOF program will be discussed in more detail in Chapter 5. Several of the important flight quantities, generated by the simulation, are shown in Figure 4-2. The most distinguishing characteristic of the trajectory, from a computational modeling standpoint, deals primarily with the Mach range reached by the projectile in a typical flight. The Mach profile for a typical trajectory shows that modeling the transonic flight regime is a necessary part of an effective design study, since a large portion of the flight falls within a Mach 0.9-1.1 range.

Aerodynamic design studies are limited by the amount of time required to produce accurate flight data, whether by experimentation or numerical simulation. It is not economically feasible to generate results for every possible design, in all relevant flow regimes. Typically, realistic flight points chosen for investigation provide sufficient information to characterize the aerodynamic qualities of the design. It was necessary to specify two Mach flight points which would be used to evaluate the overall effectiveness of the deformed projectiles. These flight points were chosen on the basis of not only the trajectory profile, but also on some knowledge of the proposed trajectory flight plan to be used for this specific guidance implementation.

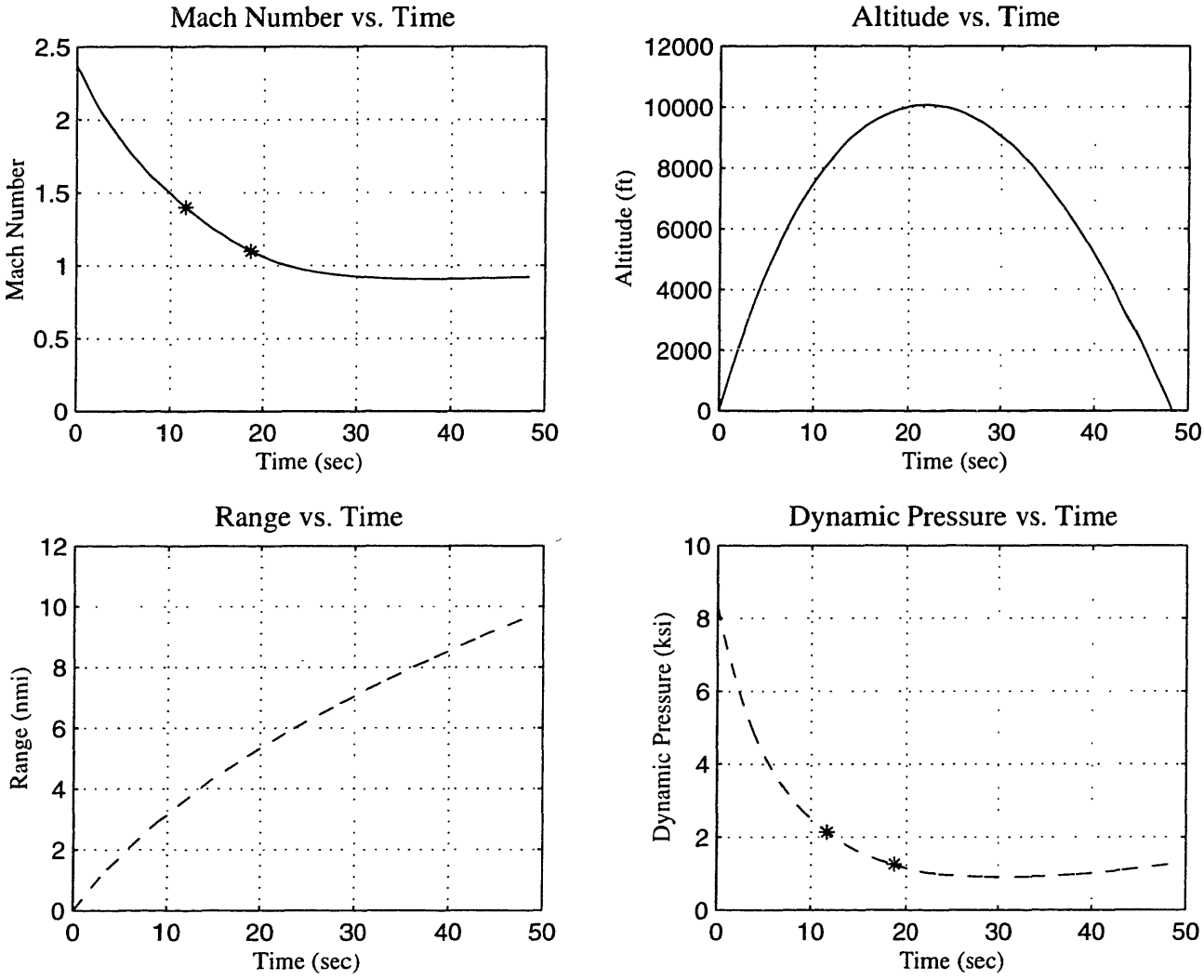

Figure 4-2: Typical Flight Envelope for the NATO Standard Projectile

The limiting factor in the flight plan proposed for this fixed-trim guidance application dealt with the time delay caused by the acquisition of a GPS tracking signal. The delay amounted to approximately ten seconds of unguided initial flight, within which despinning of the fuze section of the shell could take place as well as the distortion of the projectile. Viewing Figure 4-2, the delay means that actual control does not begin until a significant portion of the initial velocity has been lost. Design points for this investigation, shown with asterisks in Figure 4-2, were chosen to reflect the controlled flight envelope. Since the actual control authority of the guided projectiles is dependent on the dynamic pressure ($q = 1/2\,\rho V^2$), and this pressure drops significantly in the early stages of the flight, it was decided to focus the design evaluation on the beginning of the controlled flight. Two Mach conditions, 1.1 and 1.4, were chosen as important flight points; since they bracketed the flight time when the majority of the trajectory offset would be achieved. These two Mach numbers provide the basis for the design review of the different fixed-trim guidance concepts.

The choices made in the discussion above set the stage for the numerical simulation of the non-axisymmetric projectiles. Flow variables and Mach ranges have been set according to the flight profile of a typical ordnance trajectory. The only additional flow parameter required for the viscous numerical code was the Reynolds number. This number was calculated for all of the design simulations on the basis of the actual velocity of the projectile flight at *sea-level* conditions. The Reynolds number is definitely dependent on the altitude of the projectile, but the solutions were very weakly dependent on this variable and a reasonable reference used for all the simulations was sufficient.

4.2 Basic Results

This section presents the actual numerical results for the preliminary phase of this investigation. It is organized by first presenting the baseline pitch moment and normal force derivatives for the standard projectile configuration, displayed in Figure 4-1, over a range of Mach numbers. The next section outlines the bulk of this investigation, which is the study of the two fixed-trim guidance concepts, followed by the analysis of the aero-torque generation calculated for the strake surface features. The variables which describe each guidance concept have been outlined already in Section 1.2, but will be discussed in more

detail with the results from the numerical simulations. The end of this section delves into a broader aerodynamic survey of the deformed projectiles by presenting a computational study on the influence of the various fuze distortions on the actual aerodynamic coefficient derivatives. This is followed by Mach sweep predictions on a candidate shape from each design concept.

In an effort to make the results more understandable, a definition of the various terms, normalizations, and directional conventions used in this study is necessary. The aerodynamic coefficients described in this investigation are functions of the various forces and moments acting upon the projectile. Using established conventions, force coefficients have been non-dimensionalized by the standard parameters of dynamic pressure ($q = 1/2\,\rho\,V^2$) and reference area ($S = 1/4\,\pi\,d^2$); with the reference length (d), the velocity (V), and density (ρ). The maximum diameter of the projectile has been set as the reference length, which for the projectile in this study is 4.995 inches. The pitching moments, in addition to the parameters above, have been normalized by the reference diameter of the shell.

The most convenient coordinate frame to apply for projectiles is the aeroballistic axis system shown in Figure 4-3. The origin of the coordinate system is located at the center of mass of the standard projectile. Although it was realized that the shell's center of gravity will be offset by the various fuze distortions, a standard location was needed in order to effectively compare the numerical results. The definition of the angle of attack and the side-slip are needed in Section 4.2.5, when the influence of the fuze distortions on coefficient derivatives is discussed. It was attempted, for the purpose of clarity, to make use of the most conventional system so that results would not be clouded by questions of direction or sign changes.

4.2.1 Baseline Projectile Results

A diagram of the baseline projectile used in this study has already been given in Figure 4-1. The 5in54/Mk64 projectile has a very similar profile to the 5in54/RAP examined in the validation cases in Section 3.1.2, but the slight differences neccesitate a complete study of the baseline aerodynamic derivatives for this shell. The focus of this particular investigation is on the fixed angular trim conditions which can be generated by various asymmetric fuze distortions, therefore knowledge of the baseline shell's reaction to changes in angle of attack is essential.

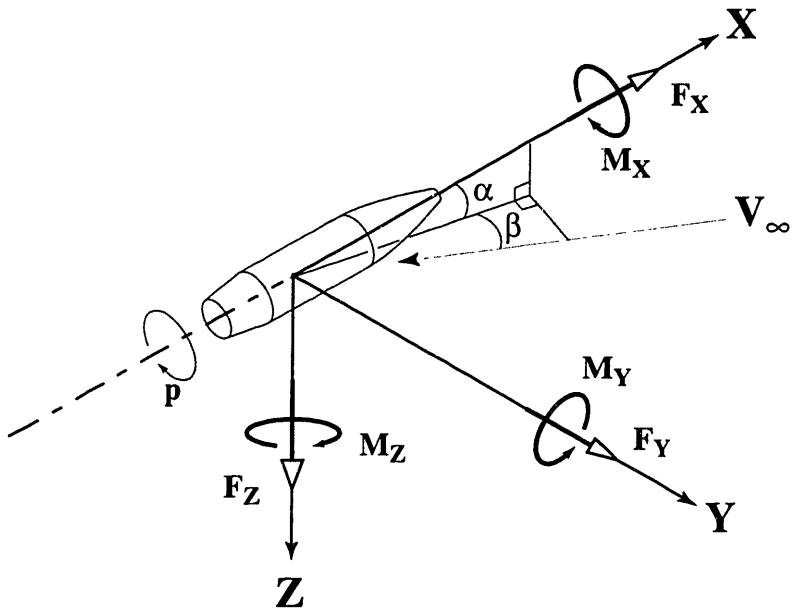

Figure 4-3: Aeroballistic Coordinate System

The baseline characteristics for the normal force derivative are shown in Figure 4-4. These results show much the same character as the validation predictions in Section 3.1.2. In the supersonic regime, there is a general increase in the normal force generated by the shell body, due to angle of attack, from an increase in Mach number. This Mach trend is seen in all of the experimental data for ballistic projectiles. The sensitive transonic Mach region, in the area from Mach 0.9-1.1, is characterized by rapid changes in the aerodynamic derivatives, which are very dependent on the specific geometry of the shell. The transonic predictions for the Mk64 baseline show rather benign transonic trends in the normal force derivative, with the largest change coming at approximately Mach 0.95.

The baseline pitch moment derivative Mach trends are shown in Figure 4-5. The supersonic characteristics of the Mk64 again closely follow the trends seen in the previous validation study, with the pitch moment sensitivity to changes in angle of attack falling off slightly with increasing Mach number. The large pitch moment bubble, seen with the 5in54/RAP, does not occur with the Mk64 baseline shell. As mentioned in Section 3.1.2, the peak in the pitch moment slope in the transonic regime is a function of the shell's boat-tail geometry and the position of the shocks in this region. The Mk64 does not exhibit the same abrupt motion of the shocks in the transonic regime. The profile of the Mk64 is slightly different from the 5in54/RAP, which could account for the change in its behavior. Small

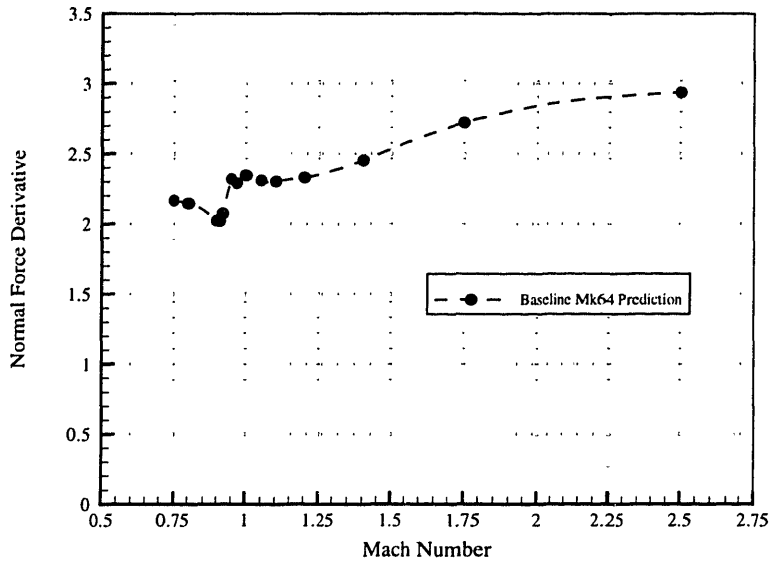

Figure 4-4: Normal Force Coefficient Derivative Baseline

changes in a shell's geometry can greatly affect the local velocity of the flow, which would produce radically different shock characteristics.

The baseline Mk64 trends, for both the normal force and pitch moment slopes, appear very benign and do not exhibit large fluctuations in the transonic regime. These characteristics are not illogical though, since the Mk64 is a mature ordnance projectile which has been used and re-tested for optimum flight qualities and stability. Benign changes in the static aerodynamic coefficients would certainly improve the accuracy of the projectile, causing fewer errant trajectories and better gust response characteristics. Using a very stable platform as a control vehicle for this investigation is beneficial so that changes due to the various fuze asymmetries can be isolated and studied.

4.2.2 Sliced Fuze Design

The first relevant issue in the investigation of the slice design was the choice of parameterized variables which would effectively explore the aerodynamic characteristics of this kind of surface asymmetry. One of the most severe constraints on the sliced fuze design was the amount of volume extracted from the standard shell. An estimate was reached on a reasonable limit for this volume, which translated into a boundary on the furthest longitudinal position from which volume could be extracted. It was decided to place this

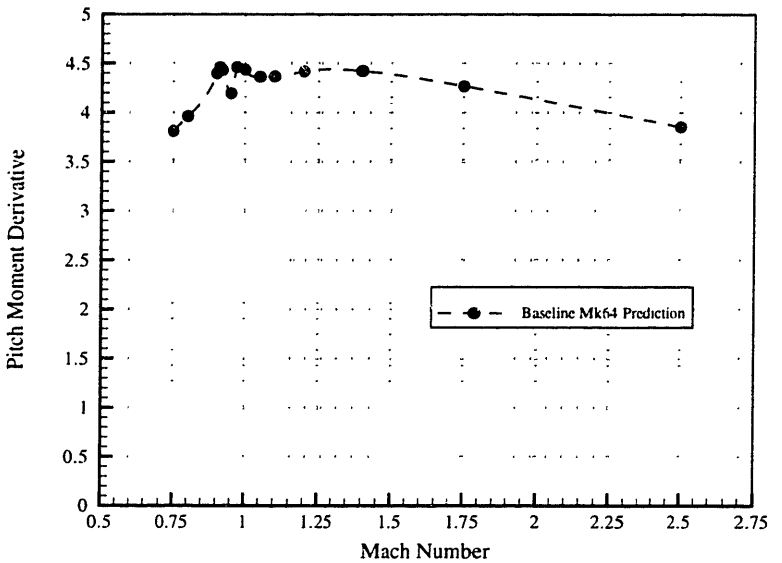

Figure 4-5: Pitch Moment Coefficient Derivative Baseline

limit, for the standard projectile, at 2.7 inches from the original shell nose. An additional experimental shape, which moved the slice plane 0.5 inches forward to 2.2 inches, was also generated to investigate the sensitivity of the control authority to the longitudinal position of the slice plane. The second parameter for the slice design was chosen as the slice angle. It was decided to vary the slice angle around the 45° line, since a simple flat plate momentum transfer analogy places the maximum at this value. These two parameters seemed reasonable since together they completely describe a plane cutting through the projectile.

Flow solutions were obtained by varying both the slice angle as well as the pivot locations. As discussed in Section 4.1, each candidate shape was numerically simulated at Mach numbers of 1.1 and 1.4. Results for the normal force coefficient and pitch moment coefficient generated by the various slice cases are shown in Figures 4-6 and 4-7 respectively. The first easily seen quality is that there is a rather strong increase in the force and moments generated by the deformed shell as the position of the slice pivot point is moved further aft. This trend seems to demonstrate the fact that the forces generated by the slice design are dependent on the slice plane area, since moving the pivot point further back on the fuze causes a much larger shell cross-section to be intersected.

Variation of the slice angle provides a much more subtle change in the slice plane area, leading to interesting results. Normal force and pitch moment variations with slice angle

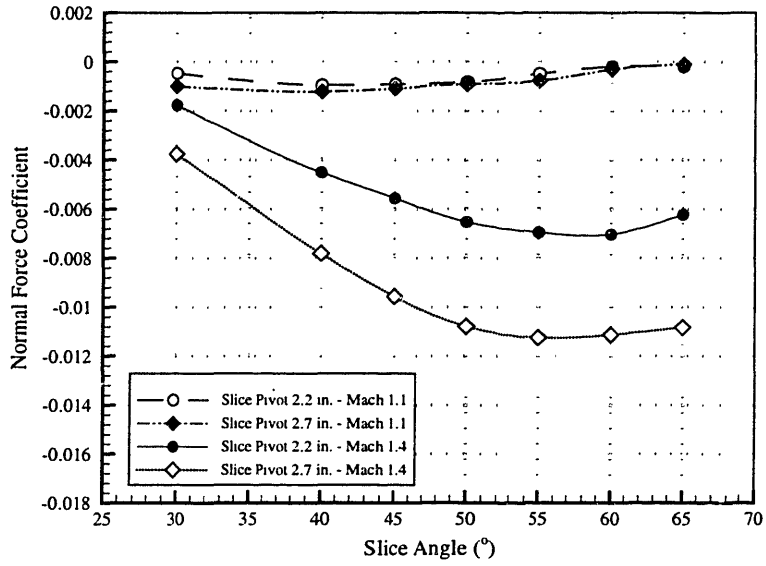

Figure 4-6: Variation in the Normal Force Coefficient with Slice Angle

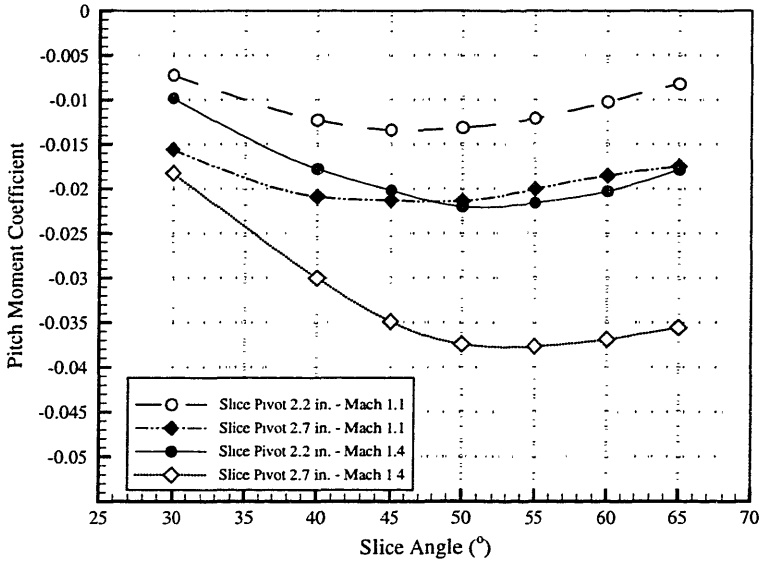

Figure 4-7: Variation in the Pitch Moment Coefficient with Slice Angle

exhibit different behavior at the two Mach numbers. This is not unexpected considering the discussion in Section 3.2 on the sliced projectile, in which significant changes in the character of the flow field were seen at different Mach numbers. In that section it was shown that in the transonic flow regime the slice feature creates a severe shock wave off of the slice edge and causes a separated flow region to occur aft of the slice. The size and severity of the separation region is extremely sensitive to not only the Mach number of the free stream but also to the slice angle, since both influence the local velocity of the flow.

The trends of sliced fuze in the transonic regime can be further explored through Figure 4-8, which illustrates the pressure distribution on the shell at Mach 1.1 for various slice angles. The competing nature of the dominant effects in the flow are exhibited in this figure. A large contribution to the normal force is produced in fuze section of the deformed shell, where a considerable amount of the flow momentum is transfered to the slice plane. Unfortunately, at the pivot junction between the slice and the symmetric shell body a shock wave is generated and a large pressure recovery ensues, resulting in a loss of normal force and in some cases separated flow. The competing influences of the purely inertial, flow momentum transfer to the slice plane; and the severe compressible-viscous interaction behind the slice produce a very dis-ordered trend in the variation of the aerodynamic qualities with slice angle. Due to the strong interaction of viscous and compressible effects on the performance of the slice design, the simple *flat plate* analogy used to explain the pivot location trend can no longer be used so loosely.

Figures 4-6 and 4-7 seem to imply that the slice angle with maximum control authority will be dependent on the specific Mach number. Although this complicates the selection of an *optimum* design from a simple evaluation, it is clear that an appreciable amount of normal force and moment is being generated by the slice distortions. Despite the extreme sensitivity of the normal force to Mach number and slice angle; the pitch moment, which dictates the trim condition of the projectile in flight, is somewhat better behaved, and has a clear maximum of approximately 50° in the two Mach regions investigated.

4.2.3 Bent Fuze Design

The bent fuze distortion was parameterized with the same reasoning as the sliced fuze. A diagram of this particular design was already displayed in Figure 1-2. The volume constraint, important with the slice design, was not an issue with the bend design since the

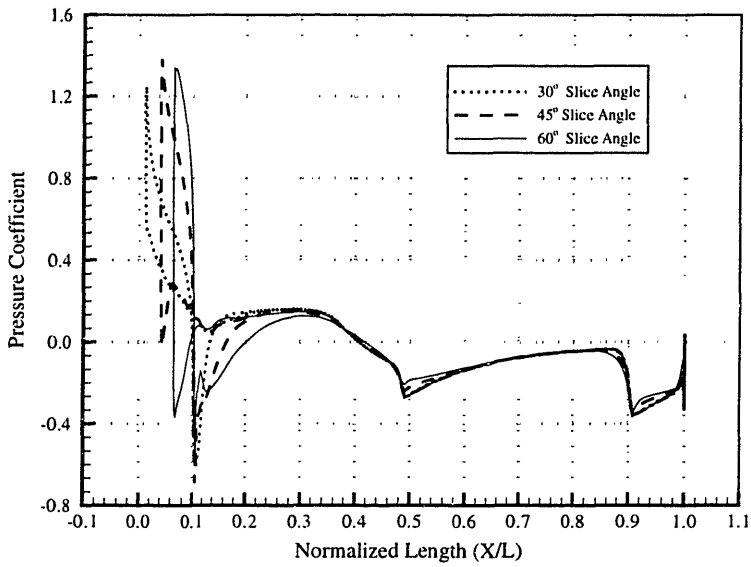

Figure 4-8: Pressure Distribution for Various Sliced Shells at Mach 1.1

fuze volume was only being deformed and not removed. An upper limit on the furthest aft position to initiate bending, which was derived purely from the geometric limits of the fuze, was set at 4.25 inches from the shell's nose. In addition to this position, further simulation were completed on hinge positions of 3.25 and 2.25 inches, in order to effectively map the sensitivity of the control authority to this variable. The other parameterized feature selected for the bent fuze investigation was the bend angle, which was chosen in a range from 0-24 degrees. It was hoped that choosing such extreme angles would help examine any non-linear effects that occurred due to the severe angle of attack of the flow over the bent fuze.

The coefficient results for the bent shell study have been organized in a slightly different manner from the sliced fuze study. The first results presented, in Figures 4-9 and 4-10, show the variation of the two aerodynamic coefficients with bend angle for various bend hinge positions simulated at Mach 1.1. This figure shows the same outcome as seen in the sliced case, that increasing the overall region of the shell influenced by the distorted surface increases the effectiveness of the augmentation. This suggests that, for both of the fuze distortions, a good plan for maximum control effectiveness is to choose the beginning of the control surface on the furthest aft position possible given internal volume and surface constraints.

The next results from this study, displayed in Figures 4-11 and 4-12, show the variation

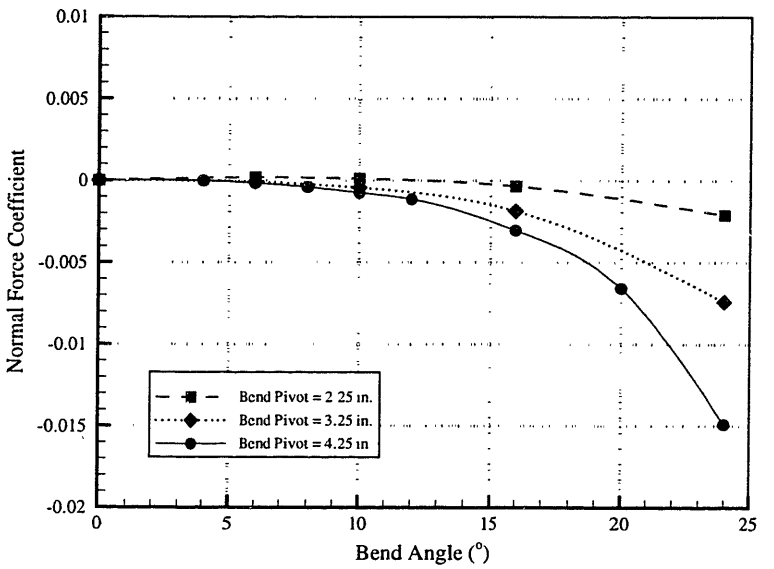

Figure 4-9: Sensitivity of Normal Force Coefficient to Pivot Location

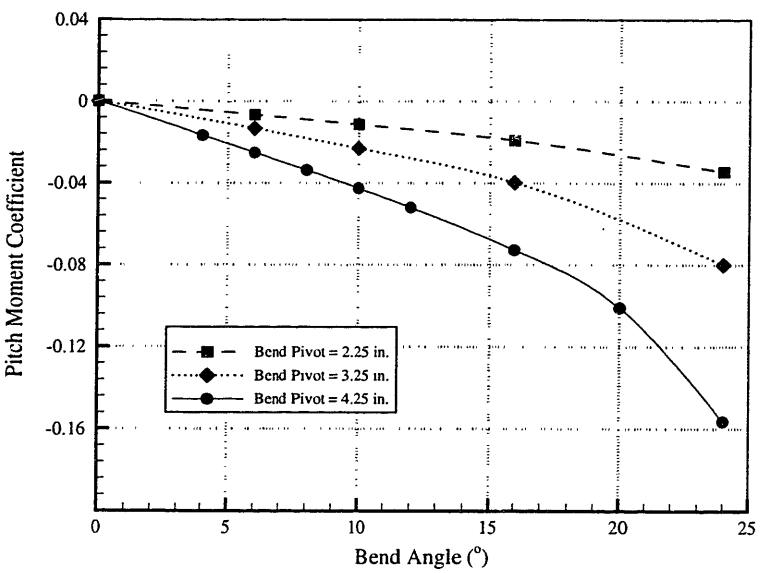

Figure 4-10: Sensitivity of Pitch Moment Coefficient to Pivot Location

of pitch moment and normal force as a function of the fuze bend angle for two Mach numbers, 1.1 and 1.4, taken at the furthest bend hinge position of 4.25 inches. These results show a much clearer trend in the angular parameter than was seen with the slice cases. The aerodynamic coefficients both increase monotonically throughout the range of bend angles chosen, and in fact exhibit nearly linear behavior for angles ranging from 0-10 degrees. It should be noted that the pitch moment generated by the bend is far in excess of any value seen with the slice designs. Since the trim condition of the shell is dependent on the pitch moment value, this suggests that far greater trim conditions can be achieved with the bent fuze. The question of evaluating the various designs will be throughly discussed in Chapter 5 with the derivation of a design metric.

A deeper insight into the local effects of the bent fuze can be seen in Figure 4-13, which shows the pressure distribution taken along the shell body at various bend angles at Mach 1.1. It is evident from this figure that the lift generated over the fuze section is directly related to the bend angle. The strength of the shock wave produced by the bend (shown by the strong pressure changes aft of the bend hinge) is also a function of this angle. These two effects compete with each other in the production of lift and moment over the entire shell body. Significantly higher moments are generated as the bend angle is increased due to the position of the lift producing region on the augmented shell. The self-nullifying character of the bend augmentation is very similar to the results seen with the sliced configurations, except that the effects of the bend are local to shell fuze and do not propagate siginificantly down the length of the projectile.

The pressure distribution results from Figures 4-13 and 4-8 show that even though the upper surface pressure over the bent fuze never reaches the magnitude seen over the sliced shell, the *lift* producing region extends much farther along the shell. Although lift is lost across the hinge location, this loss is not nearly as severe as that seen in the transition over the slice edge. The surface gradients over the junction between the slice and the shell body are much larger than in the bent shell cases, and even tend to cause flow separation at certain slice angles. The changes in the velocity of the flow as it propagates down the shell are directly related to the gradient of the projectile surface, albeit in a complex and perhaps non-intuitive manner. The gradients in the velocity affect not only the momentum of the flow, but also the interaction of viscous forces on the body. These effects contribute to the surface pressure, and therefore to the lift generated by the different fuze distortions.

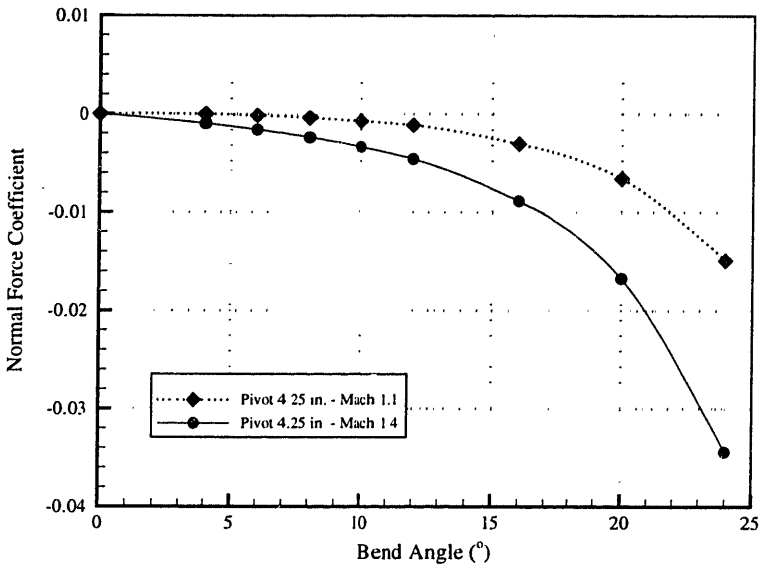

Figure 4-11: Variation in the Normal Force Coefficient with Bend Angle

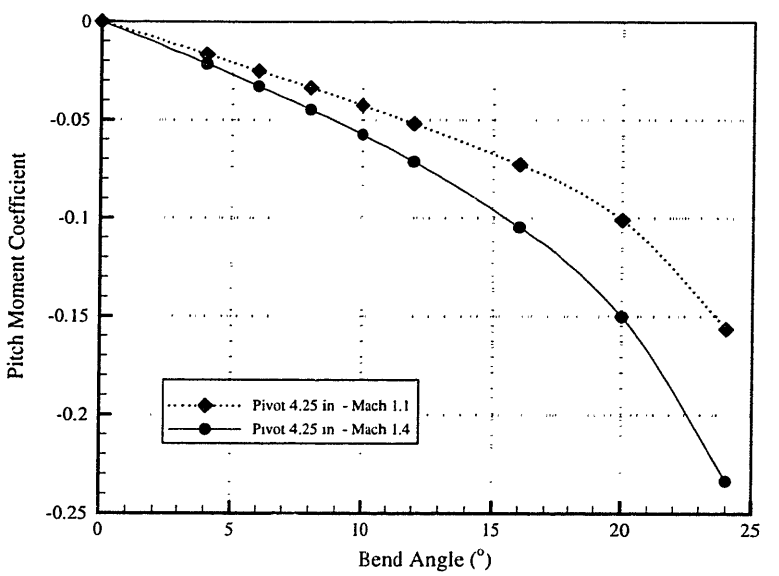

Figure 4-12: Variation in the Pitch Moment Coefficient with Bend Angle

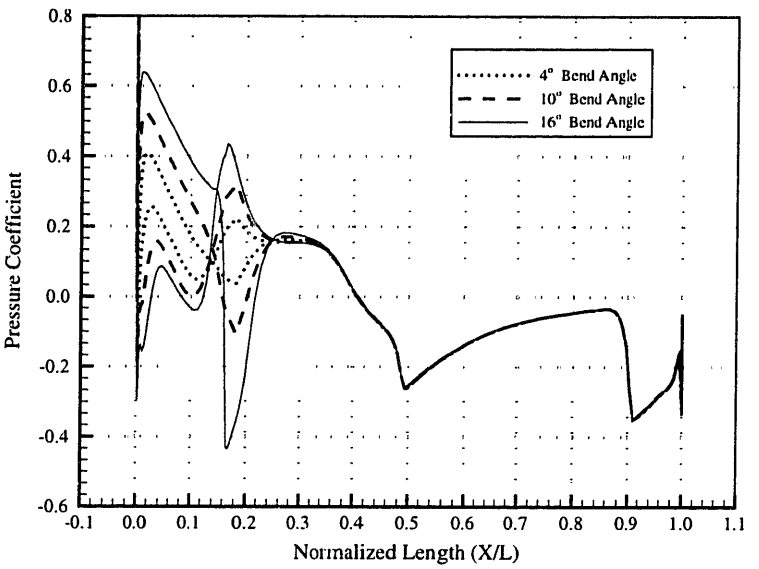

Figure 4-13: Pressure Distribution for Various Bent Shells at Mach 1.1

4.2.4 Strake Study

The following results are a slight deviation from the discussion of fuze augmentation comparisons discussed in the previous sections. As mentioned in Section 1.2, fixed-trim guidance for spin-stabilized projectiles requires two necessary features; sufficient trim force for control of the projectile trajectory, and sufficient roll control of this actuation force so that the direction of the trajectory offset can be effectively commanded. The first piece of the puzzle has been addressed in the previous sections. This section displays the results for a study completed on various aero-torque surface features. These *strakes*, which have been discussed already in Section 1.2, must be designed to provide enough roll torque for the initial despinning process, followed by the production of sufficient roll moment for actuation, even at lower Mach levels and dynamic pressures.

A full 3-D diagram of the strakes was displayed previously in Figure 1-3 and most closely resembles a corkscrew. The basic geometry of the surface features can be reasonably parameterized by the quantities height, width, and cant angle. Figure 4-14 shows a 2-D explanation of the three main geometry parameters which describe the strake. The strakes' main function is to redirect flow traveling over the body in a direction tangential to the shell surface. This deflection causes forces to be generated on the shell due to the change in momentum of the flow, similar in principle to the flow over vanes. Without shocks

or the presence of significant viscous forces; the force generated by the strake, from a simple Bernoulli argument, should be linearly dependent on the magnitude of the angular deflection. This angular deflection is directly related to the cant angle of the strakes as they wrap around the projectile body.

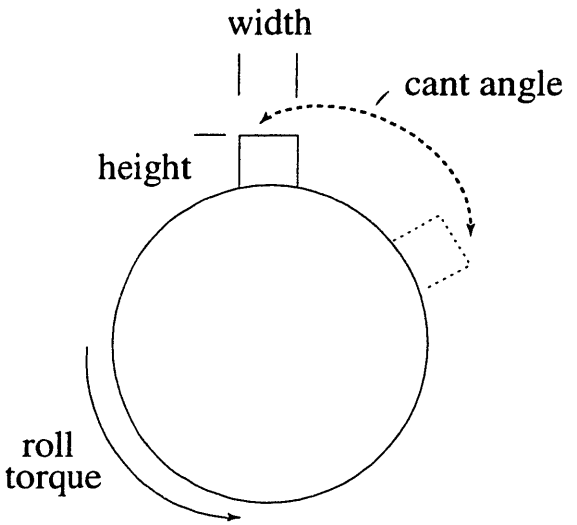

Figure 4-14: 2-D Diagram of Strake Geometry

The strake concept makes use of two surface features, which are geometric mirror images of each other, since the end goal of this design is to produce a roll moment on the shell fuze. This goal dictates that the forces produced by the strakes should be equal in magnitude and positioned opposite in direction, causing only a moment to be generated about the center-line of the shell. The cant angle of the strake determines the total deflection angle of the fluid passing over the body. The height of the strake changes the area of the surface which deflects the flow. The width of the strake is mainly dictated by structural concerns, and was chosen as a reasonable size which could be machined without difficulty. The standard width for the strakes, used in all of the numerical simulations, was one-quarter of an inch.

The main parameter for the strake study was the degree of cant angle, since that determined in some sense the amount of roll moment produced by the strakes. The results for the cant angle parameterization of the strakes have been broken up into two sections, outlining the other two necessary test parameters of height and Mach number. Comparisons at three different strake heights are shown in Figure 4-15. These results not only reinforce the infered linear dependency of the roll moment on the cant angle, they also show that increasing the height of the strakes increases the roll moment. The relative height of the

strakes alters the area of the surface which deflects the flow. The torque generated by the strakes is produced by the reaction force from the flow momentum transfer, therefore the taller the strake the more roll moment.

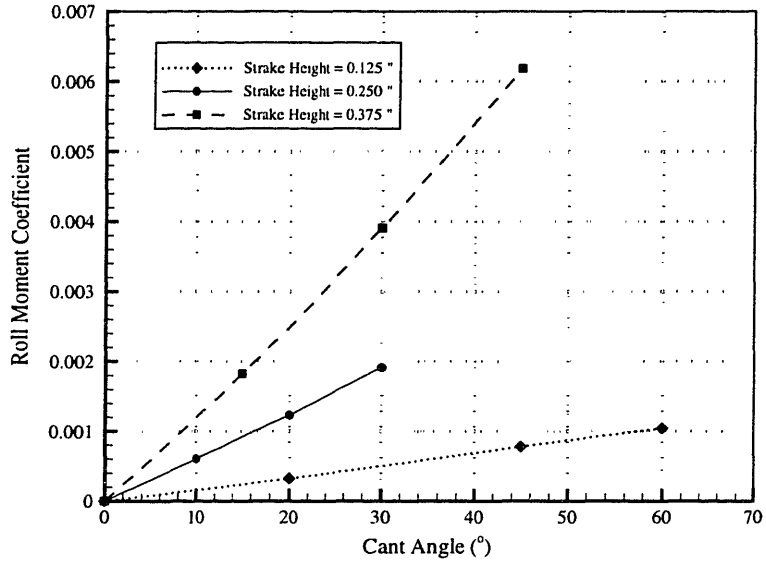

Figure 4-15: Variation of Strake Roll Moment with Height

The second result, shown in Figure 4-16, displays the roll moment coefficient sensitivity to the Mach number, taken from the strake geometry with a height and width of 0.25 inches. The diagram shows that the roll moment coefficient produced by the strakes is almost completely independent of the Mach number. Of course, the actual roll moment generated by the strakes is dependent on the dynamic pressure, which increases as the square of the Mach number, so a much larger roll torque would be expected at higher Mach numbers. The Mach insensitivity does provide an interesting result though; the effectiveness of the strakes is mostly insensitive to changes in the viscous and compressible forces at the shell surface. The change in the boundary layer height, from one Mach number to the next, does not overtly affect the efficiency of the strakes. This is somewhat understandable since the strakes project well outside of the viscous layer of the shell, and no control blanking or other viscous influences are apparent in the results.

The strakes appear to closely follow classic Bernoulli relationships; if not quantitatively than at least in a qualitative sense. The roll torque produced by the strakes is linearly dependent on the cant angle for all geometries and Mach numbers tested. In addition the

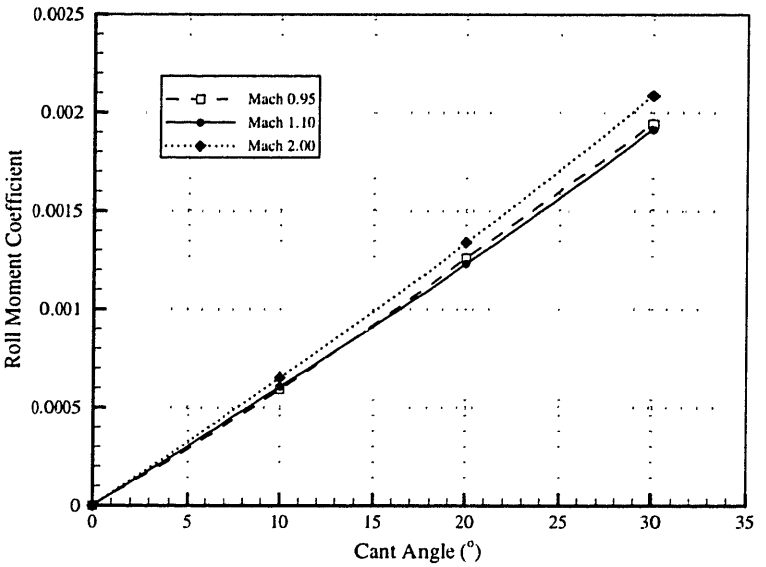

Figure 4-16: Variation of Strake Roll Moment with Mach Number

roll torque is clearly dependent on the height of the strake, or more specifically the area of the strake surface which deflects the flow. This conclusion makes the determination of a reasonable strake geometry possible, given a specific roll torque requirement. The cant angle and height of the strake can be adjusted to facilitate a wide range of control bandwidths. The one difficulty with this design is that it does not allow roll torque scheduling throughout a ballistic flight, according to the relative dynamic pressure, since the current design is static. One possible option is to allow limited actuation of the strakes by controlling their height in a mechanically viable way. The clear trend in the roll torque as a function of the strake height would make this form of actuation possible, given a suitable dynamic device for altering the strakes in flight.

4.2.5 Coefficient Derivatives

The parameterized behavior of the two deformed fuze designs is the first step in the basic description of the static aerodynamic qualities of the asymmetric projectiles. The next two sections are intended to discuss the effects that the augmentations have on both the nominal projectile coefficient derivatives, as well as a more in depth look at the sensitivity of control force and moment generation as a function of Mach number. Due to the time and resources required for numerical simulations, it was impossible to complete simulations of all

the possible designs at all flight conditions useful for this design study. To accomplish some reasonable picture of the overall aerodynamic characteristics of these distorted shells, it was necessary to choose a candidate shape from each design concept and use that geometry for a broader investigation.

The two geometries that were chosen for the derivative and Mach sweep studies were the 50° slice case and the the 10° bend case, both with fuze distortions in the furthest aft position. Section 4.2.2 and 4.2.3 have already demonstrated the the optimum longitudinal position for the two augmentations is located as far down the fuze as physical constraints will allow. The 50° slice case was chosen because the design showed close to maximum generation of normal force and pitch moment at both of the Mach numbers tested. The 10° bend design, while not the optimum bend case tested, was selected because it represented a viable deformed geometry, and produced a significant amount of control authority.

In order to assess the asymmetric shell's control authority at the trim angle of attack and to analyze the stability of the new configurations, it was necessary to study the effect the fuze alterations had on the baseline coefficient derivatives. Simulations were performed on the standard projectile, the sliced case, and the bent case over a range of attack angles from 0-4 degrees, at Mach numbers of 1.1 and 1.4. Figures 4-17 and 4-18 show the variation in normal force and pitch moment produced by the two shell designs as a function of angle of attack. These results show that altering the fuze of the shells has very little effect on the slopes of the pitch moment and normal force coefficients at either of the Mach numbers tested.

The forces produced by the configurational asymmetries generate a constant offset over the range of attack angles investigated. While the simulations were limited to small angles of attack no greater than four degrees, this is a reasonable range to study since it is extremely unlikely to have stable flight under angles much greater than this value. A study has been completed on the two asymmetric projectile designs to test the changes to the side force and yaw moment slope with respect to the side slip angle. On axisymmetric projectiles, these derivatives are not an issue since the shell reacts the same way to motions of yaw or pitch. Since the angle of attack study showed that the static derivatives were not affected by the fuze distortions, it was necessary to check this result with respect the side slip angle. The study was conducted at a Mach number of 1.1, over a beta range from 0 to 4 degrees, using the same 50° slice and 10° bend designs as in the alpha study.

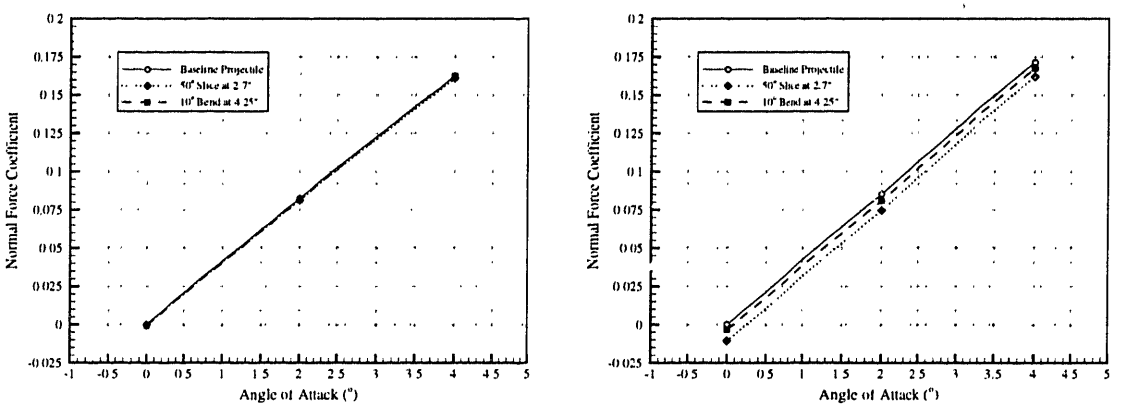

(Mach 1.1 Case) (Mach 1.4 Case)

Figure 4-17: Normal Force Coefficient vs. Angle of Attack

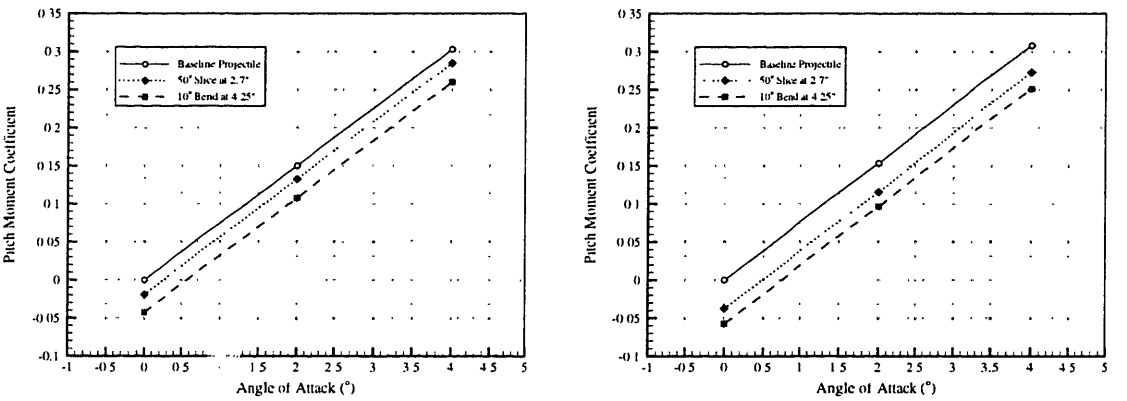

(Mach 1.1 Case) (Mach 1.4 Case)

Figure 4-18: Pitch Moment Coefficient vs. Angle of Attack

Figure 4-19 shows the results of the side force and yaw moment taken over a sweep in side slip angle. The figure shows that very little effect is felt on the side force from the distortions, however the yaw moment is altered appreciably in the sliced projectile case. The 50° slice geometry changes the yaw moment slope by approximately 5%. While this is certainly not a large change, further study needed to be completed to address this possible problem. Additional predictions were made using 50° sliced configurations with different slice pivot positions. Since the control force generated by the sliced configurations changes very rapidly with this parameter, it was an effective way to test the limits of the changes in side slip derivatives. Figure 4-20 shows the percentage change in side force and yaw moment beta derivatives as a function of slice pivot point, for a 50° slice taken at Mach 1.1.

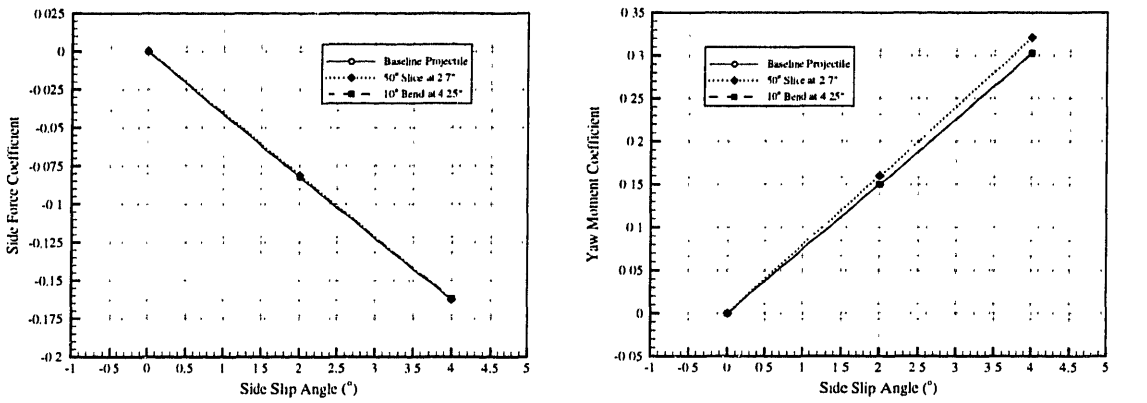

Figure 4-19: Side Force and Yaw Moment Sensitivity to Side Slip Angle

The results in the yaw moment derivative show a possible problem could exist for some slice configurations. Moving the pivot point to 3.5 inches resulted in a change in the yaw moment slope of almost 10%. This is a significant deviation from the baseline value and, given the results for the alpha sweeps, would result in dissimilar pitch and yaw moment sensitivities to changes in the body angle. Asymmetric aerodynamic derivative characteristics can cause severe changes in the trim behavior of spinning projectiles, possibly leading to catastrophic instability [16]. The change in the yaw moment slope can probably be attributed to the large change in the shell profile as the slice plane is moved further aft. The projected area of the projectile, in the pitch plane, begins to be severely altered when so much of the fuze volume is removed. Despite this problem, in the range of slice configurations which satisfied the internal volume constraint, the change in yaw moment slope was not that large. This problem could be a significant consideration if the slice distortion is moved further down the length of the shell.

4.2.6 Mach Sweep Investigation

It has been discovered in Section 4.2.5 that the nominal aerodynamic derivatives are not greatly affected by the presence of the deformed control surfaces. The next step, in a more thorough investigation of the aerodynamic qualities of the asymmetric projectiles, deals with their sensitivity to changes in Mach number. A parametric study has already been completed describing the trends in the control aerodynamic properties for different geometries at two Mach numbers, 1.1 and 1.4. It is extremely costly to investigate all

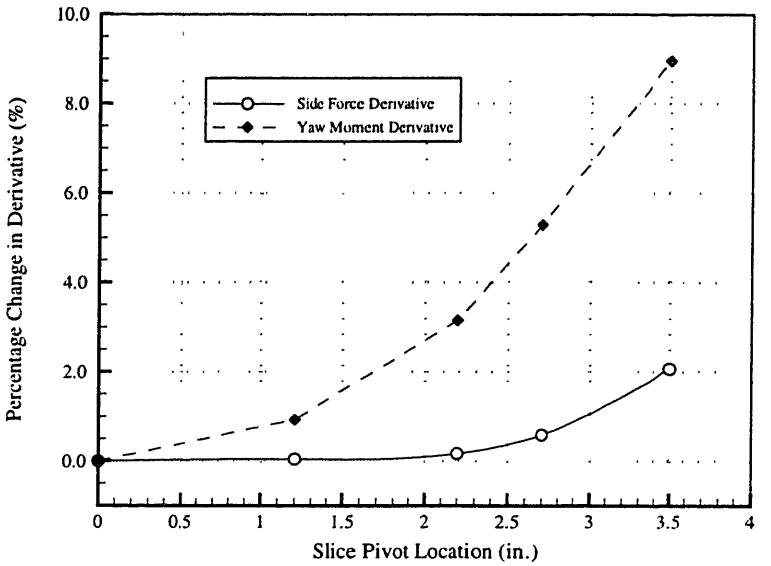

Figure 4-20: Side Force and Yaw Moment Sensitivity to Pivot Position

possible designs at all relevant flight points, therefore candidate shapes need to be chosen in order to facilitate an effective Mach sweep study of the augmented projectiles. The same candidate geometries implemented in the coefficient derivative study mentioned in Section 4.2.5 were also used in this Mach investigation. The purpose of the investigation was to isolate the specific Mach dependencies of the control forces and moments generated by the fuze distortions, in order to assess the effectiveness of the two designs over a complete flight.

Simulations, between Mach 0.75 and 2.00, were completed on both the 10° bend geometry as well as the 50° slice geometry. All results presented in this section were taken at zero angle of attack, in order to characterize the nominal aerodynamic qualities of the two fuze designs. Figure 4-21 shows the drag coefficient of the two projectiles taken over the investigated Mach range. The interesting point of this graph is that the two shells exhibit the standard drag profile, which shows a sharp increase in the drag at the supersonic barrier of Mach 1.0. This figure also predicts that the sliced projectiles produce a much larger drag at both subsonic and supersonic speeds. This is probably due to the geometry of the sliced shell nose, which exposes a large cross-sectional surface area directly into the free stream.

The next two diagrams, Figures 4-22 and 4-23, display the normal force and pitch moment produced by the two designs over the Mach range. The supersonic characteristics of

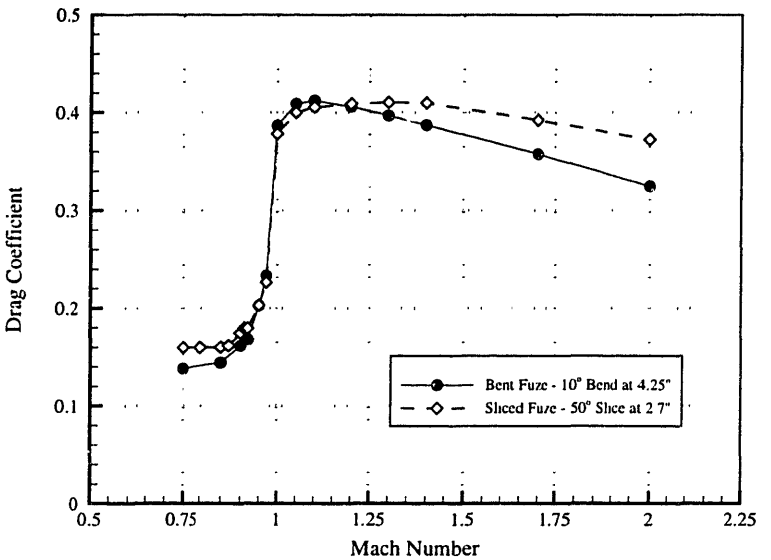

Figure 4-21: Drag Coefficient vs. Mach Number

the two designs are both fairly well behaved, demonstrating an increase in the magnitude of the normal force and pitch moment coefficients with increasing Mach number. The transonic region is where the trends get interesting for the two coefficients, as one might expect from the sensitive nature of this flow regime. It has already been mentioned that vehicles in the transonic region can exhibit extremely large fluctuations in all of the aerodynamic characteristics. The flow is extremely sensitive to the specific surface features of the vehicle, which can lead to vastly different looking flow solutions over very small changes in Mach number.

The bend design experiences a very large peak in both the normal force and pitch moment coefficient Mach profiles in the transonic regime. The maximum of this peak occurs at a Mach number of approximately 0.92. The discussion in Section 3.1, which outlined the boat tail effects experienced by projectiles in the transonic regime, showed that a peak in the pitch moment coefficient occurred at Mach 0.92. This coincidence is highly suggestive of a similar phenomena causing the peaks in the coefficients Mach profiles for the bend case. The capability to output force distributions has been developed to examine the local effects of the different fuze distortions on the force coefficients. The Mach sensitivity of the coefficients gives information about the overall resultant forces on the shell body, but it tells nothing about what regions of the projectile are producing these effects.

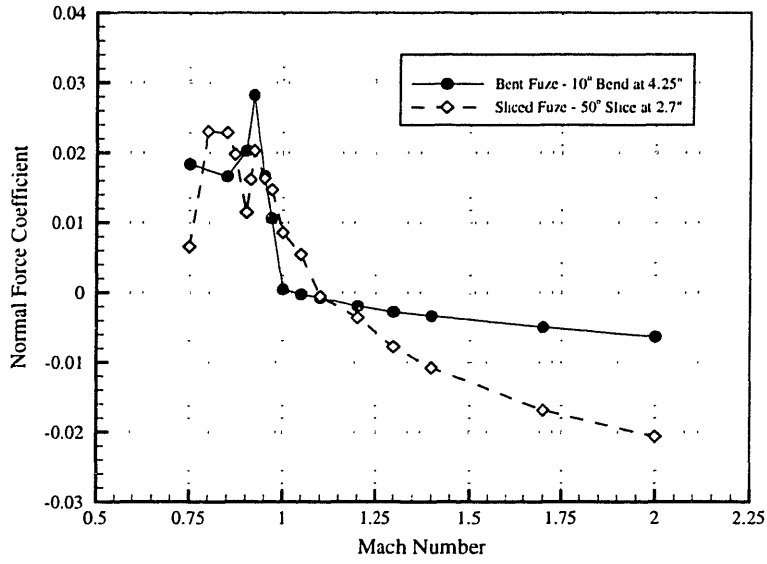

Figure 4-22: Normal Force Coefficient vs. Mach Number

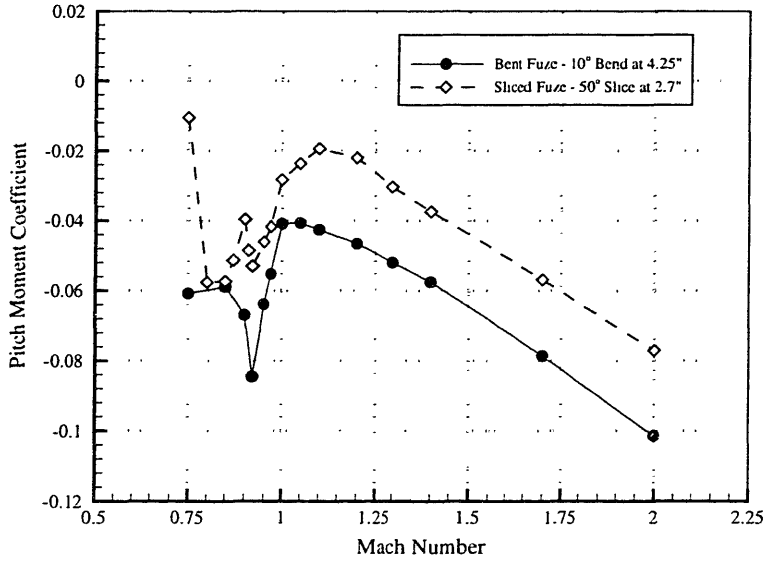

Figure 4-23: Pitch Moment Coefficient vs. Mach Number

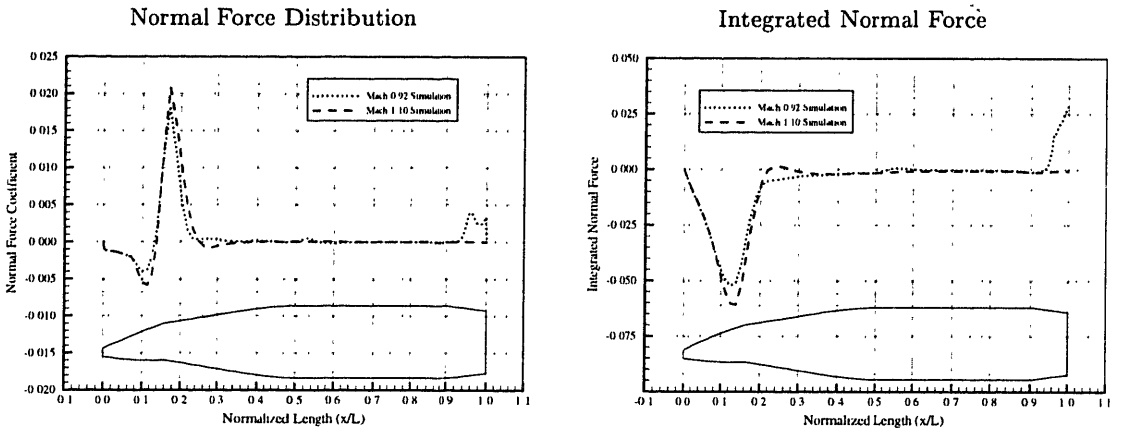

Figure 4-24: Transonic Normal Force Distributions of the Bent Shell

Figure 4-24 shows a diagram of the longitudinal distribution of the normal force, displaying the local quantity as well as the integrated development of the normal force along the bent projectile. The two cases shown are taken from Mach 0.92 and Mach 1.1, both examples of flow regimes within the transonic regime. Both show that the normal force generated by the bend is completely lost in the pressure recovery region behind the bend hinge. The two distributions are almost identical up to the point of the boat tail, when the Mach 0.92 case exhibits a large positive normal force. This normal force, and the pitch moment that is created due to its presence, are caused by the same perturbation to the position of the shocks on the boat tail as seen in the Chadwick nominal shell validation data. The presence of the bend causes a small perturbation in the velocity of the flow along the shell which is amplified as it accelerates around the boat tail. The slight velocity difference between the upper and lower surface moves the relative position of the shock surface on the boat tail, which changes the pressure distribution in that region.

The normal force and pitch moment are products of this pressure difference, from the dissimilarity in shock positions on the upper and lower boat tail surface. In the Mach 1.1 case, the velocity of the flow over the boat tail becomes completely supersonic. The position of the shock surface moves from the boat tail to the base of the shell, causing the pressure to equilibrate on the upper and lower surface. The same velocity perturbation caused by the projectile at angle of attack in the transonic regime, shown in the transonic coefficient validation case, is also seen with the bent shell. The large normal force and pitch moment spike generated by the bent shell, seen over the transonic region in Figures 4-22 and 4-23, is

due to the indirect change in the flow velocity in the boat tail region, rather than any direct control force generated on the fuze. While this result is interesting, it does not say too much about the effectiveness of the bend design in the transonic region, since the specific bend parameterization of the fuze has little to do with the production of the large normal force and pitch moment seen in the transonic regime.

In the case of the sliced fuze, it has already been demonstrated in Section 3.2 that significant flow field changes occur in the transonic regime. The slice distortion has a tendency to cause severe gradients in the flow at the slice junction with the body. This can lead to the presence of re-entry flow conditions if the inertia of the main flow is sufficiently small to allow the adverse pressure gradients behind the slice to alter the flow direction. Figure 4-25 shows the longitudinal normal force distribution over the 50° slice case at Mach 0.92 and 1.1. The slice configuration creates a large disturbance to the pressure and velocity of the flow over the entire shell body. The strange behavior seen in the subsonic portion of the coefficient profiles is almost entirely due to the viscous separation of the flow as it passes over the slice. The region of slow moving fluid on the upper surface of the shell makes a clean analysis of the coefficient trends very difficult. The re-entry flow region generated by the slice propagates down the shell causing all kinds of bizarre pressure and velocity effects in the transonic regime.

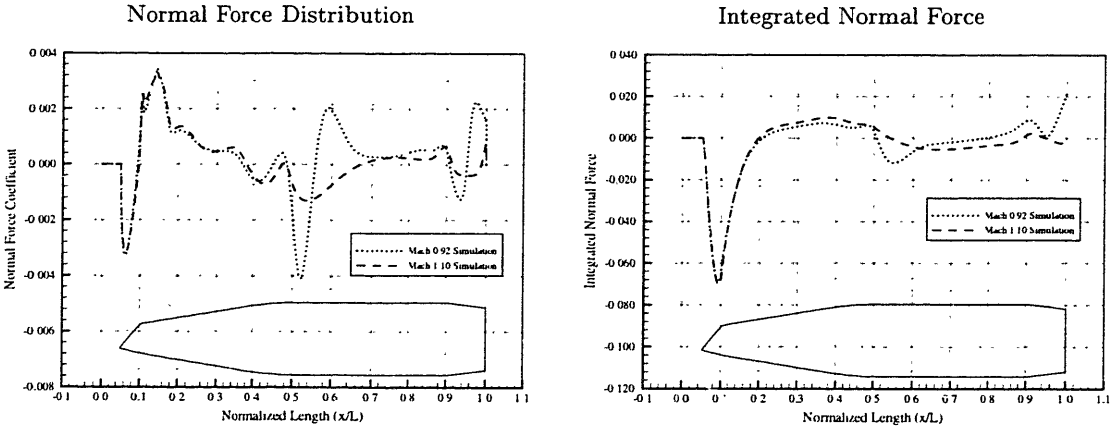

Figure 4-25: Transonic Normal Force Distributions of the Sliced Shell

Chapter 5

Design Performance Evaluation

The preliminary results for the asymmetric projectile design study have been documented in Chapter 4. The main focus of the aerodynamic study consisted of numerical predictions of the basic forces and moments generated by the two asymmetric design concepts. The next step in the design process is to create a suitable design metric to evaluate the various fuze geometries, in order to select a parameterization which will offer the optimum control authority and trajectory offset during the flight. The previous chapters have focused on the aerodynamic characteristics of the deformed shell geometries without any reference to the actual dynamics inherent in spin-stabilized projectile motion. This chapter will attempt to take the information gained from the computational study, and utilize it to effectively evaluate the designs based on a broader picture of the projectile dynamics.

A complete description of the complicated motion of a high spinning rigid body requires a six degree-of-freedom simulation which accounts for all the dynamics of the body. In the case of a projectile in flight, this system of equations is complicated by the aerodynamic forces acting on the body, which are non-linear functions of the projectile's position, velocity, and acceleration. The common approach in ballistic avionics is to linearize the equations about a trim point, and treat the motions of the body as perturbations from this trim state. This modeling technique neccesitates creating a large aero-data base which consists of the basic aerodynamic derivatives for the projectile as a function of Mach number. The motion of the projectile can then be solved by stepping the trajectory in time; calculating the forces and moments on the body, and projecting the position and velocity of the shell to the next time-step.

It is difficult to glean any meaningful physical insight from this numerical recipe, since the calculations are cumbersome and completely non-analytic. Making evaluations of preliminary aerodynamic designs based on this system would be almost impossible. It was necessary to devise a design metric which would provide reasonable information on the effectiveness of the different designs, and incorporate a sufficient understanding on the dynamics of the augmented projectiles. In order to accomplish this goal, it was decided to decouple the projectile dynamics into two separate systems of equations for angular motion and translational motion. In this case, angular motion describes the dynamics of the projectile in the pitch-yaw plane, while translation accounts for the ballistic trajectory of the shell treated as a point mass in flight.

The decomposition was designed so that a suitable angular trim condition could be defined using the pitch-yaw motion of the asymmetric shells, followed by a more complete description of the effects of this trim state on the ballistic trajectory. The trim angle problem is addressed in Section 5.1, which starts from a numerical description of the angular motion of the shell, followed by a derivation of a reasonable trim condition for this motion. The trim condition is the basis for the design metric, which is used to evaluate the designs from the results described in Section 4.2. Section 5.2 continues the evaluation procedure by examining the changes in the trajectory of the deformed shells, using a 3-DOF simulation tool. The final step in the evaluation process is Section 5.3 which investigates several additional *secondary* metrics used to evaluate the overall performance of the projectile designs.

5.1 Trim Metric Evaluation of Results

Numerical simulation of the motion of a body is a robust way to display the actual dynamics described by a complicated system of the equations. The physical constraints on ordnance projectiles most often require that they be statically unstable, necessitating a high rate of spin for gyroscopic or dynamic stability. The specific projectile used for most of this study is indeed unstable, demonstrated by the positive sign of its pitch moment derivative. This means that without sufficient spin, perturbations to the projectile's angle of attack in flight will lead to catastrophic, *tumbling* motion of the shell. The high spin rate gives the projectile dynamic stability by introducing a large angular momentum in the longitudinal direction

of the shell body, which couples with the moments caused by angular perturbations to generate precessional motion.

5.1.1 Angular Motion of the Projectile

A complete system of equations describing the precessional motion of a spinning projectile in flight can be derived using Newton's statement about the time rate of change of linear momentum equaling the sum of applied forces. The relationship between the angular rates of the system and the resultant moment falls directly from these equations. The difficulty lies in the choice of axis system in which to express the motion of the projectile, since the rotation of the projectile can result in ambiguity over whether the axis is fixed in inertial space or spinning with the body. The choice of an axis system naturally produces exactly the same motion; the differences in the formulations are only a function of the complexity necessary to decompose the moments on the body. Since the static coefficients calculated for this study were consistent with the aeroballistic axis system, this system has been implemented to derive the basic angular equations of motion.

An excellent derivation of the aeroballistic moment equations and the development of an analytic solution for these equations using the *tricyclic theory* can be found in a technical report by Vaughn [35]. A detailed development of this derivation is not useful for the present application, therefore only a summary of the relevant equations and assumptions will be introduced. The use of an aeroballistic axis system, shown in Figure 5-1, as a directional framework provides the most natural development of the angular motion of spinning projectiles. This non-rolling axis system, which defines the angular position of the projectile in terms of the angle of attack (α) and side slip angle (β), results in a very simple description for the moment equations about the y and z body axes, using several reasonable assumptions.

Using the aeroballistic axis system, the applied aerodynamic moments on the projectile's body can be easily broken down into linearized coefficients of the wind-axis angles and their derivatives. The introduction of a trim moment (M_0) in the applied moment equation is necessary to generate the motion of the asymmetric projectiles. Since the direction of the trim moment depends on the orientation of the non-rolling fuze section, which is fixed in inertial space, a direction convention must be devised. Figure 5-2 shows a 2-D diagram

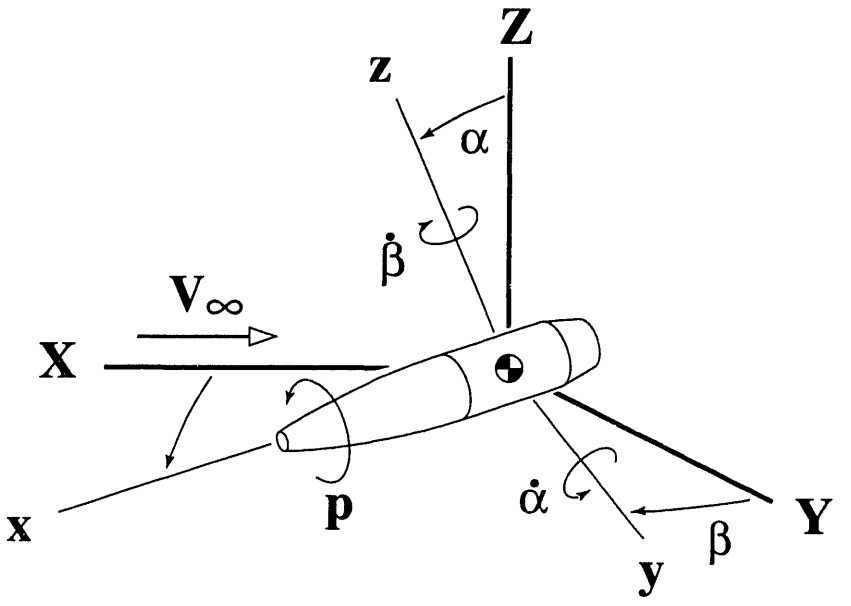

Figure 5-1: Gyroscopic-Wind Axis System

of the fuze roll angle referenced to the non-rolling body axes. In this system the fuze roll angle (θ_{fuze}) is referenced to the direction of the trim moment of the shell. This can be the source of confusion since the force produced by the distortion is 90° out of phase with this orientation, but it is the most natural way to define the trim quantities.

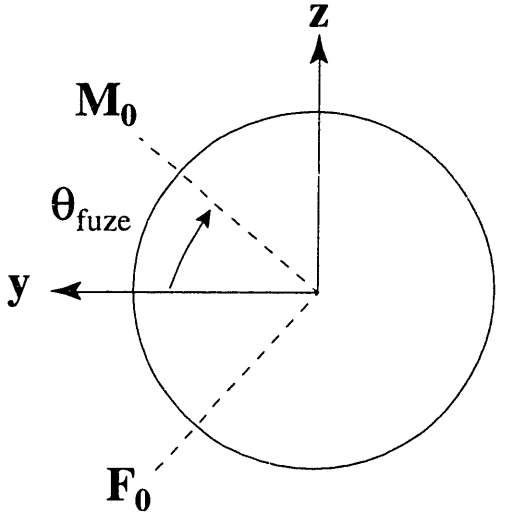

Figure 5-2: Definition of Fuze Roll Angle

The following system of equations follow from the definition of the trim moment direction taken in the aeroballistic framework.

$$\sum \mathrm{M_y} = I\ddot{\alpha} - \dot{\beta}pI_x \tag{5.1}$$

$$\sum \mathrm{M_z} = -I\ddot{\beta} - \dot{\alpha}pI_x \tag{5.2}$$

where the applied moments on the body are

$$\sum \mathrm{M_y} = \mathrm{M}_\alpha\alpha + (\mathrm{M}_q + \mathrm{M}_{\dot{\alpha}})\dot{\alpha} + \mathrm{M}_{p\beta}(p\beta) + \mathrm{M}_0\cos(\theta_{\mathrm{fuze}})$$

$$\sum \mathrm{M_z} = \mathrm{N}_\beta\beta - (\mathrm{N}_r + \mathrm{N}_{\dot{\beta}})\dot{\beta} + \mathrm{N}_{p\alpha}(p\alpha) + \mathrm{M}_0\sin(\theta_{\mathrm{fuze}})$$

These two equations follow from the following assumptions:

1. The applied aerodynamic moments can be derived based only on moments due to q, r, α, β, $\dot{\alpha}$, and $\dot{\beta}$; plus Magnus moments combining roll rate and angle.

2. A symmetry assumption, therefore products of inertia are practically zero; which means $I = I_{yy} = I_{zz}$, and $I_{xx} = I_x$

3. The assumption that the roll rate is constant, therefore $\dot{p} = 0$

4. The damping and aerodynamic lag moments can be grouped together, essentially saying that $q = \dot{\alpha}$ and $r = -\dot{\beta}$

This set of equations was numerically integrated in order to produce a reasonable picture of the angular motion for spinning projectiles. Figure 5-3 shows a diagram of the angular trajectory of the shell taken in the α-β plane. The motion was achieved by taking the trim moment produced by the bent projectile at Mach 1.1, which corresponds to $C_{\mathrm{m0}} \approx 0.1$, and directing it in the yaw plane such that $\theta_{\mathrm{fuze}} = 0$. The coefficient derivatives for the applied moment equation were taken from experimental predictions at Mach 1.1. The most important aspect of these derivatives was the pitch moment slope, which gave $C_{\mathrm{m}\alpha} = 4.0$. The motion of the projectile under the augmented control moment, directed in the yaw plane, precesses about a trim position in the pitch plane. This result is important to the definition of the trim metric used to evaluate the asymmetric fuze designs.

Figure 5-4 shows the time history of the angular trajectory simulation. The motion was taken over approximately one period, and showed that the projectile oscillated around zero

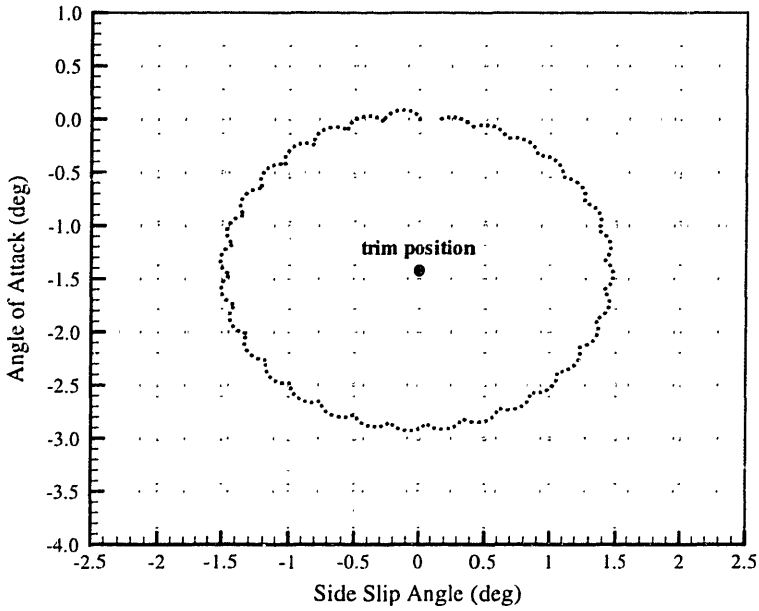

Figure 5-3: Motion of Projectile Nose in α-β Plane

side slip and a trim angle attack of approximately -1.43 degrees. This steady state result corresponds to a value equal to $-C_{m0}/C_{m\alpha}$ in degrees. The projectile was given zero initial conditions in order to isolate the effects of the moment produced by the fuze distortion. These results suggest that the motion of the projectile generates precessional orbits about a trim position which is related to the moment produced by the deformed fuze, in addition to the pitch moment coefficient derivative of the shell body. This conclusion is the foundation on which a trim state for the angular motion of the projectile was defined. The trim state allows a design metric to be derived which compares the asymmetric fuze parameterizations from the standpoint of optimum dynamic performance.

5.1.2 Steady Trim Derivation

The numerical simulations given in Section 5.1.1 provide the framework and justification for the definition of a suitable design metric for this study. The basis for this metric comes from a calculation of an *average* resultant force on the deformed projectile, which follows from a summation of the nominal force produced by the fuze distortion in addition to the force generated by the projectile body at the trim condition. The trim position of the angular motion of the shell was displayed in Figure 5-3 and deals with the trim angle around which

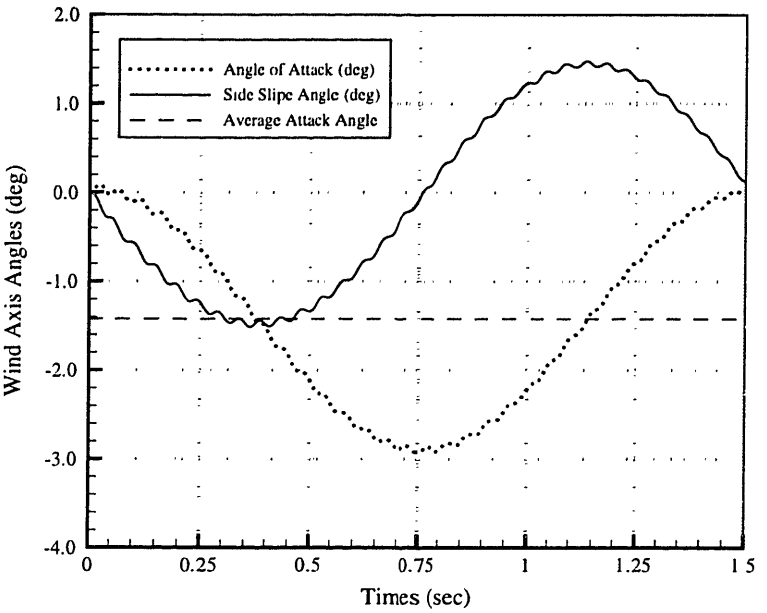

Figure 5-4: Angular Motion of Projectile Nose in Time

the projectile makes precessional orbits in the α-β plane. In a linear sense, these trimmed precessional orbits inherent the same stability properties as the nominal angular trajectory of the shell. *Stability* under this definition implies that perturbations of angular position will result in orbits which not only do not grow in time but also maintain a coherent attraction basin. This attraction basin is the trim position, which is used to calculate the resultant force on the shell.

Derivation of the resultant force on the shell at the trim angle follows most easily from the assumption of a steady state solution to Equations 5.1 and 5.2. This implies that all rate variables in the equations are set to zero. In order to simplify the treatment of this trim metric, the moment from the fuze distortions is assumed to be directed completely in the yaw plane, therefore $\theta_{\text{fuze}} = 0$. From this simplification, the moment equation in the z axis immediately falls out, which follows the results found in the angular simulation in which a zero average side slip angle was shown for one period of motion under the same fuze conditions. In coefficient form, this leaves an equation for the moment in the yaw plane as the following

$$\sum C_{\text{m}} = (C_{\text{m0}} + C_{\text{m}\alpha}\, \alpha_{\text{trim}}) \tag{5.3}$$

The simplification ignores all the precessional motion seen in the angular simulations, but maintains the static relationship between the moment produced by the deformed fuze and the moment generated by the body. It can be seen from this equation that given an unstable, positive pitch moment derivative; a positive augmented moment will result in a negative, pitch down, trim angle. The resultant force, now directed in the z axis, can then be easily calculated using the trim angle from Equation 5.3 and the force generated by the projectile asymmetry (C_{z0}).

$$\sum C_z = (C_{z0} + C_{z\alpha}\, \alpha_{\text{trim}}) \tag{5.4}$$

Under most flight conditions, a positive normal force generated by the fuze distortion will also result in a positive pitch moment. It can be seen from Equation 5.4, as mentioned in Section 1.1, that the trim angle generated on statically unstable projectiles will be opposite in direction to the nominal force produced by deformed fuze. The two effects produced by using asymmetries on the shell fuze fight each other in terms of the overall control authority of the projectile. This result is a definite weakness of fixed-trim control for these projectiles, but can be overcome by placing the control force sufficiently forward of the projectile's center of gravity, in order to maximize the pitch moment produced by the asymmetry.

In order to compare the control effectiveness of the deformed shells with other designs, it was deemed necessary to compute the forces in velocity centered axes. The pertinent coefficient, trim lift, can be found using a rotation of the normal and longitudinal body forces, which incorporates the drag of the projectile into the metric. As seen from Figure 5-3, the precessional orbits of the projectile are really quite small, showing angular magnitudes in the range of one degree, so the trim coefficient is not significantly altered by the rotation.

$$\begin{aligned} C_L\,(\text{trim}) &= C_z \cos(\alpha_{\text{trim}}) - C_x \sin(\alpha_{\text{trim}}) \\ &= \left[C_{z0} - C_{m0}\left(\frac{C_{z\alpha}}{C_{m\alpha}}\right)\right] \cos\left(\frac{C_{m0}}{C_{m\alpha}}\right) + C_x \sin\left(\frac{C_{m0}}{C_{m\alpha}}\right) \end{aligned} \tag{5.5}$$

Calculation of the trim lift, therefore, is found to be an extremely coupled equation of all body centered forces and moments. Use of this quantity as the defining metric in the evaluation of the shell geometries incorporates the basic dynamics of the gyroscopic motion inherent in spinning projectiles, while reducing the complicated precessional orbits into a steady state position.

5.1.3 Asymmetric Projectile Trim Results

The derivation of the trim lift as the design metric for this aerodynamic study necessitates revisiting the results from the investigation displayed in Section 4.2. A reasonably careful explanation of the aerodynamics of the asymmetric shells was attempted in that section, leaving only performance evaluation questions for the final presentation. While some of the results of the performance criterion are evident from the trends in pitch and normal force, one can see from the conclusions reached in Section 5.1.2 that it is still important to incorporate both of these quantities in the overall evaluation of the asymmetric projectile designs.

Figure 5-5 shows the variation in the trim metric with slice angle for two different slice pivots (2.2" and 2.7") at Mach numbers of 1.1 and 1.4. The first conclusion that can be made from these results is that placing the slice pivot position in the furthest aft position is the optimal slice configuration. The trim lift trend with slice angle is very flat, but appears to have a maximum around 50° for all the cases tested. This is an interesting result because in Section 4.2.2 the trends in slice angle for the two Mach numbers were distinctly different for both normal force and pitch moment. This can be attributed to the fact that the lift generated at the trim condition is a function of both the nominal control force and moment. The interaction between the two, captured in Equation 5.5, appears to scale the resultant trim force produced by the asymmetric projectile. In other words, although a larger slice angle generates a larger trim angle, this gain is canceled since the configuration also produces a larger control force oriented in the opposite direction.

Figure 5-6 shows the trim metric trend as a function of bend angle. In this control design there are really no surprises from those seen in the pitch and normal force results in Section 4.2.3. The lift generated by the projectile at trim increases with increasing bend angle. The different bend geometries show that the optimum placement of the bend hinge is the furthest aft position possible on the shell body. The trends at the two Mach numbers appear to be quite similar, the only difference being that the trim lift-bend angle slope is larger in the Mach 1.4 flow condition. All of the trends with bend angle are quite linear except at extremely large angles, greater than 20 degrees.

The trim metric trends over a complete Mach sweep for a candidate geometry from each of asymmetric design concepts is shown in Figure 5-7. The supersonic region shows

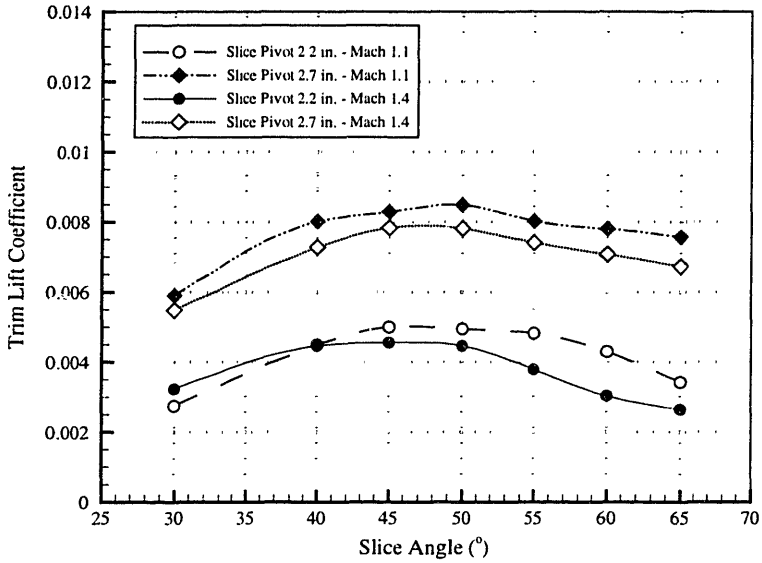

Figure 5-5: Variation in the Trim Metric with Slice Angle

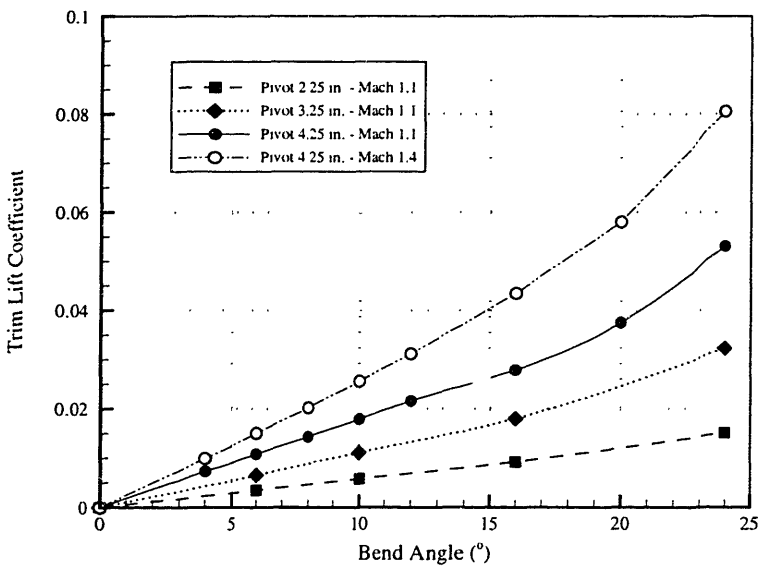

Figure 5-6: Variation in the Trim Metric with Bend Angle

very well behaved trends, with increasing Mach number leading to increased trim lift. The trends in the transonic regime are a result of the sign change in the normal force, displayed in the results from Sections 4.2.2 and 4.2.3. The sharp peak in the trim lift generated by the bent configuration at Mach 0.9 is directly related to the forces produced in the boat tail region, which have already been documented in the normal force and pitch moment distribution plots for that configuration.

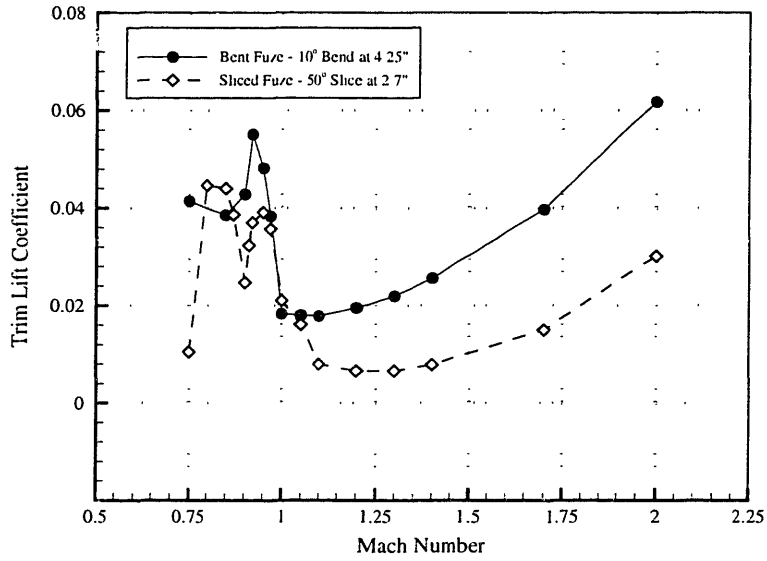

Figure 5-7: Variation in the Trim Metric with Mach Number

The major conclusion which can be reached from the trim lift Mach trend is that the bent configuration is superior to the slice design over almost the entire flight profile of the projectile. Since the candidate slice design represents the optimum configuration given the volume constraints already discussed, it appears that the bend design is a superior concept. This conclusion needs to be supported by direct numerical simulations of ballistic trajectories using the two asymmetric projectile designs. The next section presents results using a modified 3-DOF simulation tool, which calculates a complete projectile trajectory, and allows roll controlled nominal force and moments to be introduced into the dynamics. This added facet makes performing a reasonable measure of the control effectiveness of the two designs possible through directly observing their trajectory offset potential.

5.2 Trajectory Simulations

The angular motion simulation presented in Section 5.1.1 represents a *first cut* attempt at describing the dynamics of the augmented projectiles. The main reason for designing this capability was to provide some proof that the trim conditions assumed in the derivation of the design metric were reasonable. Unfortunately, the angular motion of the spinning shells is limited in its ability to provide useful information about the effects of the fuze distortions on the overall ballistic trajectory. A simulation program, which incorporates the translational dynamics of ballistic projectiles, has been implemented to make predictions on position, velocity, and heading during a complete flight. This model takes into account the control force and moment, generated by the asymmetries, by incorporating them into the trim state of the projectile and the calculation of external forces at every time step.

The simulation is only a model of the dynamics present in a real ballistic trajectory and makes many assumptions in order to simplify the problem. The main assumption of the simulation is that the projectile exists in its trim state at every instant in time. This is certainly not true since it has been shown that the control forces, due to the fuze distortions, cause the projectile to precess about its trim state with a specific period. The aerodynamic forces on the body are calculated by using linearized aerodynamic coefficients, which are setup as functions of the flight Mach number. Further steps are also taken to compensate for atmospheric density changes. The end result is a fairly robust simulation program, which uses only three degrees of freedom; but accounts for changes in the projectile spin, orientation, and direction of the fuze control force and moment.

The simulation has also been modified to take into account the time rate of change of the flight path angle ($\dot{\gamma}$), and its effect on the projectile orientation. The high spin rate and curvature of the ballistic trajectory causes the projectile to yaw to account for the directional change in the angular momentum. This angular trim state is called the *yaw of repose* and can be analytically modeled by treating the projectile as a point mass, solving for the change in flight path angle, and using the spin rate of the projectile to calculate the trim side slip angle. Simplifications to this basic idea lead to the following equation:

$$\alpha_{\text{repose}} = \frac{p\, I_{xx}\, \dot{\gamma}}{qSd\, C_{m\alpha}} \tag{5.6}$$

The yaw of repose is maximum near the apex of the shell flight, where the curvature of the

trajectory is greatest. The *equilibrium* yaw angle induced by this gyroscope effect generates a side force on the projectile throughout the flight which causes a large cross range drift.

Section 4.1 outlined the typical initial conditions for an ordnance projectile trajectory. The three important states; initial launch angle (Q_e), velocity (V_0), and spin rate (P_0) were all documented in Table 4.1. In order to draw comparisons for the various trajectory studies, the same initial values have been used for all the numerical simulations. The other important condition for the simulation is the time in which control is initiated. It has already been mentioned that a minimum ten second delay exists for the acquisition of GPS for position information. This delay represents the minimum time in which control of the ballistic trajectory can begin. All results in this section initiate the control of the shell ten seconds into the flight.

Useful information about the effects of the asymmetric control features can only occur when the complete Mach characteristics of the projectile are known. Mach sweeps have been completed for only two designs: the 50° slice case with pivot at 2.7", and the 10° bend case with bend hinge at 4.25". The nominal force and moments produced by these fuze distortions have been implemented into the trajectory simulation to provide an accurate measure of the trim state of the projectile during the flight. The simulation completes a calculation of the trim conditions, already documented in Section 5.1.2, at every time step. The only difference between the trajectory offset and the trim metric is that the effect of the trim is integrated over a complete flight, and the simulation takes into account the change in dynamic pressure.

5.2.1 Cross Range Offset

The initial ballistic simulations were arranged to illustrate the offset to the cross range trajectory. This was accomplished by placing the roll angle of the fuze in a constant direction during the flight. Figure 5-8 shows a cross range trajectory comparison for the two asymmetric designs, as well as the nominal flight of a standard projectile. The effects of the yaw of repose are clearly evident from this diagram, which shows a baseline cross range drift of almost 700 feet for a 50 second flight. The slice distortion is only able to cancel the nominal drift of the shell. The bent design shows far superior performance, altering the cross range of the projectile by almost 1500 feet. This trajectory offset is probably not significant enough for object tracking, but could improve the overall accuracy of the shell.

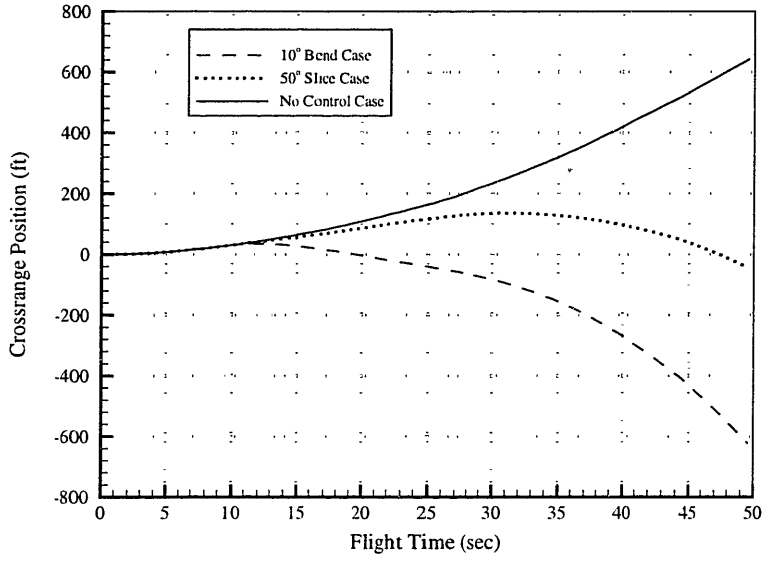

Figure 5-8: Cross Range Trajectory Comparison

The other interesting result from these simulations is the calculation of the trim angle reached by the projectile during the flight. Given the discussion in Section 5.1.1, this trim angle represents a reasonable measure of the motion of the shell. The stable precessional motion of the projectile displayed a maximum radius equal to the trim angle, thus migrations of only twice the trim angle are the maximum departure of the shell in flight. Figure 5-9 shows the trim side slip angle reached during the three simulations of the asymmetric designs and nominal shell outlined above. The large discontinuity in the diagram, ten seconds into the flight, represents the onset of control. The ballistic simulation results show that trim angles greater than 1° are never reached throughout the flight, signifying that the angular excursions of the projectile are not unreasonably large. Non-linear aerodynamic characteristics of the basic static derivatives are unlikely at these small angles.

5.2.2 Foot Print Trajectory Study

Simulations have also been completed for the two design concepts on a fuze roll angle sweep from 0 to 360°. Results from this *footprint* study are shown in Figure 5-10. Notice that the nominal terminal location of the shell, without control, has been subtracted off to display only the offset to the trajectory. This can be viewed as the available boundary in which the asymmetric designs could steer the projectile for better target accuracy. The main

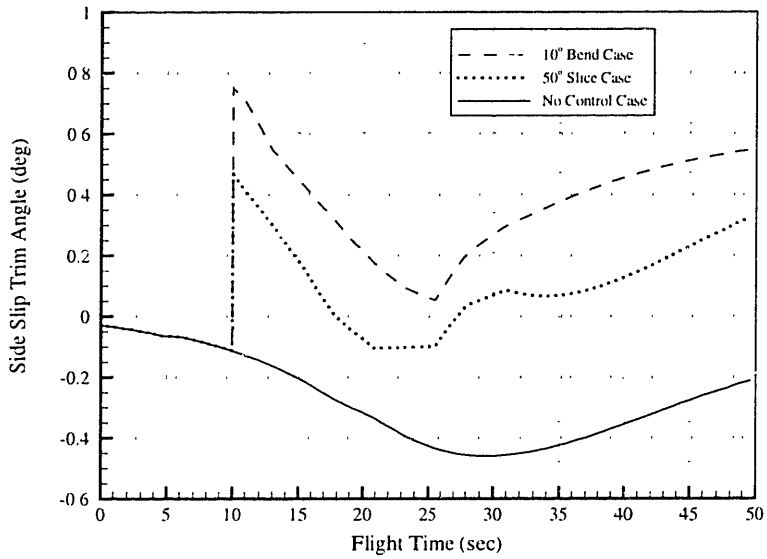

Figure 5-9: Side Slip Trim Angle Comparison

conclusion to be reached from this diagram is that the bent configuration is far superior to the slice design in terms of trajectory offset. Trim metric calculations, taken at Mach 1.1 and 1.4, showed that the bend design exhibited superior performance, establishing that the design metric provides a useful evaluation of the fuze augmentations.

5.3 Secondary Metrics

The two most important measures of the overall performance of the asymmetric projectiles have now been completed. The trim lift represents a simplified way to examine the different design parameters and select a configuration with optimum control authority. The results of the angular motion of the spinning projectiles showed that the trim angle was a reasonable measure of the steady-state motion of the deformed shells. The trajectory simulations were implemented to support the choice of the trim lift as a proper design metric for this study, by studying the actual offset to the terminal flight position of the shells using the two design concepts. Evaluation of the design concepts using both of these procedures showed that the bend distortion provided the most control authority.

There does exist some additional factors which could influence the choice of designs for usage in a fixed-trim guidance scheme. These are secondary metrics in that they do not

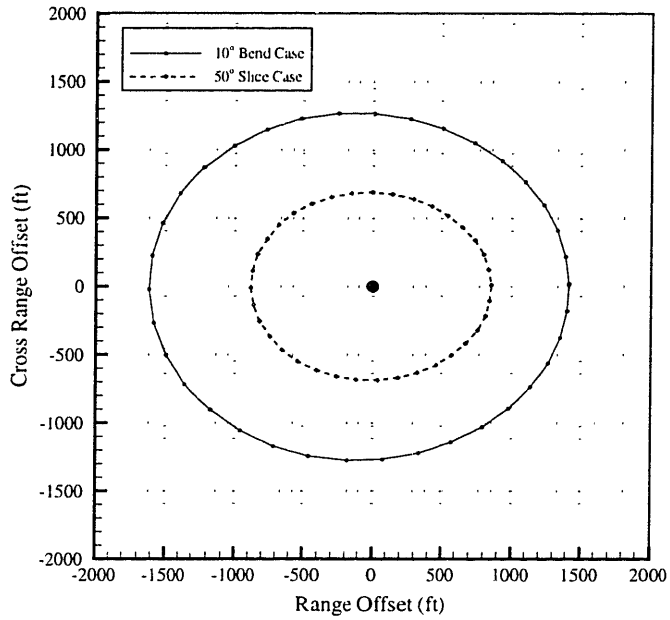

Figure 5-10: Foot Print Trajectory Comparison

directly affect the trim conditions reached by the projectile and are therefore not really considered in either of the evaluation procedures of the last two sections. This section will attempt to present some motivation for examining some additional aerodynamic factors which are affected by the fuze distortions in order to more fully investigate the strengths and weaknesses of the designs.

5.3.1 Sensitivity of Drag

The evaluation procedure outlined in the previous sections ignores the drag and range penalties due to the fuze distortions. A drag increase could potentially come from two main sources, which are both tied into the basic premise of fixed-trim control. The first source comes from the fact that slicing or bending the fuze of a projectile has the potential to increase the drag by increasing the cross sectional area seen by the free stream, as well as changing the position and strength of the shocks emanating from the shell body. Figure 5-11 shows the drag coefficient variation at Mach 1.4 for the two design concepts with respect to the two main parameters in the designs, slice angle and bend angle. The diagram shows that an appreciable change in the drag does occur when these parameters are altered, with a maximum increase of approximately 10%. The designs demonstrate a significant penalty in order to deform the projectile surfaces sufficiently for effective trajectory control.

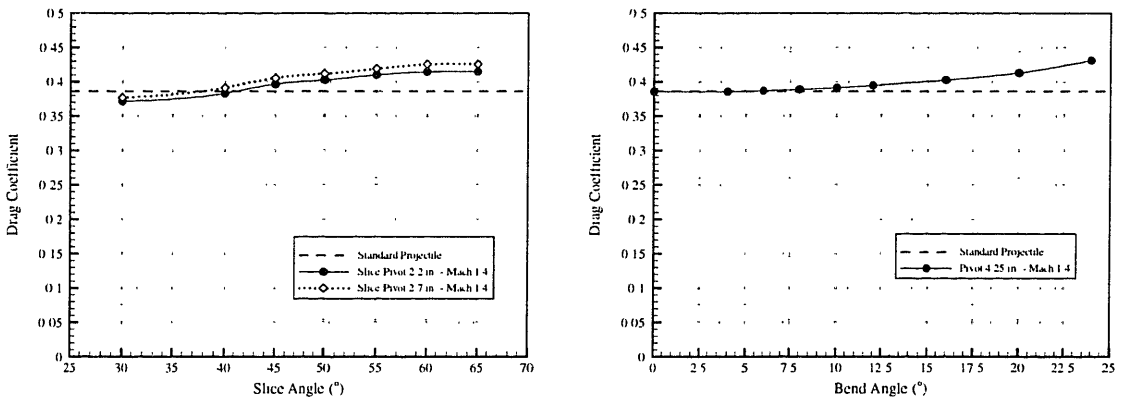

(Slice Case) (Bent Case)

Figure 5-11: Variation of Drag with Design Parameter

This result can be illustrated in a broader context by Figure 5-12, which shows the drag Mach profile for an example from each design concept, in addition to the the results from the baseline shell. This figure shows that the 10° bend design pays very little drag penalty, while the 50° slice concept has a significant increase in the drag coefficient in the supersonic Mach regime. This is due to the large, flat surface which is created from slicing the projectile fuze. The slice surface generates a significant amount of normal force, but pays a penalty from absorbing free stream momentum by generating higher drag.

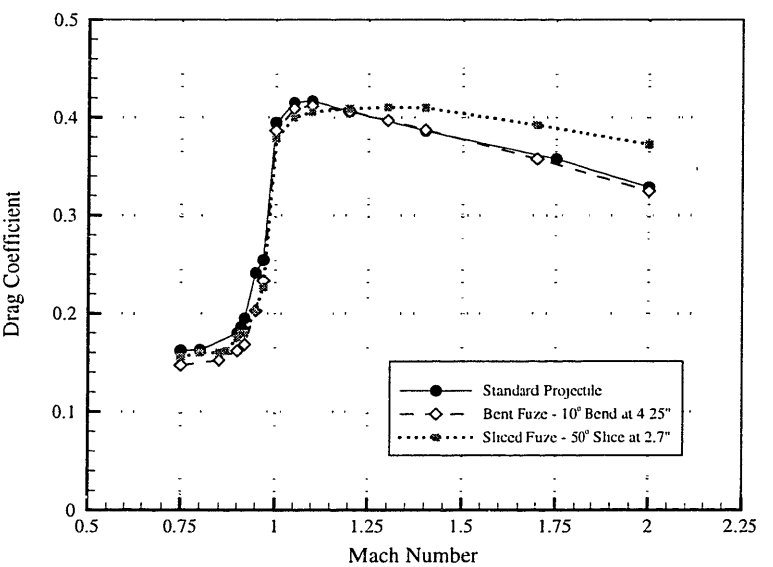

Figure 5-12: Variation of Drag with Mach Number

The other drag penalty which occurs from implementing fixed-trim control comes from the basic fact that a projectile flying at a trim angle generates larger drag. The same effects which produce a large normal force at the trim angle, also generate significant forces against the forward motion of the projectile. Figure 5-13 shows a simple illustration of this result for the two design concepts by displaying the percentage drag increase as a function of angle of attack at Mach 1.1. Figure 5-9 showed that angular motion in the range of two degrees was certainly possible with the augmentation schemes tested in this investigation. This could lead to drag increases as much as 5%. While this number may not seem like a huge price to pay for effective control of a spinning projectile, expansion of the control concepts to larger bend angles or slice surfaces would certainly lead to a significant increase in drag penalty.

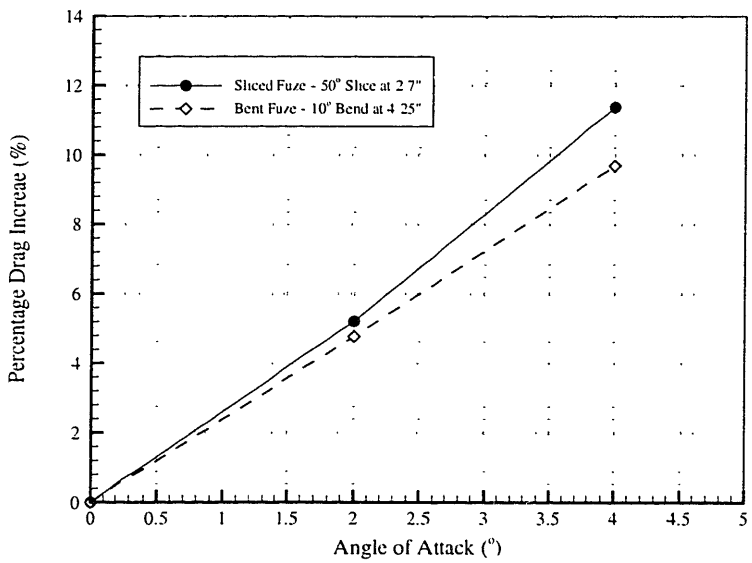

Figure 5-13: Variation of Drag with Angle of Attack

The effect of this drag increase can be illustrated by Figure 5-14 which shows the results from a calculation of the change in the range of a ballistic projectile with variation in drag. This diagram was created by fractionally increasing the drag in trajectory simulations using the 3-DOF simulation program outlined above. It is unlikely that the fuze distortions will increase the drag so uniformly in all Mach numbers, and yet Figure 5-14 is a good approximation of the sensitivity of the trajectory range to the shell drag. Thousands of feet of potential range can be lost with only a few percentage points of drag increase. This

range decrease results in less effective munitions and the potential for greater endangerment of military personnel.

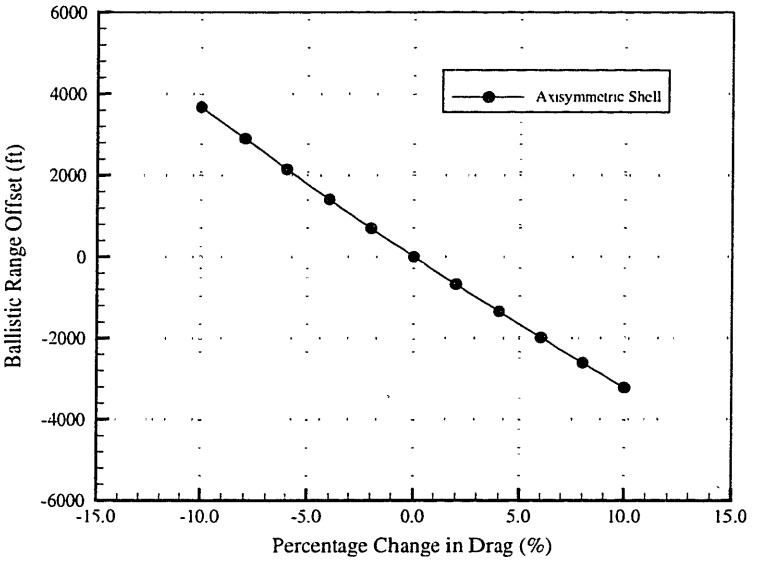

Figure 5-14: Sensitivity of Range to Drag Coefficient

Drag was not a high priority for this aerodynamic design study, since it did not directly affect the evaluation of the control authority generated by the asymmetric shells. This section was made to motivate some additional concern on the possible penalties which exist from implementing fixed-trim control. The drag characteristics of the two designs are not very good since care has not been taken to make the configurations optimal with respect to this parameter. Further study needs to be done to address this problem, which could introduce more subtle alterations to the fuze surface for drag reduction purposes. At this time, the asymmetric projectile designs tested in this study will adversely affect the ballistic range of gun-launched munitions.

5.3.2 Sensitivity of Magnus Effects

Experimental studies have already been mentioned which show a relationship between boundary layer thickness and Magnus effects [19, 17]. The presence of the various fuze distortions has a definite influence on flow field and boundary layer propagation along the surface of the shell, making their influence on Magnus forces a distinct possibility. A computational study has been completed to make some reasonable predictions on the influence

of the asymmetries on Magnus effects. These investigations have been performed by placing a spinning boundary condition on the unaltered section of the shell, and placing the body at 4° angle of attack. The simulations are extremely costly to perform, therefore a specific flight condition of Mach 1.1 was chosen in order to determine a reasonable *order of magnitude* for the change in the Magnus force and moment.

In order to ascertain the relationship between the angular position of the deformed fuze and the Magnus effects, two fuze angles have been chosen: 0 and 180 degrees. These angles, which are defined based on Figure 5-2, effectively bound the influence of the fuze distortions by reversing the position of the convex portion of the surface geometry (the junction between the slice plane or bent fuze section and the shell body). This section of the asymmetric shells has been shown to be the region in which changes to the boundary layer are greatest because of the acceleration of the flow around the surface feature. Flow separation phenomena in the simulations completed on the sliced projectile designs also support the conclusion that the position of the fuze distortions has important consequences on the propagation of the boundary layer.

Figure 5-15 shows the results of the study for the bend augmented designs. The calculations have been prepared in terms of changes in the nominal results from the baseline shell, in order to clearly assess the deviations in Magnus effects. Results show rather staggering changes in the side force of as much as 20-50% at the bend angle of 20°. Deviations from baseline Magnus moments are less extreme, probably due to the placement of the center of Magnus force close to the shell c.g., but still change as much as 10-20%. These results can be further supplemented with actual side force and yaw moment distributions shown in Figure 5-16. The distributions are taken from the 20° bend configuration, but are representative of all of the bend geometries. The main feature to notice is the difference in the development of the Magnus force and moment for the two fuze orientations. The $\theta_{\text{fuze}} = 0$ condition implies that the fuze is bent into the wind, thus the boundary layer on the leeward side of the shell is enlarged.

Results of numerical simulations of the sliced fuze design show qualitatively the same Magnus influences. The change in the baseline side force and Magnus moment are shown in Figure 5-17 for a range of slice pivot locations. The changes are actually more drastic for this particular design than the bent fuze. This makes reasonable sense given all the results presented earlier on the flow separation which occurs over the slice pivot under certain flow

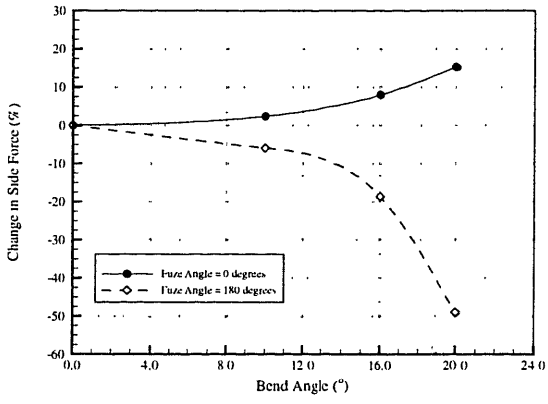

(Change in Side Force)

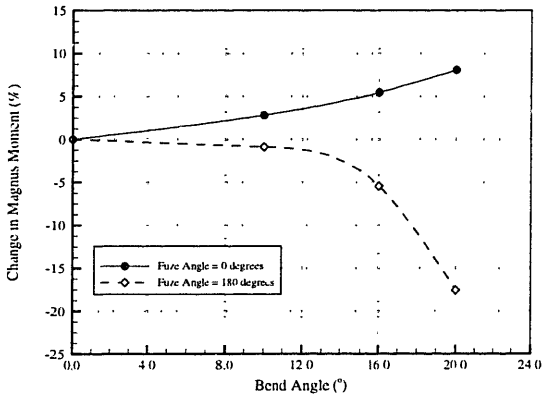

(Change in Magnus Moment)

Figure 5-15: Sensitivity of Magnus Effects to Bend Angle

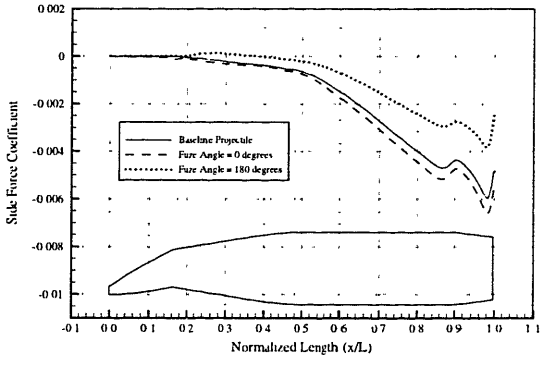

(Side Force)

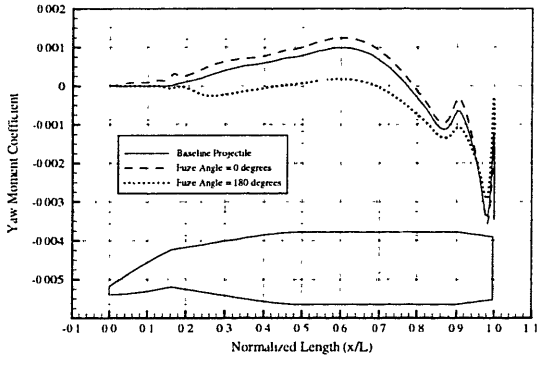

(Yaw Moment)

Figure 5-16: Longitudinal Distribution of Magnus Effects for Bent Shell

conditions. The large velocity gradients over the slice junction with the shell body cause the boundary layer to thicken as it propagates down the shell, generating an increase in Magnus forces. The distribution results, shown in Figure 5-18, for the slice design with pivot location at 3.5 inches support this conclusion. The thickening of the boundary layer immediately after the slice distortion causes effects which propagate downstream, generating increased Magnus force and moment along the shell. The Magnus forces are increased when the slice junction (pivot) is on the leeward side of the shell surface. The re-entry flow phenomena and pressure distribution results all support the conclusion that the boundary layer is being severely altered in this region.

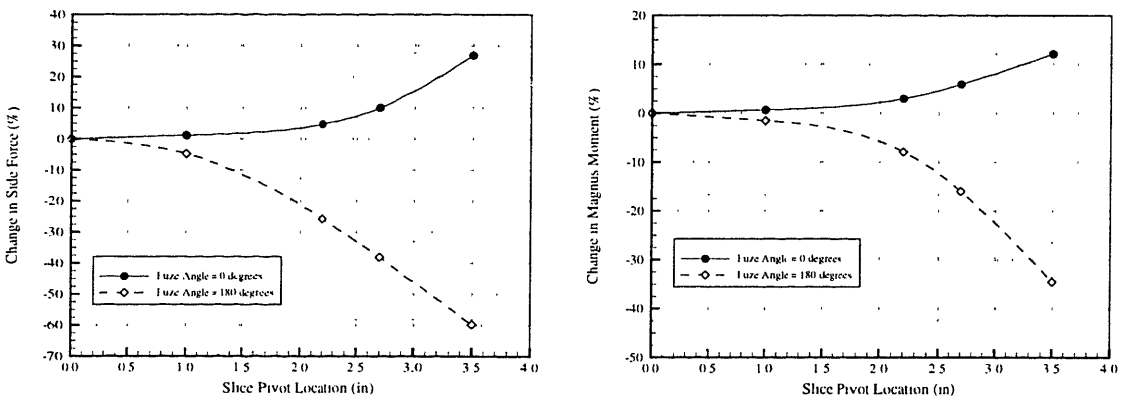

(Change in Side Force) (Change in Magnus Moment)

Figure 5-17: Sensitivity of Magnus Effects to Slice Pivot Position

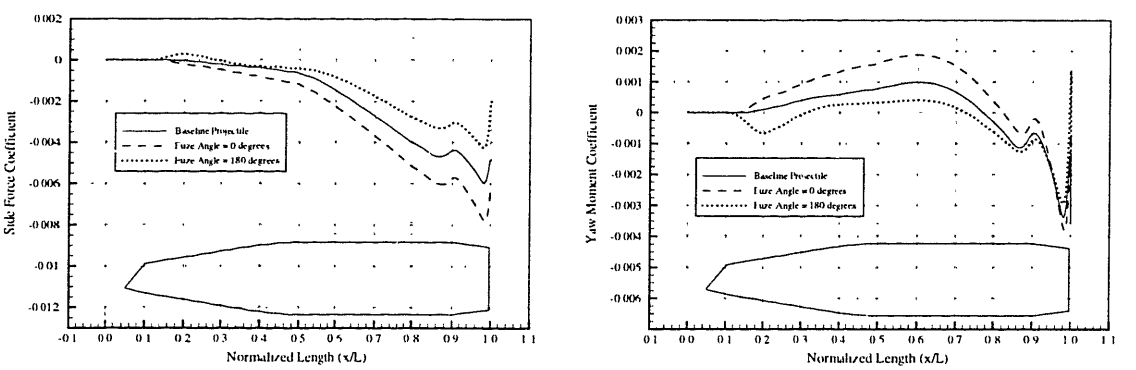

(Side Force) (Yaw Moment)

Figure 5-18: Longitudinal Distribution of Magnus Effects for Sliced Shell

The main phenomena, which generates Magnus effects, is a distortion of the boundary layer on the leeward surface of a spinning shell which alters the circumferential pressure

distribution, generating a side force and yaw moment with changing angle of attack. The fuze distortions appear to alter the thickness of the boundary layer in the region of the junction between the surface distortion and the shell body. The perturbation to the boundary layer propagates downstream altering the development of the Magnus forces along the shell. The overall result is an increase in the Magnus force when the convex portion of the fuze asymmetries is on the leeward side of the shell ($\theta_{\text{fuze}} = 0$), and an equally drastic decrease in the Magnus force when the orientation of the fuze is reversed ($\theta_{\text{fuze}} = 180$). Now that at least an approximate determination of the influence of the fuze distortions on Magnus effects has been accomplished, the question of the possible influence on the motion of the projectiles must be addressed.

The most important aspect of Magnus effects, from a dynamics standpoint, is the moment generated on the shell. This conclusion can be seen from a linear analysis of the angular motion of a spinning projectile. Numerical predictions of this motion have already been carried out in Section 5.1.1, but an approximate analytical solution also exists to the system of moment equations using the tricyclic theory [35, 7]. In the non-rolling aeroballistic axes, shown in Figure 5-1, the tricylic solution for the angular motion of a spinning projectile is given by

$$\bar{\alpha} = \bar{\alpha}_{\text{n}_\text{o}}\, \text{e}^{(\lambda_1 + \text{i}\omega_1)\text{t}} + \bar{\alpha}_{\text{p}_\text{o}} \text{e}^{(\lambda_2 + \text{i}\omega_2)\text{t}} + \bar{\alpha}_{\text{e}} \tag{5.7}$$

where the complex yaw ($\bar{\alpha}$) consists of a high frequency nutation ($\bar{\alpha}_{\text{n}_\text{o}}$), a slower precessional motion ($\bar{\alpha}_{\text{p}_\text{o}}$), and a zero frequency term ($\bar{\alpha}_{\text{e}}$) which represents the equilibrium yaw caused by trim moments and the yaw of repose. The three modes described by these dynamics were all captured numerically in the angular motion in Figure 5-3. The damping and frequency terms in Equation 5.7 are represented, using standard notation, by the aerodynamic coefficients as

$$\lambda_{1,2} = \frac{qS}{2\text{m}\text{V}} \left[C_{\text{z}\alpha}(1 \mp \tau) + \frac{\text{m}\text{d}^2}{2I_y} C_{\text{m}\text{q}}(1 \pm \tau) \pm \frac{\text{m}\text{d}^2}{I_x} C_{\text{n}\text{p}\alpha}\, \tau \right] \tag{5.8}$$

$$\omega_{1,2} = \frac{pI_x}{2I_y} \left[1 \pm \frac{1}{\tau} \right] \tag{5.9}$$

where

$$S_g = \frac{p^2 I_x^2}{4 I_y q S d C_{\text{m}\alpha}} \qquad \text{and} \qquad \tau = \frac{1}{[1 - 1/\text{S}_\text{g}]^{1/2}}$$

This system of analytic equations use the same linear assumptions mentioned previously for the derivation of the trim metric. The approximations degrade the overall solution, but they provide a clear description of the importance of the various aerodynamic coefficients to the motion of spinning projectiles. The necessary and sufficient conditions for dynamic stability in the linear case, using the definitions above, are

$$S_g > 1 \qquad \text{and} \qquad \lambda_{1,2} > 0 \tag{5.10}$$

The first condition is a statement about gyroscopic stability for a spinning body. The spin rate and physical geometry of the baseline projectile is designed so that this factor is greater than 1.5 throughout the ballistic flight, with its minimum value at launch, therefore gyroscopic stability is not an issue for these shells. The condition on the damping factors for the two modes of motion is a more serious and potentially troublesome area. Equation 5.8 shows the functional relationship of several aerodynamic derivatives on the damping terms. Studies have already shown, in Section 4.2.5, that the normal force coefficient derivative ($C_{z\alpha}$) exhibits an extremely weak dependence to the distortions placed on the fuze section. The damping derivative (C_{mq}) has a stabilizing influence on both of the modes of motion. Its dependence on projectile asymmetry has not been undertaken in this study, but could possibly be an important factor for later consideration.

The Magnus moment coefficient plays the most pivotal role in the dynamics of spinning projectiles because it simultaneously dampens one mode of motion while destabilizing another. The results for the numerical simulations of the spinning asymmetric shells showed significant changes in the Magnus moment, which were dependent on the orientation of the fuze section with respect to the spinning shell body. The 3-DOF simulation, discussed in Section 5.2, has been altered to produce the linear damping coefficients using Equation 5.8. In order to ascertain the influence of Magnus moment on the dynamic stability of the projectiles, the baseline reference condition has been compared with results increasing and decreasing the Magnus moment by 20%. Trajectory results for the two damping factors are shown in Figure 5-19, under the same initial conditions stipulated in Table 4.1. While this percentage boundary might seem rather excessive, results at Mach 1.1 showed changes to the Magnus moment, due to the fuze distortions, which well within this envelope.

Linear analysis shows that the nutational motion of the symmetric projectiles is only

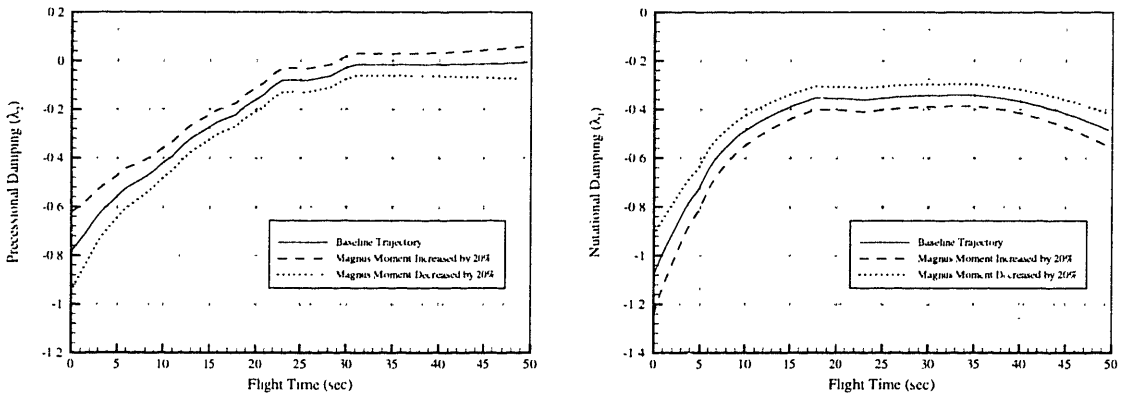

(Precessional Damping) (Nutational Damping)

Figure 5-19: Variation of Damping Factors with Time of Flight

marginally stable during a ballistic flight, therefore even small changes to the Magnus moment have the potential to drive the nutational motion of the shell unstable. The instability of the Magnus-enlarged projectiles, which occurs around 30 seconds into the flight, takes place completely within the transonic regime. This result makes the numerical predictions on the sensitivity of the Magnus effects at Mach 1.1 reasonable if not a bit conservative, considering the increase in viscous phenomena in transonic flow conditions. It was mentioned in Chadwick [7] that the marginal stability of the projectiles during the descending flight is counteracted by the non-linear Magnus moment effects which occur as yaw angle increases. The fuze distortions could influence the stability of the projectiles through the changes in the Magnus moment, but the linear analysis presented here is not sufficient to ascertain whether non-linear Magnus moments will effectively stabilize the shell in flight. A clear link, though, has been made between the projectile asymmetries and a possible stability problem due to increases in the Magnus moment characteristics.

Chapter 6

Final Design and Conclusions

The initial results and evaluation of the basic asymmetric design concepts has now been presented. This chapter follows the performance analysis discussion with a complete review of fixed-trim guidance configurations as well as final conclusions derived from this study. Section 6.1 reviews all the information gained from the computational investigation in light of the criteria set forth in Chapter 5. An attempt is made to highlight the essential flow features and problems associated with each design. The section concludes with some observations on particular design strategies and further iterations which could provide improved aerodynamic performance. These configuration ideas are based mainly on pressure distribution results from the basic designs, as well as further thought into the limitations placed on the design by the initial constraints of the problem.

Section 6.2 takes up this theme of iterative design established by the previous section. Several additional projectile configurations, which are based on small modifications to the original concepts, have been numerically tested . This section is meant to provide some motivation that the basic design ideas studied in this investigation are certainly not the last word on the subject of configurations for fixed-trim guidance. Small deviations from these initial geometries, which required very simple surface alterations, can provide substantial increases in performance. The two most promising projectile configurations are explored in Section 6.2 and aerodynamic results from numerical simulations are presented for these configurations. An attempt is also made to explain the aerodynamic benefits of these designs, using comparisons based on the results from the initial asymmetric configurations.

Section 6.3 presents the final words and conclusions of this investigation based on the

results obtained from both the initial designs as well as subsequent *improved* concepts. This section is meant to act as a recapitulation of the major themes observed in the study of asymmetric projectile configurations for fixed-trim guidance. Section 6.1 outlined several weaknesses present in the current schemes, and this topic is reviewed in light of all the evaluation results. Some time is also spent discussing strategies and future research which could provide a more complete justification of the results obtained in this study. There are several areas in which significant information is lacking on the aerodynamic characteristics of these deformed shells, which would be required if a practical implementation is going to be considered. In addition, given the results found in Section 6.2, there is some motivation to loosen the constraints imposed on the shell configurations and treat the problem as an exercise in design optimization, using all the methods available with this strategy. A more robust and complete analysis, using this methodology, could reap significant performance and aerodynamic improvements over the designs tested in this study.

6.1 Weaknesses of Initial Design

A thorough evaluation of the basic designs has already been attempted in Chapter 5. This section is only meant to outline some of the major themes and weaknesses inherent in the two design configurations tested in this study. Pressure coefficient and force distribution results have provided the bulk of the information needed for this evaluation. Integrated quantities, such as force and moment coefficients, while beneficial to providing an accurate dynamic model of the vehicle, often obscure the real aerodynamic characteristics. These quantities say almost nothing about local flow effects involved with the configurations. The largest benefit of implementing computational tools for aerodynamic design evaluation, over the usage of experimental methods, is that a complete description of all pertinent local quantities are computed over the entire flow field. This *excess baggage*, which requires significant cost in memory and storage requirements, can be used to make more enlightened evaluation and analysis. Knowledge of the local flow quantities allow the designer to focus his attention on the *root* strengths and weaknesses of a particular configuration.

Robust analysis is especially important in this design study because the flow conditions, over the pertinent Mach regimes, are extremely sensitive to geometric changes in the projectile surface. Sections 3.2.1 and 4.2.2 have outlined the essential flow features for the sliced

projectile configuration. It is evident from the results that the severe surface change in the junction between the slice plane and the shell body is the dominating factor for these designs. Slice plane surface area is certainly important for directing the maximum momentum from the free stream, but substantial losses in lift are seen in the pressure recovery region where flow separation occurs. The same basic flow features are seen with all of the different slice angles, in which the flow accelerates around the slice junction. Force distributions have shown that there are substantial differences in the force generated in the regions of the different slice features, but this large variance is lost in the pressure recovery region.

The characteristics of the slice configuration improves in the supersonic Mach regime, since the increase in Reynolds number means that viscous effects are not as dominant. The comparisons between OVERFLOW and FELISA in Section 3.2 have shown the change in the character of the flow field as Mach number is increased. The slice distortion exacerbates the boundary layer thickening and other viscous phenomena in the transonic flight regime. This affects the position and strength of shocks on the body, which in turn influences the local flow velocity and pressure. The interaction between viscous and compressible forces along the shell body produces a host of problems in the overall performance of the slice design.

The problems which exist with the bent projectile configurations are similar in nature to the weaknesses in the sliced shell. The surface gradients in the bend design are not nearly so severe, relieving the problem of flow separation, but the large pressure recovery region which develops as the flow is forced around the junction of the bent section with the shell body remains a large problem. Pressure recovery is an inherent feature of many lifting bodies, but the placement and severity of this region marks good designs from impractical geometries. The region which can be distorted on the projectile is a difficult constraint, since it does not allow a reasonable surface area for gradual pressure redistribution. The quick change in the local flow velocity over the short fuze section creates strong shock waves, which emanate from the area around the bend hinge. Compressible effects, coupled with boundary layer interaction, result in a severe loss of lift reducing the overall effectiveness of the bend design.

The hard constraints placed on the asymmetric projectile configurations tested in this study leave little room for alterations. The main impetus behind the specific configurations tested in this study was that the two fuze distortions were easily generated in flight with

small explosives. The initial goal was to construct a design which could fit inside a standard axisymmetric fuze casing. The large constraints imposed by this requirement have limited the effectiveness of the two designs and have lead to the problems associated with viscous separation and severe pressure recovery. The vast benefits which have been achieved with airfoil designs, for instance, have mainly come from the freedom to adjust the complete 2-D profile according to flight speed or similar design points. The asymmetric configurations tested in this study left very little freedom for an optimal profile selection, since volume and surface constraints practically dictated the class of fuze distortions which could be performed.

This weakness in the basic strategy for fixed-trim control of munitions plays an important role in the overall effectiveness of the designs. Complex surface distortions, which would require significant in-flight modifications, have not even been examined in the initial phase of this study. Increasing the articulation of the fuze distortions could lead to improved aerodynamic qualities. The next section discusses two modified projectile designs derived from the initial asymmetric concepts. These two configurations have been produced by relaxing the basic physical constraints adhered to with the initial design concepts, resulting in substantial increases in performance.

6.2 Final Design Concepts and Strategy

The previous section outlined several of the inherent weaknesses with using asymmetric fuze distortion for fixed-trim guidance. The physical constraints initiated in the problem lead to two simple design concepts; bending and slicing. These basic schemes are relatively simple alterations to the axisymmetric fuze which can be performed during the actual flight. This section takes the basic forms already studied in the previous chapters, and spawns some additional variations based on the results from the initial investigation. Two specific configurations have been chosen to demonstrate the increased performance which can be achieved through only minor variations in the initial design schemes.

Section 6.2.1 outlines the results found for the first of these *second phase* designs. The basic, root asymmetries have lead to some interesting flow and pressure effects. Pressure distribution results have shown substantial lift generated by both the slice surface and the bent fuze region. The problem is that the sharp surface junction between the fuze distortion

and the shell body leads to a severe pressure recovery region. The basic premise behind the first design is to show if a combination of the initial schemes, which makes use of the strengths of both designs, could generate significantly higher trim forces. This hybrid form would require a significantly more complex deployment mechanism, but could provide better performance despite the weaknesses inherent in the two designs.

Section 6.2.2 examines the basic physical constraint which requires launching an axisymmetric projectile. The design alteration explored in the example for this topic is to allow the basic fuze frame to exhibit a slight elliptic cross section, while the remainder of the projectile volume maintains its axisymmetric geometry. The reasoning behind this study is to explore whether three dimensional changes to the fuze could improve the aerodynamic performance of the initial fixed-trim guidance designs. The allowance for slight cross sectional asymmetries on the fuze section, which comprises very little of the overall mass of the shell, would have almost no effect on the mass or aerodynamic characteristics of the spinning projectile body. Using this slightly altered frame, the two initial design schemes are tested in order to assess the level of improvement which can be achieved.

6.2.1 Hybrid Sliced and Bent Configuration

The hybrid design presented in this section is based on pressure coefficient results found for both initial design concepts. Originally the sliced design seemed like a viable option since it created such a large actuation surface on the fuze section of the projectile. The junction between the slice surface and the shell body presented many kinds of problems since the severe gradients in the flow lead to large lift losses and boundary layer separation. Viscous effects, exacerbated by the slice, produced extremely disordered conditions along the remainder of the projectile body ruining all the benefits gained over the fuze section. The bent shell produced a much smaller pressure rise on the fuze surface, but since the deformed section extended further down the length of the shell, a larger force and moment were generated. Unfortunately, distorting the fuze with bend angles larger than 10 degrees tended to form subsonic pockets of flow on the bottom surface of the shell, in addition to compression shocks. The strong shocks caused pressure changes which destroyed some of the force generated by the bent fuze. In addition, drag increased dramatically at larger bend angles, since the cross-sectional area of the projectile was increasing.

These weaknesses in the two designs resulted in a slight alteration to the initial con-

figuration which basically consisted of combining the strengths of the two fuze distortions. The hybrid shell design was generated by performing both slicing and bending actions on a standard fuze. The slice surface created produces a large normal force, but the addition of a bent fuze reduces the relative angle of the junction between the slice plane and the fuze surface. In addition, the bend lowers the pressure on the bottom surface of the shell resulting in an even larger generation of normal force over the slice region. Hybrid shell designs, with a bent fuze section of 10° and slice angles varying from $30 - 65°$, were numerically tested at a Mach number of 1.1. Comparisons with the standard slice configuration on the basic aerodynamic coefficients of normal force and pitch moment are shown in Figure 6-1.

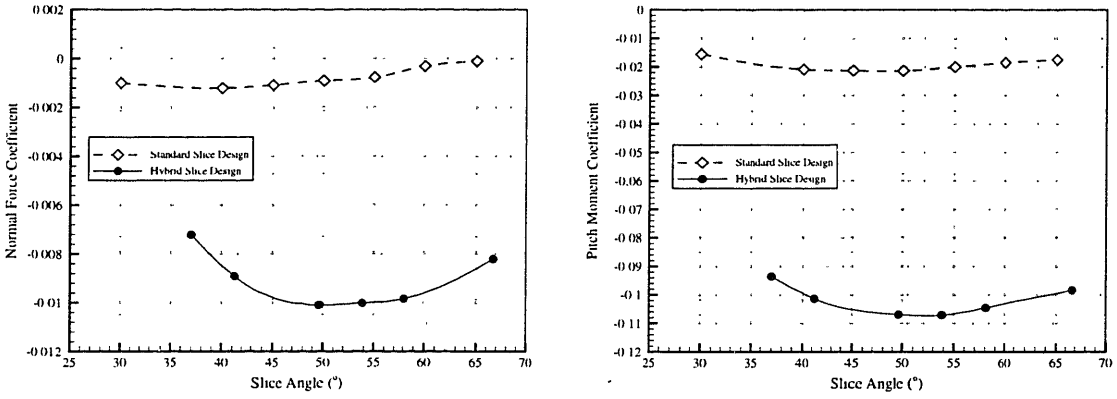

(Normal Force Coefficient) (Pitch Moment Coefficient)

Figure 6-1: Basic Aerodynamic Characteristics of Hybrid Design

These results at Mach 1.1 demonstrate a substantial increase in both normal force and pitch moment of nearly 400%. The dramatic aerodynamic performance of this hybrid design attests to the benefits which exist for simple modifications to the initial schemes. The two design concepts each have undesirable flaws, but these weaknesses can be overcome by more careful placement of the fuze distortions. The drag generated by the hybrid design was not substantially different from the 10° bend design, which is perhaps 1-3% higher than the baseline projectile. The reasons for the improved aerodynamic characteristics of the hybrid design can perhaps be better observed from pressure and pitch moment distribution comparisons taken from the 50° case, shown in Figure 6-2. The separated flow region on the upper surface of the shell is substantially decreased by changing the relative angle between the slice plane and the fuze surface, without adversely affecting the large force producing region on the slice surface.

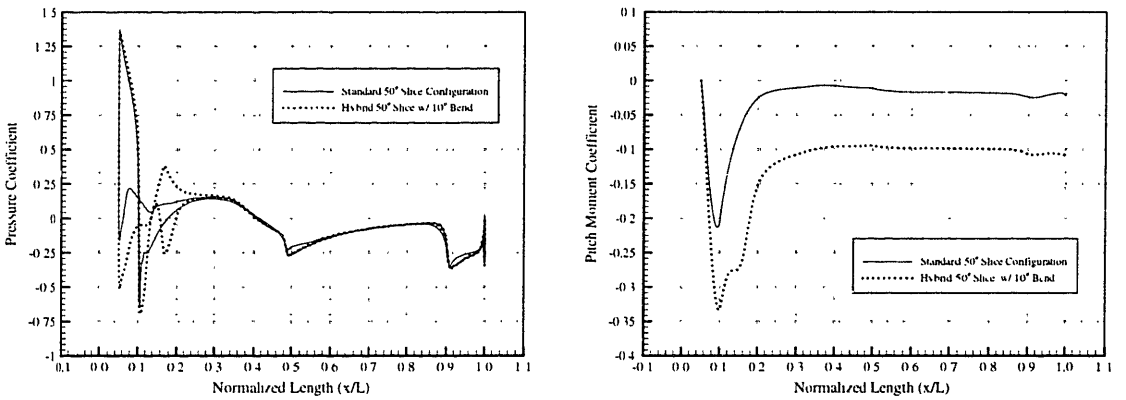

(Pressure Coefficient Distribution) (Pitch Moment Distribution)

Figure 6-2: Aerodynamic Distributions Along Hybrid Design

It is reasonable to expect substantial improvements with respect to the trim metric for the hybrid design. Figure 6-3 shows a comparison of the variation of trim lift with slice angle for the standard and hybrid configurations. Again, the overall performance of the hybrid shell at Mach 1.1 is almost 400% greater than the standard design. As a reference source, the trim lift generated by the 10° bend design is also included. The hybrid design generates a larger trim lift than the two basic designs combined, establishing that the hybrid design is aerodynamically a better vehicle. The increased level of performance will significantly affect the trajectory offset generated for a ballistic flight. Although a complete Mach sweep has not been performed with the hybrid design, one could expect Mach characteristics similar in nature to the standard slice design. This would lead to thousands of feet in extra offset. In fact, decreasing the volume sliced from the fuze could probably provide sufficient increases in the trim lift, and would have more internal volume and better drag characteristics.

The main point behind combining the two initial design concepts into one hybrid design is to support the idea that increasing the flexibility with respect to the complexity of the augmented surface can substantially increase performance. Using more articulated slice surfaces or even tailoring the complete fuze into an aerodynamic lifting body definitely opens up the possibility for a significantly improved design which provides more trim lift, more internal volume, and possibly even less drag. The initial schemes were a good start in examining design concepts for asymmetric fuze configurations, however a vast array of geometries exist which could provide better aerodynamic characteristics.

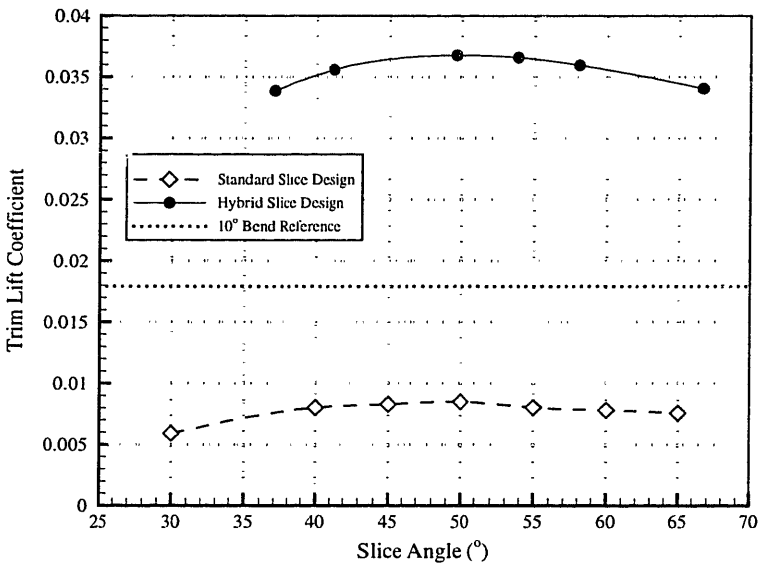

Figure 6-3: Trim Metric Characteristics of Hybrid Design

6.2.2 Elliptic Asymmetric Fuze Designs

This section looks at the benefits which exist from easing the hard constraint on launching the augmented projectile in an axisymmetric condition. This reasoning can be applied to many types of designs, however the specific example discussed in this section is to allow a non-circular fuze section to be used as the base frame for the initial design schemes. By allowing slightly elliptic cross sections for the fuze section, substantial improvements in performance can be realized without significant penalty in the aerodynamic properties of the baseline shell.

The elliptic nature of the cross section of the fuze has been parameterized by setting the axis ratio at the fuze nose. The ellipticity is then uniformally blended over the length of the fuze until a circular fuze joins with the shell body. A 2-D diagram illustrating the basic geometry as well as the axis ratio definition is shown in Figure 6-4. The main point behind this design is that the elliptic cross section increases the available surface for augmentation, makes the fuze a better lifting body, but still maintains an axisymmetric condition over the remainder of the projectile. The hope is that because the fuze section represents such a small part of the mass and volume of the shell, the gross aerodynamic characteristics of the projectile body will be unaffected.

The two fixed-trim guidance concepts of slicing and bending the new elliptic fuze were

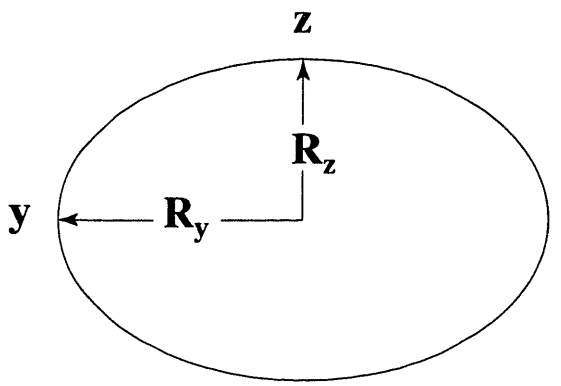

$$\text{Axis Ratio} = \frac{R_y}{R_z}$$

Figure 6-4: Diagram of the Elliptic Cross Section

both investigated in this study. Since this brief investigation was focused on the effects of the fuze ellipticity, a configuration from both of these initial designs was chosen for testing. The base fuze distortions chosen were the 10° bend at 4.25", and the 50° slice at 2.7". The aerodynamic characteristics of these two designs at Mach 1.1 are shown in Figure 6-5 as a function of the axis ratio parameter defined in Figure 6-4. Substantial increases in both the normal force and pitch moment generated by both of the augmented shells can be seen from these results. The larger width of the bent fuze creates an increase in normal force and moment of almost 200%. The sliced design is also affected by the ellipticity, which produces a significantly larger slice surface for redirecting the momentum of the free stream. The maximum increase due to the elliptic fuze, with respect to the standard slice design, is approximately 300%.

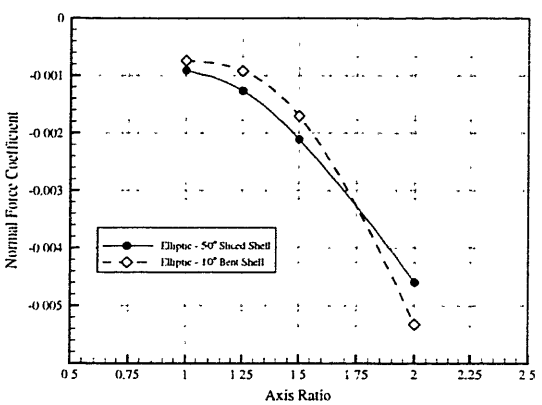

(Normal Force Coefficient)

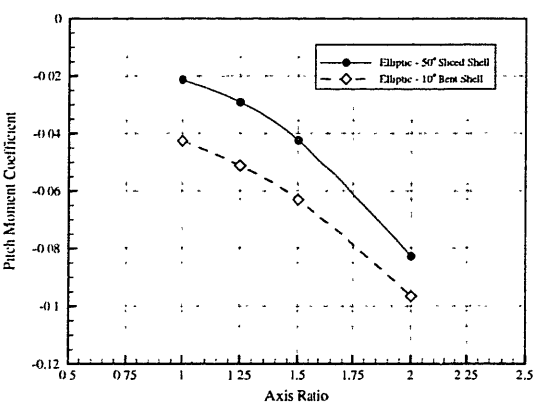

(Pitch Moment Coefficient)

Figure 6-5: Basic Aerodynamic Characteristics of Elliptic Designs

The pressure distribution results, taken along the symmetry plane, show no significant differences between the elliptic designs and the standard configurations. This shows that the changes to the fuze cross section very weakly affect the pressure along the centerline of the shell. The performance gains are all based on the fact that the projected surface of the fuze has increased. The increase is not that dramatic, but the forces and moments produced by the distortions are very sensitive to the fuze geometry. A more local illustration of the effects of the ellipticity can be seen in Figure 6-6 which shows a comparison of the pitch moment distributions for each of the design concepts. The elliptic fuze simply allows more force to be generated by the two basic augmentations which increases the overall effectiveness of the designs. Some of the benefits of the elliptic cross section are lost in the pressure recovery region, but a better lifting body is still created with the new fuze geometry.

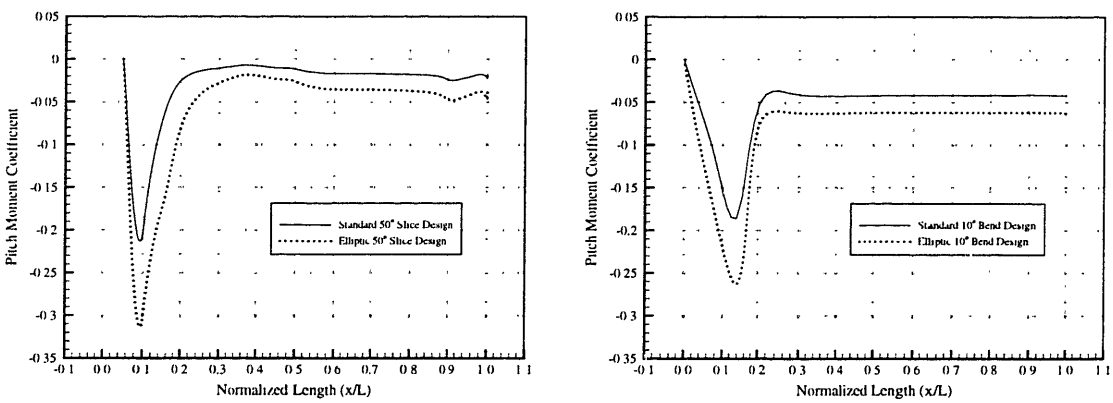

(Elliptic Slice Design) (Elliptic Bend Design)

Figure 6-6: Pitch Moment Distributions Along Elliptic Designs

The trim characteristics of the elliptic designs, shown in Figure 6-7, demonstrate substantial increases in overall performance. Even a modest change in the axis ratio of 1.5 generates approximately double the trim lift of the standard configurations. The benefits of using a non-circular fuze cross section would be significantly tainted if the ellipticity influenced the baseline aerodynamic characteristics of the projectile. Figure 6-8 shows the change in the normal force and pitch moment derivative, as well as the drag coefficient, as a function of the axis ratio of the fuze. These results support the conclusion that the small alterations to the fuze have very little effect on the baseline derivatives and drag of the projectile. For increases of the overall performance on the order of 150%, a maximum deviation of approximately 3% is seen in the pitch moment derivative. Thousands of feet of extra

trajectory control could be produced with very little change in the nominal aerodynamic characteristics of the shell.

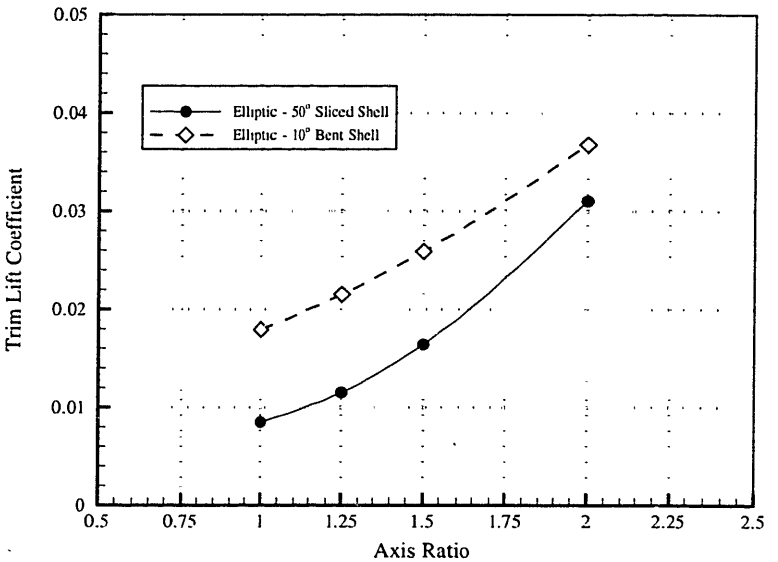

Figure 6-7: Trim Metric Characteristics of Elliptic Designs

The two designs outlined in this section have explored the possibility of permitting slight deviations in the original constraints of the design problem, by either increasing the complexity of the fuze distortions or allowing slight asymmetries in the nominal fuze configuration. These two designs are by no means the limit to what can be accomplished with this general methodology. Permitting more freedom with respect to the deformed surfaces could produce great benefits in performance without significant penalties. The problem with the initial designs is that they were horrible aerodynamic lifting bodies, with all kinds of problems with separation and pressure recovery. The slight alterations tested in this section are extremely simple changes to the basic configurations. More elaborate aerodynamic tailoring of the fuze might provide even better performance characteristics. Unfortunately, the alterations would force a relaxation on the constraint of launching the shell symmetrically, since complex shape changes in flight might be impossible.

The main problem with allowing asymmetries at launch condition deals with the instabilities which can exist in the angular motion of spinning almost-symmetric projectiles. The subject of missiles having configurational asymmetries has been addressed by many authors [23, 10, 16, 22]. The reason that this present study has not delved too deeply into

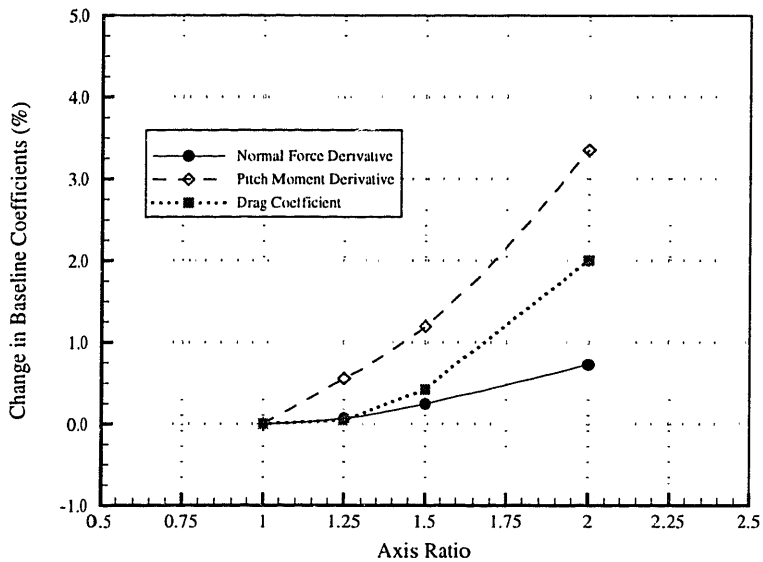

Figure 6-8: Sensitivity of Baseline Characteristics on Elliptic Fuze

the instabilities of the deformed shells at launch is that the plan was to launch the projectile in an axisymmetric state, and then distort the fuze during the flight. None of the problems associated with spinning asymmetric shells were apparent in these designs, since the deformed fuze section would be made independent from the main spinning body by a semi-frictionless bearing system. One purpose of this section is to motivate the idea that allowing slight asymmetries at launch would provide no additional stability problems than the strategy of augmenting the shell after launch.

The main sources of instability for spinning asymmetric projectiles deal with problems which exist if the roll rate of the shell approaches the natural pitch frequency. This resonance condition can lead to unbounded angles of attack in the presence of mass or aerodynamic asymmetries, since the trim angle of attack generated by the asymmetry rolls at the rate of the body. The high spin rate of these ordnance projectiles, at around 255 Hz, places the roll frequency orders of magnitude greater than the pitch frequency of a typical ordnance projectile in any flight regime. This *super-resonant* condition relieves many of the possible problems inherent with spinning asymmetric bodies. After a detailed analysis, Murphy [21] concluded that the motion of asymmetric missiles in super-resonant conditions exhibit behavior which is well approximated by the tricyclic motion of symmetric projectiles with average moment and force coefficients. In other words, since the frequency of the roll

rate is so much greater than any other motion, the trim forces and moments produced by aerodynamic asymmetries will be *averaged* out of the overall dynamics of the spinning shell.

The other issue of spinning asymmetric bodies, in addition to the aerodynamic characteristics, is the inertial mass asymmetry which exists due to the offset of the center of gravity. The handling of the effects of products of inertia (J_{xz}) on the angular motion of spinning vehicles was addressed by Hodapp [15]. The conclusion from this paper was that for projectiles in the super-resonant spinning region, the tendency of a spinning body is to trim at an angle equal to the inclination of the principal axis (δ_α) which can be derived from the equations of motion as

$$\delta_\alpha \simeq J_{xz}/(I - I_x) \tag{6.1}$$

Products of inertia in other planes can be handled in a similar manner. This equation assumes that $I \approx I_{zz} \approx I_{yy}$, which is a reasonable assumption even for the elliptic fuze.

Calculations, which make the very conservative assumption of a constant shell density, have shown two things concerning the asymmetric shells. First, that even with the maximum axis ratio tested of 2.0, the elliptic fuze projectiles have values of I_{zz} within fractions of a percentage of I_{yy}. The small elliptic portion of the shells and the large volume in the rest of the projectile body results in very little effect on the inertial characteristics. The second conclusion found from the inertial calculations is that the product of inertia (J_{xz}) created by any of the fuze distortions constitutes less than one percent of the value of the principal moment of inertia (I). This result, taken with Equation 6.1, means that the trim angle reached at large spin rates, generated by any of the projectile designs studied in this investigation, would be bounded by a fraction of a degree. These results were all obtained by assuming a constant shell density over the projectile body and solving for the offsets to the volume. In reality the fuze section has a lower density than the remainder of the shell, and the effects from fuze asymmetries would be even less than the results found in these calculations.

In general, the allowance for slight asymmetries on the fuze section has been shown to have very little effect on both the aerodynamic or mass properties of the nominal shell. The use of an elliptic fuze cross-section generated significant performance increases, giving the augmentation concepts better aerodynamic properties. Limited flattening of the fuze does not alter the overall aerodynamic coefficients of the projectile body because the changes

represent insignificant modification to the volume or surface distribution of the shell. These small alterations, though, have a dramatic influence on the trim forces and moments generated by the fuze distortions. Similar shape modifications, including limited aero-tailoring of the fuze volume, could result in even better performance. The hybrid shell and the elliptic fuze concepts demonstrate relatively simple alterations to the initial designs which generate significant improvements without influencing nominal projectile characteristics. The relaxation of some of the hard constraints on possible design configurations is the key to improving the potential for fixed-trim control.

6.3 Conclusion and Future Work

A computational approach for predicting the control authority of an augmented projectile with an asymmetric fuze design has been successfully implemented. This computational approach was supported by the implementation of a host of numerical tools and analysis packages, all outlined in Section 2.3. Validation studies, which reinforce the overall ability of the computational tools utilized in this investigation, have been extensively reviewed in Section 3.1. These studies demonstrated the fidelity and accuracy of the predictions made with numerical simulations, as well as their usefulness in predicting local quantities of flow velocity and pressure distributions. The use of these basic results has become embedded in all of the subsequent analysis of the asymmetric projectile configurations.

Two basic fuze configurations have been tested in the initial phase of this investigation. The two designs, the sliced and the bent concepts, have been evaluated in Section 5.1 using a metric which calculates the trim condition of the shell given the forces and moments generated by the asymmetries. This measure of control authority provides reasonable determination of *optimum* aerodynamic performance. The results have shown that bending the fuze, given the physical constraints imposed by the fuze geometry, provides significantly more control force than the sliced fuze. Naturally, this result comes out of a significant level of examination, of not only the integrated aerodynamic quantities, but also local flow field distributions.

The trajectory control produced by these designs over a complete ballistic flight reached over a thousand feet. Certainly this does not represent offsets significant enough for complex guidance or moving target tracking, but it does allow for the reduction of the dispersion

of the gun-launched munitions. The weaknesses of these designs has been outlined in Section 6.1. These weaknesses are generally a result of the finite volume available in the fuze as well the hard constraints on possible surface distortions due to the original flight plan. The strategy, which served as the background for this study, was to launch the projectiles symmetrically and then alter the fuze in the beginning stages of the flight with small explosives. The stability issues which might exist from this violent perturbation to the projectile velocity and heading have not been studied in this investigation, however this unlocking maneuver is certainly not a trivial matter.

Section 6.2.2 of this thesis attempted to motivate the conclusion that limited alterations to the fuze section of a fast spinning projectile would have very small effect on both the aerodynamic and mass characteristics. The benefits from more complex fuze shapes and hybrid asymmetric designs have been shown in Section 6.2. These designs were achieved by relatively simple modifications to the basic concepts, and yet substantial increases in trim performance resulted. The essential question then could be how significant fuze alterations would have to be to alter the baseline characteristics of the nominal projectile body. The initial results of this study showed that the fuze asymmetries did not greatly affect these nominal qualities, leaving some room to believe that additional modifications could be created with even better aerodynamic performance.

Although at the onset several shell configurations seemed promising, there is some motivation for re-stating this design evaluation in the form of an optimization problem, and using design methods based on this premise. Inverse methods exist which shape the surface according to prescribed pressure or lift distributions. This problem is inherently a 3-D problem, but significant improvements could be realized without substantial numerical cost. The hard constraints which exist on keeping the original fuze surface axisymmetric place some difficulty on making use of these more elaborate aero-tailoring methods, since the size of the design space is significantly reduced and local freedom for fuze surface alteration is limited. Inverse methods are very good at searching a large design space and optimizing over a very complex, multi-dimensional series of constraints. Unfortunately, the solutions produced by this kind of methodology are often not physically realizable and require some information on a target aerodynamic performance criteria. This target setting, usually expressed as a pressure or flow distribution goal, can sometimes be very difficult to generate.

Future work could make use of the basic design concepts tested in this investigation, and

use the results to optimize around a particular design. The design routine would have to take into account viscous and compressible effects, since they have been shown to have very significant influences on the overall performance of the asymmetric shells. An elaborately formed optimization problem could even be made to take volume and drag constraints into account. Another important factor would be to include the results from all of the Mach regimes tested for a proper characterization of the augmented projectile. The difficulty of this multi-domain problem is choosing the weightings for each of the constraints, as well as deriving a suitable cost function. The trim metric used in this investigation would probably not serve as a good model because it only takes into account a limited piece of the problem. Trim lift was used for this study because it represented a simple, analytically derived function which could be evaluated at discrete Mach points. It is obviously not complete because it does not include drag, stability, or volume constraints in any fundamental way.

Chapter 5 made an attempt to address all the factors involved in the performance of the asymmetric projectiles, but naturally was limited by the intuition of the researcher. The secondary forces, mainly influenced by viscous effects, were only peripherally studied in this computational investigation. More elaborate examination of the changes in Magnus effects as a function of the fuze distortions must be completed before serious implementation of the design concepts is considered. Another factor not even considered in this investigation was the effect of the deformed fuze on damping coefficients. Computational results have only recently been achieved which address the subject of predictions of damping derivatives in conjunction with spinning projectiles using rotating reference frame formulations [39, 29, 38]. These numerical studies have produced some fairly good comparisons with experiment but have concentrated on higher Mach numbers, which exhibit very little unsteady effects. Transonic predictions are probably quite a few years away, and may require significant theoretical development.

Accounting for asymmetries would probably require a numerical tool which allows fully moving grids. These codes are only in the infant stage of development, but would give a great deal of flexibility in predictions on the complete aerodynamic characteristics of vehicles in flight. Time accurate modeling could also be possible which would allow the prediction of aerodynamic lags and transient information. The computational cost of this kind of study is prohibitive, and presently would not be reasonable for large design studies. The methods used in this study, given the computational resources available, were reasonably planned to

generate the most information on the augmented projectiles without making excessive and costly numerical simulations. An attempt was made to fill all the necessary holes in our knowledge on the basic aerodynamics of the projectiles by establishing trends coupled with reasonable intuitive conclusions.

The limitation on resources made generating a simulation at every flight point, for every design completely unreasonable. Despite this constraint, pressure distribution resul s and more localized profiles contributed greatly to an understanding of the root causes for the performance trends seen with the different designs. The vast quantity of data generated by computational simulations can be used as a powerful tool for educated inferences about strengths and weaknesses of a design. The results outlined in the previous chapters have focused on both quantitative measurements as well as qualitative explanation of the trends found in the various studies. This is important in the overall understanding of how exactly the deformed features are affecting the flow field around the projectile body. Substantial unforeseen viscous-compressible interaction was observed in many of the simulations. These phenomena influenced the local propagation of both pressure distribution and the boundary layer, as well as the global quantities of normal force and pitch moment.

Local flow visualization was the key to the second phase design schemes outlined in Section 6.2. These concepts represented only small departures from the initial configurations, and yet generated substantially higher performance. It is certainly possible to generate additional fuze geometries which exhibit even better aerodynamic qualities by relaxing the hard surface and volume constraints placed on the fuze. Although this study of fairly simple geometric distortions certainly does not represent the aerodynamics for every possible fuze design, it does provide sound information on the possibilities for using subtle changes in the fuze surface to affect the performance of projectiles in flight. The results presented for the various designs have certainly confirmed that significant aerodynamic control authority can be generated with a wide variety of fuze distortions. It is certain that subsequent studies, which borrow from the results gained in this investigation, will allow the practical implementation of configurational asymmetries for fixed-trim guidance and control.

Appendix A

CMATD Aerodynamic Investigation

A substantial aerodynamic investigation has been completed on the CMATD projectile, which was an experimental shell designed by Draper laboratory to initially function as the frame for the asymmetric shell design. A diagram of the projectile is shown in Figure A-1 and closely resembles the geometry of the Mk64 standard shell. The main difference between the CMATD and the Mk64, which was used as the baseline for all the results presented in this thesis, is a slightly enlarged fuze section. This region was enlarged on the CMATD to accommodate the placement of internal hardware, including any possible motors for surface actuation devices. At the beginning of this investigation Draper Laboratory was completing wind-tunnel tests on the CMATD for use in a research project on fixed-trim guidance with canard control. The geometry of the CMATD was different enough to require experimental data in order to assess the basic aerodynamic qualities of the shell.

The first major task of this investigation, after the validation studies outlined in Section 3.1, was to perform baseline computational simulations on the CMATD in order to predict all relevant static coefficients. Aerodynamic predictions on the CMATD were completed using the viscous code OVERFLOW over a range of Mach numbers. These results were presented to Draper Laboratory and comparisons between the wind-tunnel data and the numerical predictions were reasonable, although significant discrepancies did exist. These differences could not be numerically explained, therefore significant additional time was taken to exactly match the wind-tunnel conditions by performing simulations of the

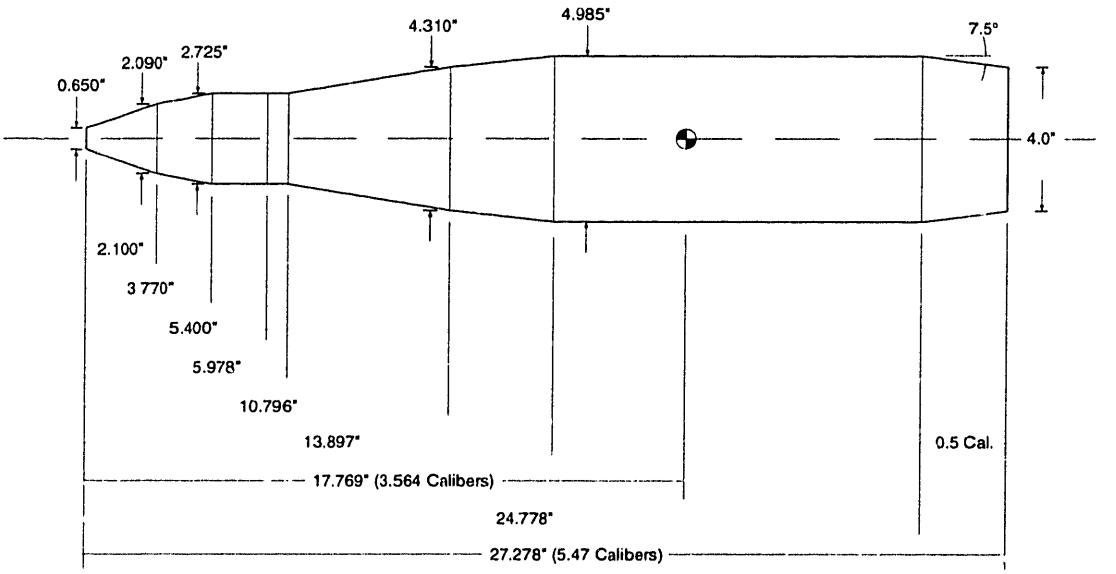

Figure A-1: Diagram of the CMATD Projectile

CMATD projectile with a sting attached to the base of the shell. The results of this particular study did not really fit within the framework of this thesis, thus the decision was to include any CMATD predictions in a suitable appendix.

Results from the validation study completed on the 5in54/RAP, presented in Section 3.1.2, exhibited a large peak in the pitch moment derivative in the transonic region between Mach 0.85 and 0.95. This peak is a common aerodynamic feature of ordnance projectile which have a substantial boat-tails. The CMATD exhibits this same behavior, which can be best described as being analogous to the Mach tuck behavior of airfoils. In the transonic regime, the position of the shocks on the boat-tail region of a projectile is very sensitive to the local velocity of the flow. This local velocity can be affected by many factors including the taper and length of the boat-tail; the boundary-layer thickness in that region; and the flow field and pressure distribution at the base of the projectile. As the velocity increases to the sonic barrier, the position of the shocks moves along the boat-tail, until they reach a final position at the base of the shell. The large pitch moment derivative change, seen in the transonic regime, is caused by the relative movement and position of the shocks on the upper and lower surface of the projectile. This position changes rapidly in the Mach region from 0.85 to 0.95, due to the transonic local velocity on the boat-tail, leading to violent shifts in the pitch moment.

Wind-tunnel data on projectiles is most often performed by mounting the body on a

sting, which causes no interference to the flow over the front of shell body and creates a stable framework to complete various experiments. Unfortunately, the presence of the sting significantly affects the pressure and flow velocity in the base region of the projectile. In transonic conditions, where disturbances from the base can propagate upstream, substantial aerodynamic interference can occur due to the sting. A base mounted sting might affect the peak in the pitch moment derivative, since the movement of the shocks as Mach number increases dictates the trend of this coefficient. This conclusion was the motivating factor behind performing simulations of sting-mounted CMATD projectiles.

The wind-tunnel data completed on the CMATD is not available for public disbursement and is presently considered classified. This is the biggest reason that baseline predictions on the CMATD were not included in the validation section. It is apparent from comparisons between the experimental data and the two numerical studies, though, that the relatively small disturbances in base region flow, due to the sting, lead to large changes in the static coefficient derivatives. Figure A-2 shows a comparison of the normal force derivative from numerical predictions taken on the standard and sting-mounted shell. This result demonstrates the significant aerodynamic interference created by the sting. Although the data from the wind-tunnel tests has been deemed classified, permission has been given to state that the computational predictions made on the sting-mounted CMATD compared favorably and were well within 5% of the experimental results. This conclusion not only illustrates something very interesting about the interference from a sting-mounted apparatus during wind-tunnel studies, but also validates the numerical predictions made using OVERFLOW.

The transonic sensitivity of the peak in the pitch moment derivative on base region flow would suggest that there could be considerable influences due to a sting. Figure A-3, which shows the Mach trends for the pitch moment derivative, supports this conclusion. The presence of the sting has not only significantly altered the size of the pitch peak, but also the position as well. An important point to notice in both Figure A-2 and A-3 is that the supersonic predictions for the standard and sting-mounted configurations are almost identical. This result supports the conclusion that the differences in the predictions from the two CMATD configurations is due to the disturbance propagation from the sting at critical transonic Mach numbers. The presence of the sting exacerbates the movement of the shocks on the boat-tail, generating a larger fluctuation in the pitch moment over the shell body.

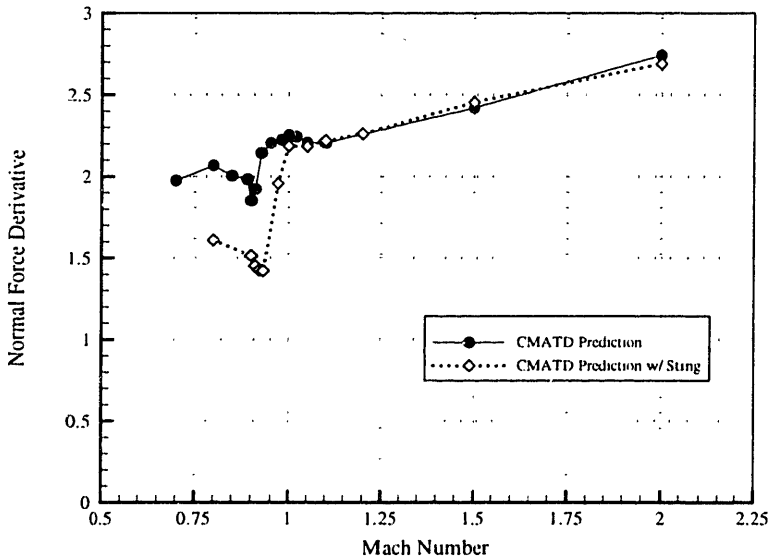

Figure A-2: Normal Force Derivative Comparisons for CMATD

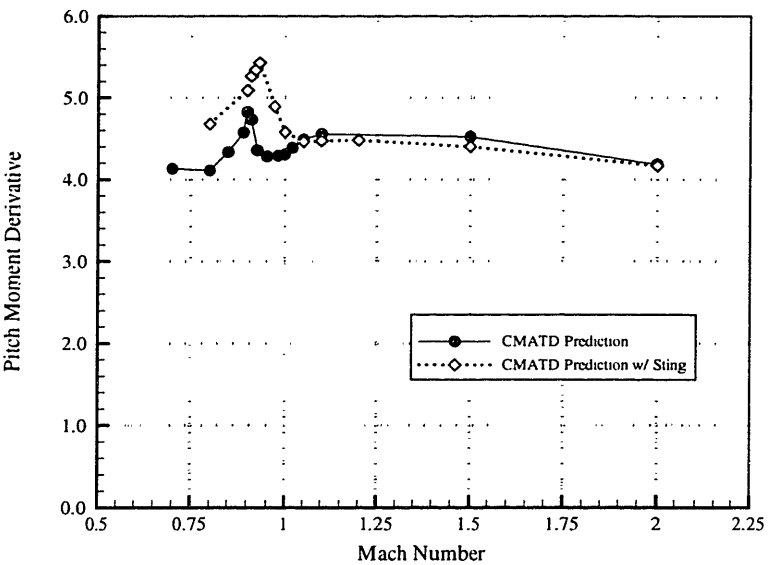

Figure A-3: Pitch Moment Derivative Comparisons for CMATD

A better illustration of the transonic sting interference effects can be seen from normal force and pitch moment distributions taken at critical Mach numbers in the peak region of the pitch moment derivative. Figure A-4 shows the distribution comparisons for the two CMATD configurations at Mach 0.90 simulated at an angle of attack of 4°. This figure positively identifies the boat-tail region as the location of the discrepancy in the aerodynamic predictions. As stated above, the influence of the sting changes the local characteristics of the flow in the boat-tail region affecting the position of the shocks and causing substantial changes in the nominal static derivatives of the shell. The normal force and pitch moment development over the projectile is nearly identical until the boat-tail region.

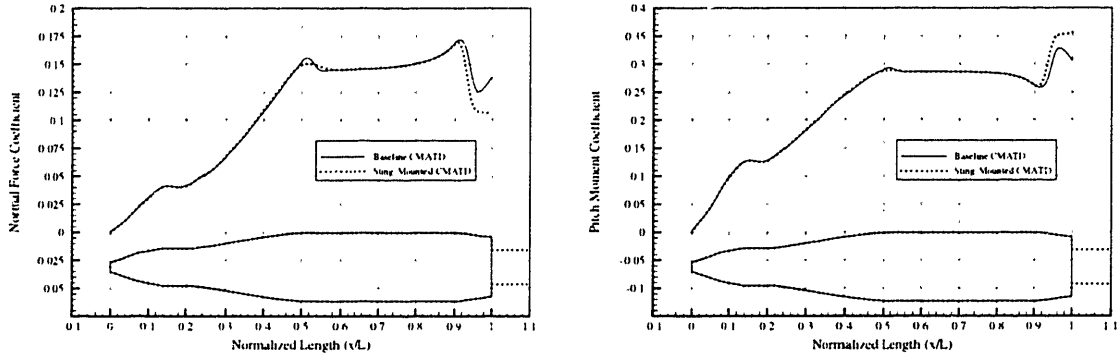

(Normal Force) (Pitch Moment)

Figure A-4: Comparison of Aerodynamic Distributions for CMATD

These conclusions can be further illustrated by pressure field contours in the base region of the projectile, taken from the same two simulations at Mach 0.90, which are shown in Figure A-5. The pressure contours in the base region of the shells are absolutely different for the two configurations. The pressure field in the sting-mounted CMATD is considerably more stable and ordered, which is not unreasonable considering the damping effects of the sting. This flow characteristic was noticed for almost all of the transonic projectile simulations, which exhibited a considerable level of unsteadiness in the base region. The other main point to notice in Figure A-5 is the location and size of the sonic boundary, outlined in black, which is considerably different for the two configurations. The standard configuration shows larger pockets of supersonic flow which extend further down the length of the boat-tail. This supports the the original conclusion that interference from the sting cause local velocity changes, which lead to deviations in the boat-tail shock location and strength.

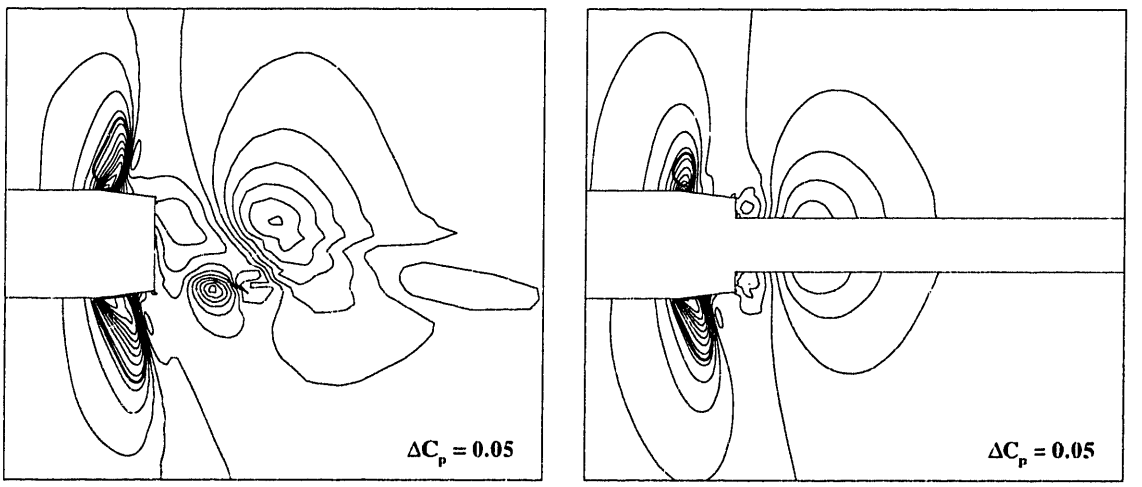

(Standard Shell) (Sting-Mounted Shell)

Figure A-5: Comparison of Pressure Fields for CMATD Boat-tail

The baseline CMATD results have established several important points concerning the computational predictions used in this study. The transonic numerical results used in this investigation demonstrate high fidelity and accuracy with respect to the actual flight condition. It appears in this case that the wind-tunnel experiments provided data which was not accurate. This conclusion can only be made from the high precision in the comparisons of numerical predictions with experimental data, as well as the severe discrepancies between the sting-mounted projectile and the standard shell results. The numerical predictions illustrate that substantial interference effects are caused by the presence of the sting, which influences both the local flow field and the overall aerodynamic characteristics of the projectile. The comparisons made for the baseline CMATD also demonstrate the considerable visualization power which can be achieved by computational simulations. Flow field contours, pressure distributions, as well as integrated quantities are all available to the researcher for a more informative description of the aerodynamics involved in critical flight conditions.

References

[1] B. Baldwin and T. Barth. A one-equation turbulence transport model for high Reynolds number wall-bounded flows. TM 102847, NASA, 1990.

[2] B. Baldwin and H. Lomax. Thin layer approximation and algebraic model for separated turbulent flow. *AIAA 78-257*, 1978.

[3] P.G. Buning and W.M. Chan. *User's Manual for FOMOCO Utilities - Force and Moment Computation Tools for Overset Grids.* NASA Ames Research Center, July 1996.

[4] P.G. Buning, W.M. Chan, and Ing-Tsau Chiu. *User's Manual for the HYPGEN Hyperbolic Grid Generator and HGUI Graphical User Interface.* NASA Ames Research Center, October 1993.

[5] P.G. Buning, W.M. Chan, and D.C. Jesperson. *OVERFLOW User's Manual, Version 1.7.* NASA Ames Research Center, August 8 1996.

[6] P.G. Buning, Pamela P. Walatka, Larry F[illegible]rce, and Patricia A. Elson. *PLOT3D User's Manual.* NASA Ames Research Center, March 1990.

[7] W. R. Chadwick and J. F. Sylvester. Dynamic stability of the 5-inch/54 rocket assisted projectile (the influence of a non-linear Magnus moment). NWL Report 2059, U.S. Naval Weapons Laboratory, Dahlgren, Virginia, October 5 1966.

[8] M. F. Costello. Range extension and accuracy improvement of an advanced projectile using canard control. *AIAA 95-3461-CP*, 1995.

[9] Jan-Kaung Fu and Shen-Min Liang. Computations of aerodynamic drag for turbulent transonic projectiles with and without spin. *AIAA 93-3416-CP*, 1993.

[10] Louis S. Glover. Effects on roll rate of mass and aerodyanamic asymmetries for ballistic re-entry bodies. *Journal of Spacecraft*, 2(2):220–225, March-April 1964.

[11] C. Gracey, E. M. Cliff, F. H. Lutze, and H. J. Kelley. Fixed-trim re-entry guidance analysis. *Journal of Guidance*, 5(6), Nov-Dec 1982. (Also AIAA 81-1754).

[12] Bob Haimes. *VISUAL3 User's & Programmer's Manual.* Massachusetts Institute of Technology - FDRL, February 6 1996.

[13] Charles Hirsch. *Numerical Computation of Internal and External Flows*, volume 1. John Wiley & Sons, 1988.

[14] Ira D. Jacobson. Magnus characteristics of arbitrary rotating bodies. Technical Report 171, AGARD, 1973. As cited in J.E. Greene as well as W. Luchuk.

[15] Albert E. Hodapp Jr. Effects of products of inertia on re-entry vehicle roll behavior. *Journal of Spacecraft*, 8(2):155–161, February 1971.

[16] Albert E. Hodapp Jr. Effects of unsymmetrical stability derivative characteristics on re-entry vehicle trim angle behavior. *Journal of Spacecraft*, 11(5):300–307, May 1974.

[17] Jerome T. Kegelman, Robert C. Nelson, and Thomas J. Mueller. The boundary layer on an axisymmetric body with and without spin. *AIAA Journal*, 21(11):1485–1491, November 1983.

[18] S.H. Lo. A new mesh generation scheme for arbitrary planar domains. *Int. Journal of Numerical Methods in Engineering*, 21:1403–1426, 1985.

[19] John C. Martin. On Magnus effects caused by the boundary layer displacement thickness on bodies of revolution at small angles of attack. BRL Report 870 - Revised, Ballistic Research Laboratories, Aberdeen Proving Ground, Maryland, 1955.

[20] Jeremiah E. McGinley, Richard J. Schoon, and James O. Sweeny. Guided projectile feasibility study. Technical Report AFATL-TR-81-45, Air Force Armament Laboratory, April 1981.

[21] Charles H. Murphy. Nonlinear motion of a missile with slight configurational asymmetries. *Journal of Spacecraft*, 8(3):259–263, March 1971.

[22] Charles H. Murphy. Angular motion of spinning almost symmetric missiles. *Journal of Guidance and Control*, 2(6):504–509, Nov-Dec 1979. (Also AIAA 78-1334).

[23] J. D. Nicolaides. On the free flight motion of missiles having slight configurational asymmetries. Technical Report 858, Ballistic Research Laboratories, Aberdeen Proving Ground, Maryland, June 1953. (also IAS Preprint No. 395).

[24] C. J. Nietubicz, W. B. Sturek, and K. R. Heavey. Computations of projectile Magnus effect at transonic velocities. *AIAA Journal*, 23(7):998–1004, July 1985.

[25] C.J. Nietubicz and W.B. Sturek. Navier-Stokes code verification for projectile configurations at supersonic and transonic velocities. *AIAA 88-1995*, May 1988.

[26] S. Parks, P. Buning, W. Chan, and J. Steger. Collar grids for intersecting geometric components within the chimera overlapped grid scheme. In *AIAA 10th Computational Fluid Dynamics Conference*, Honolulu, HI, June 24-26 1991. AIAA 91-1587.

[27] J. Peraire, J. Peiró, L. Formaggia, K. Morgan, and O.C. Zienkiewicz. Finite element Euler computations in three dimensions. *Int. Journal of Numerical Methods in Engineering*, 26:2135–2159, 1988.

[28] J. Peraire, J. Peiró, and K. Morgan. *FELISA Reference Manual, Version 1.0.* NASA: Langley Research Center, December 3 1993.

[29] N. Qin, D.K. Ludlow, S.T. Shaw, J.A. Edwards, and A. Dupuis. Calculation of pitch damping coefficients for projectiles. In *35th aerospace Sciences Meeting and Exhibit, January 6-10, 1997 / Reno, NV.*

[30] Frank J. Regan. Preliminary static aerodynamic measurements on a proposed canard-controlled guided projectile. Wind-Tunnel Report 73, Naval Ordinance Laboratory, April 1974.

[31] W. B. Sturek and D. C. Mylin. Computational study of the Magnus effect on boattailed shell. *AIAA Journal*, 20(10):1462–1464, October 1982.

[32] W. B. Sturek, C. J. Nietubicz, J. Sahu, and P. Weinacht. Applications of computational fluid dynamics to the aerodynamics of Army projectiles. *AIAA Journal of Spacecraft and Rockets*, 31(2):186–199, March-April 1994.

[33] W.B. Sturek and K.R. Heavey. Computations of projectile Magnus at transonic velocities. *AIAA Journal*, 23(7):998–1004, July 1985.

[34] N. E. Suhs and R. W. Tramel. *PEGSUS 4.0 User's Manual.* Calspan Corporation/AEDC Operations, November 1991.

[35] Harold R. Vaughn. A detailed development of the tricyclic theory. Technical Report SC-M-67-2933, Sandia Laboratory, Albuquerque, February 1968. (Also NASA N69-74116).

[36] W. Vander Velde. Application of Gracey guidance to 5-inch gun projectile. Notes.

[37] W. Vander Velde. The Gracey, et. al., guidance system. Notes.

[38] P. Weinacht. Prediction of projectile performance, stability and free-flight motion using CFD. In *35th aerospace Sciences Meeting and Exhibit, January 6-10, 1997 / Reno, NV*, 1997.

[39] Paul Weinacht, Walter B. Sturek, and Lewis B. Schiff. Navier-Stokes predictions of pitch damping for axisymmetric shell using steady coning motion. *AIAA 91-2855-CP*, 1991.

THESIS PROCESSING SLIP

FIXED FIELD: ill _____ name _____

index _____ biblio _____

► COPIES: (Archives) (Aero) Dewey Eng Hum

Lindgren Music Rotch Science

TITLE VARIES: ►☑ see degree book

NAME VARIES: ►☑ Merrill (middle name)

IMPRINT: (COPYRIGHT) _____

►COLLATION: 138 p

►ADD. DEGREE: _____ ►DEPT.: _____

SUPERVISORS: _____

NOTES:

cat'r: date:

page: J155

►DEPT: Aero

►YEAR: 1998 ►DEGREE: M.S.

►NAME: GEORGE, Sean